THE UNIVERSITY *of* EDINBURGH

Learning human-like skills for cutting soft objects using force sensing

Artūras Straižys

Doctor of Philosophy

THE UNIVERSITY OF EDINBURGH

2023

Abstract

This thesis investigates the application of force sensing to learn robotic cutting of soft objects.

The automation of deformable object cutting is a promising prospect for many important areas, ranging from the food processing industry to soft tissue surgery. However, the remarkable robustness with which humans perform these tasks is far beyond the capabilities of current robotics. Humans achieve this robustness by employing various cutting strategies that rely on tactile feedback. This thesis investigates these abilities, ways of sensing and modeling these, and approaches to exploit these for robotic cutting, through four key research contributions.

The first formulates and confirms the hypothesis that forces play a key role in the robustness of cutting skills. This study investigated the human skills of scooping a grapefruit with a knife. The insight behind the hypothesis is that humans guide the knife's movement using tactile cues that arise at the pulp/peel interface. Experiments conducted in this thesis indicate that similar torque-based movement adaptation is an effective strategy in robotic grapefruit scooping. The proposed method can be used in many practical applications where cutting along the medium boundary is required; for example, in surgical excision of solid tumours within soft tissue.

A second study considered the practical implementation of robotic cutting systems that must account for a number of constraints. In many cutting tasks, the required adaptation of cutting movement is subject to a non-holonomic constraint that restricts the lateral motion of the blade. This makes it difficult to encode cutting motions using dynamical system-based methods, such as dynamical movement primitives (DMPs), otherwise well suited for learning complex reactive behaviours. The non-holonomic DMPs proposed in this thesis introduce a coupling term derived by the Udwadia-Kalaba method that guarantees run-time satisfaction of a wide range of constraints, including non-holonomic. We demonstrate how this approach can be applied to learn robotic cutting skills from demonstration.

A third study on the role of forces in surgical excisions has shown that the force modality contains valuable information for skill understanding. It was found that incision forces consist of subject-specific signatures that reflect excision assessment by experts. We proposed a generative model of excision forces, which decomposes cutting behaviour into amplitude and temporal components that encode meaningful characteristics of the observed behaviour. Along with a novel sensorised instrument developed for this study, this model can form the basis for surgical training systems with objective skill assessment and opens up many opportunities for learning human-like robotic excision of soft tissues.

Finally, these approaches were combined for learning human-like robotic elliptical excision skills, following an approach using the previously developed sensorised instrument and the model of elliptical excision forces. We introduced a generative model for pose trajectories of the blade in the elliptical excision task and used it to encode the observed excision behaviours. We demonstrate how the proposed model of excision forces can be employed to optimise the robotic behaviour with respect to the performance assessment of experts and the desired human-like characteristics of cutting forces.

This work let us analyse complex cutting tasks, techniques and skills from human demonstrations. Such analysis can lead us to understand better what underlies these skills in humans and how these can be replicated by a robot.

Lay Summary

A better understanding of what underlies the skill of cutting soft objects is critical for many important areas, ranging from surgical training to automation of kitchen tasks.

Humans demonstrate remarkable robustness in cutting despite the overwhelming complexity of physical processes involved. This raises the question of how this reliability is possible, given the seeming absence of a detailed physical model of material deformation and separation processes.

This thesis investigates complex cutting behaviours in humans and explores the potential to replicate these on a robot. Specifically, we study the role of force sensing in shaping these behaviours. In the first part of the thesis, we focus on decomposing cutting movements into fixed and adaptive components and explore how to learn these from demonstrations. This lets us to endow the robot with human-like movement adaptations in cutting tasks involving complex trajectories.

In the second part of the thesis, we look into latent characteristics of cutting forces observed in human-executed cutting tasks. This enables us to model these tasks in terms of the blade-object interaction forces and characterise the individual performances from force measurements. In the context of task automation, we show how such characterisation can be applied for optimising the robotic cutting movements to achieve the human-like characteristics of task execution. This has particular relevance in surgical robotics and the field of robot-human interaction.

Acknowledgements

I would like to express my deepest gratitude to my first supervisor, Subramanian Ramamoorthy for his steady support throughout all these years. You were always open to my ideas. Your insights and thoughtful suggestions gave me the confidence to push the boundaries of my thinking.

A big thank you to Michael Burke for being a brilliant co-supervisor. You are an example of how theoretical and practical thinking coincide. I appreciate you finding time despite the time zone difference and the demands of being a young father. I could not have done it without your guidance.

To the RAD group – Daniel, Yordan, Martin, Todor, Craig and Simon, George and other new members – thank you for being great minds.

Special thanks to Alex, for encouraging me to pursue this journey. Your joie de vivre is contagious!

Finally, to my family – this one is for you, thank you for your love and support.

To Natalija, my biggest inspiration. I am lucky to have you in my life.

This work was supported by the Engineering and Physical Sciences Research Council, as part of the CDT in Robotics and Autonomous Systems at Heriot-Watt University and The University of Edinburgh under Grant reference EP/L016834/1.

Declaration

I declare that this thesis was composed by myself, that the work contained herein is my own except where explicitly stated otherwise in the text, and that this work has not been submitted for any other degree or professional qualification except as specified.

Artūras Straižys

Publications

The following publications have been composed during the course of this doctorate:

Straižys A, Burke M, Ramamoorthy S. Generating robotic elliptical excisions with human-like tool-tissue interactions. In Proc. IEEE International Conference on Robotics and Automation (ICRA), 2024. [1]

Straižys A, Burke M, Brennan PM, Ramamoorthy S. A generative force model for surgical skill quantification using sensorised instruments. Communications Engineering. 2023 Jun 10;2(1):36. [2]

Straižys A, Burke M, Ramamoorthy S. Learning robotic cutting from demonstration: Non-holonomic DMPs using the Udwadia-Kalaba method. In 2023 IEEE International Conference on Robotics and Automation (ICRA) 2023 May 29 (pp. 5034-5040). IEEE. [3]

Straižys A, Burke M, Ramamoorthy S. Surfing on an uncertain edge: Precision cutting of soft tissue using torque-based medium classification. In 2020 IEEE International Conference on Robotics and Automation (ICRA) 2020 May 31 (pp. 4623-4629). IEEE. [4]

Contents

Figures and Tables

Figures

Tables

Chapter 1

Introduction

1.1 Preface

Humans demonstrate impressive object-to-object manipulation skills thanks to dexterous hands and the ability to learn using them. This unique set of features led early humans to create new tools from existing ones while perfecting manual skills to operate these. In this thesis we focus on the automation of cutting skills, one of the oldest tool-using skills applied by humans [7]. More specifically, we study the skills of cutting soft objects, which remain relevant to this day in activities like cooking or surgery.

The cutting tasks studied in this thesis can be defined as the controlled separation of soft objects using a blade. However, the simplicity of this general definition can be deceptive. The automation of cutting soft objects is an extremely challenging task. It involves a complex interplay between nonlinear deformation and fracture – physical processes that are extremely difficult to model accurately or efficiently. On the other hand, it seems highly unlikely that humans rely on high-fidelity models of these processes when using knives. While apparent skill demonstrated by chefs or surgeons requires years of systematic practice, even the least trained of us will outperform almost any robot at neatly cutting regular food items like cheese.

When faced with the task of making a clean cut with a blade, humans employ various strategies to handle large deformations and cutting resistance of soft objects. These involve tool manipulation strategies, such as modulation of the cutting motion, and direct manipulation of the object by a non-dominant (guiding) hand to control the deformation via shear strain. In this thesis, we focus on the former.

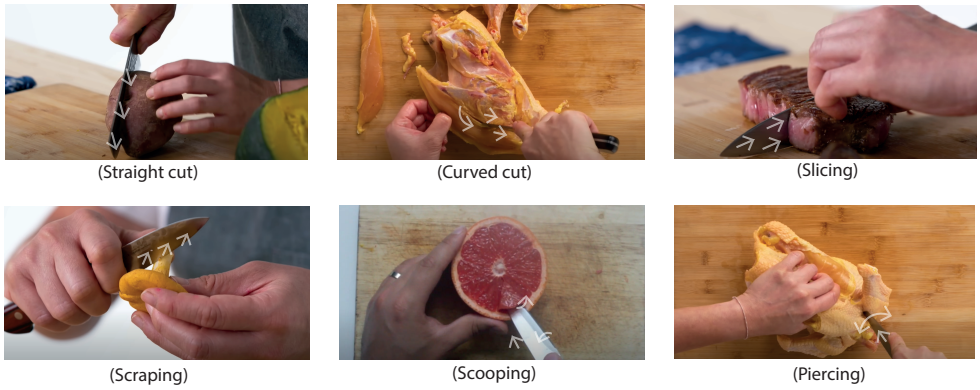

Figure 1.1: Various types of cutting motion. Images adapted from [5].

The development of tool-use strategies went hand-in-hand with the evolution of cutting tools. The sharp edge of fractured siliceous rocks allowed early humans to amplify the pressure applied by hand. However, it is the introduction of a handle that enabled the variety of possible grips for precision and control. The ulu knife [8] used by the Inuit is a great example of how cutting techniques exploit the design features of the tool. The distinct curve of the blade with a handle located above it concentrates the applied force at a small region of the blade, making it highly effective for chopping and slicing through a gentle rocking motion. Another example is a conventional knife with a pointed single-side blade that enables various cutting actions beyond slicing, such as piercing, picking and scooping – all can be performed with great precision and power [9].

We use various types of knives in our everyday lives: paring knives, bread knives, meat knives, etc. Each tool employs a distinct cutting technique (Fig. 1.1). For example, we use a serrated knife with a gentle sawing motion when cutting crusty bread. When chopping harder vegetables, we use a cleaver with a downward force applied on the back of the blade. This repertoire of cutting techniques is among the basic manual skills that most of us possess.

One point to observe is that a considerable part of cutting behaviour is anticipatory – we prescribe a particular cutting strategy before committing to cutting action, based on an anticipated blade-object interaction [10]. At a high level, the physical properties of an object to be cut dictate the type of knife to be used, and in turn, the choice of the knife determines the cutting technique. The tool's design and its relation to

the intended technique can offer valuable insight into a better understanding of the skill required for the task. In the context of task automation, we should leverage the knowledge encoded in the shape and kinematics of the tool, as well as the set of motions that form a technique.

Another part of the cutting behaviour is reactive. When cutting, we respond to sensed cutting forces by actively adjusting the blade's orientation or employing additional cutting movements. Even in the simple straight cut (Fig. 1.1), where the primary motion involves pushing the knife downwards, a minor change to the blade's orientation can significantly affect the cutting forces. For example, tilting the blade will introduce a longitudinal motion component which effectively lowers the cutting forces [11, 12] – this mechanism forms the basis for slicing techniques, which we will discuss in the next chapter.

1.1.1 Human-like cutting

Cutting skills observed in humans set an excellent reference for desired robotic behaviour. When we observe a chef or a surgeon at cutting, we can highlight the confidence of execution as we notice the apparent consistency, stability and predictability of the movements. One can also emphasize the efficiency of the cutting – the blade is manoeuvred with intent, and the cut is achieved with ease and with no wasted effort. Professional cutting is fluid and responsive – movement adjustments are subtle, judicious and timely. Because of the measured and careful trajectories, professional cutting appears safe.

These characteristics are highly desirable for robotic cutting skills in many practical applications. For example, future human-robot cooperation in the operating theatre or domestic settings will depend on organic, legible and predictable interaction between humans and machines [13,14]. An accurate model of human behaviour plays a crucial role in shared control systems, where a human operator is guided by a robot [15]. Most importantly, human-like robotic cutting behaviour is critical for ensuring safe and appropriate tool-tissue interaction in surgery [16].

There are two challenges associated with recreating human-like cutting in robots. First, defining and measuring the behaviour characteristics that reflect the skill is challenging. Despite the apparent necessity, the objective assessment of manual surgical skills remains largely elusive. The lack of universal metrics and the discrepancy between expert ratings are among the major obstacles yet to be overcome. Second, even if we can define and measure the human-likeliness of behaviour, it is not clear how to replicate this in a dynamic and highly uncertain environment.

This thesis explores how we can capture characteristic features of human-like blade-object interaction in cutting tasks. This leads to the analysis of the blade motion and the cutting forces exhibited in human demonstrations. We draw our attention to the internal structure of the cutting techniques applied by humans and raise the questions of what characteristics shape the cutting skills in humans, and how we can endow robot behaviour with these.

1.1.2 Composition of cutting behaviour

As discussed above, cutting behaviour in humans consists of anticipatory and reactive components. Fig. 1.2 shows the typical movements applied when cutting various kinds of cheese. In each case, the cut is achieved by moving the blade down through the cheese until it touches the chopping board. However, to minimize the deformations and cutting resistance, the movement is modulated to utilize the slicing effect [11]. In some cheeses with dominant viscoelastic properties, the cutting rate can drastically affect its mechanical response. While these properties can be anticipated, the actual response is extremely hard to predict. The neat cut, therefore, relies on reactive movement adjustments based on visuotactile feedback.

A similar mechanism is employed when scooping a grapefruit. Regardless of the geometry of the fruit, this type of cut is achieved by following a typical scooping motion. Because of visibility constraints, the movement is guided by tactile cues. The scooping motion proceeds until the hand senses a sudden increase in the cutting forces, which prompts the immediate blade's reorientation. Humans can actively adjust the knife based on the sense of touch without damaging the fruit or thrusting the blade inside the peel.

Figure 1.2: Various types of cheese and their cutting strategies. Firm cheeses, like Manchego, can be cut by simply pressing the blade downwards (top row). For cutting semi-soft cheeses, like Tomme, the deformations are compensated by applying a slicing-like movement (middle row). Softer cheeses with distinct viscoelastic properties, like Halloumi, are highly deformable and require dynamic adaptation of cutting movement for neat separation (bottom row). Screenshots from [6].

This thesis proposes the decomposition of these cutting movements into nominal (anticipatory) and adaptive (reactive) movement components – chapters 3, 4 and 6 build upon this idea. Fig. 1.3 shows the movement composition of curved and scraping cuts. The nominal component implements the baseline motion that achieves the cut along the desired trajectory, whereas the adaptive movement improves the robustness and efficiency of the cutting process. In general, these motion components act along different degrees of freedom. For example, the nominal cutting movement in the curved cut follows the desired cutting path by translating the knife along the normal axis and rotating about the longitudinal axis (roll). In response to the sensed cutting forces, the cutting is assisted by active modulation of the inclination angle (pitch) and the cutting depth (translation along the longitudinal axis).

These components of cutting motion are constrained. Depending on the type of cutting technique, the blade can favour one movement and discourage the others. In most cutting tasks, the movement is aligned with the direction of the least cutting resistance. When slicing, it is typically avoided to move the blade in the pure lateral

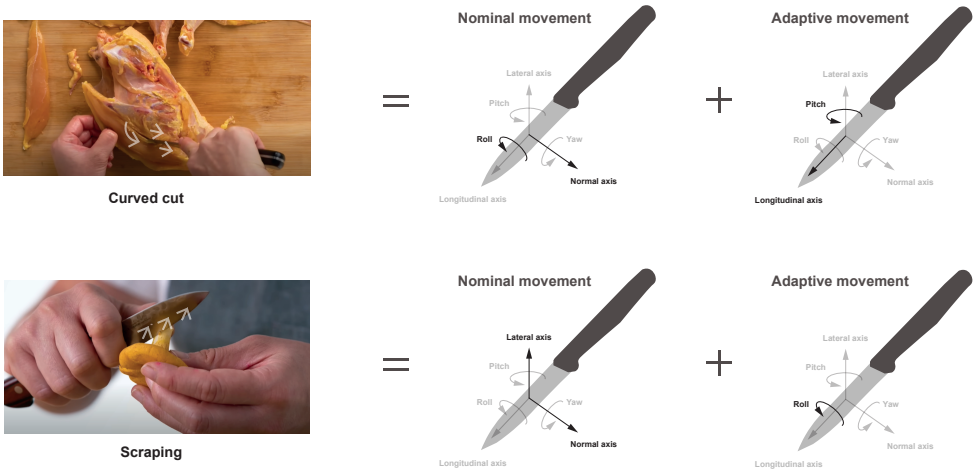

Figure 1.3: Decomposition of a cutting motion into nominal and adaptive components.

direction or to turn the knife on the spot. In other scenarios, the side of the blade can be leveraged to displace the offcut (e.g. in scooping) or to maximize the contact region (e.g. in scraping). We will return to this important subject in Chapter 4, where we investigate the non-holonomic nature of cutting motions in more detail.

The composition of cutting motions and the implicit relation between the blade's orientation and the movement direction provide a powerful structure for robot learning. Imitation learning techniques, such as Dynamic Movement Primitives (DMPs) [17], let us implicitly capture this structure from a demonstration. This thesis explores how these methods can be applied to learning cutting behaviours and constraints that underlie cutting tasks.

1.1.3 Role of cutting forces

Force-based control is a well-established field within robotic science. Robot manipulators with force and torque sensing capability show robustness to modelling errors and uncertainties. Traditionally, contact forces are controlled along the axis perpendicular to the direction of motion [18], as in deburring or polishing tasks. These compliant robot behaviours are typically achieved by a direct force loop control, or indirect, where the deviation from the commanded position is related to the applied force [19].

The cutting task, however, is unique in two important ways. First, the cutting motion of the blade is predominantly aligned with the direction of the cutting forces. Second, the cutting behaviour is not compliant – when cutting a soft object, the blade moves stiffly to initiate and propagate the crack. The cutting forces are controlled by employing additional cutting movements that change the fracture dynamics and enhance the separation process [20].

When cutting a soft object, several forces act on the blade – deformation, fracture propagation and friction [21]. These forces encode useful information about the mechanical properties of the object, as well as the state of the cutting process. This information is likely to play an important role in the reactive adaptation of the cutting motion, e.g. inducing slicing motion. However, these cutting forces are extremely difficult to predict [22], which begs the question of how the forces are mapped into an appropriate adaptation of cutting behaviour.

Numerous studies have characterised fracture dynamics in various tissues [23] and different cutting conditions [24]. However, the typical loading conditions studied in material science literature differ considerably from dynamic cutting tasks exhibited by humans. Such tasks involve complex kinematic trajectories with tight coupling between blade movement and orientation that varies throughout the execution.

This structure that underlies the cutting motion can be exploited to construct task-specific blade-object interaction models. More specifically, instead of building a comprehensive high-fidelity model of cutting dynamics capable of predicting the interaction forces for most conditions, we can look for task-specific models that describe local blade-object interactions relevant to specific cutting tasks. For example, we can learn the distribution of cutting forces from various movement adaptations around the nominal cutting behaviour. In other words, we can learn “how it feels to scrape a vegetable at various orientations of the blade” or “how it feels to cut at the interface between a softer and harder medium. In Chapter 3 we provide an example of such learning.

Given the above propositions, *cutting like humans* means to apply *human-like cutting forces* by executing *human-like cutting movements*. As discussed previously, we can encode human-like cutting movements using parameterised policies, such as DMPs. However, there are no guarantees that these will produce human-like cutting forces, which depend on the appropriate blade-object interaction and, hence, on the correct adaptive cutting behaviour (Fig. 1.4A). Given the desired (human-like) characteristics of cutting forces and the ability to measure them, we could try aligning learned motion

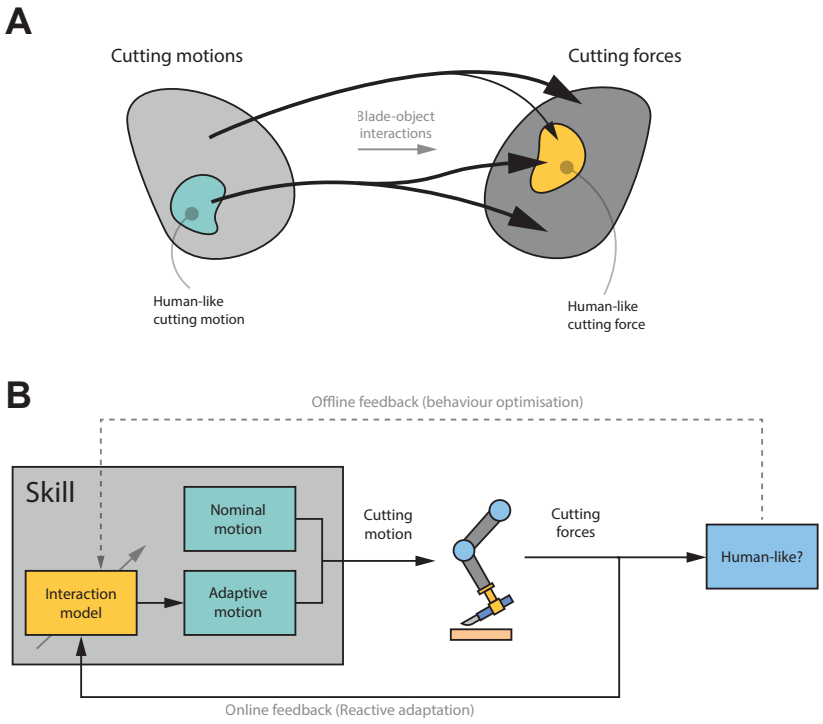

Figure 1.4: A Depending on the blade-object interaction, the human-like cutting motions can produce cutting forces that do not resemble forces from human demonstrations. To achieve human-like cutting forces under most conditions, the force-based motion adaptation must be similar to humans. **B** Reactive adaptation in real-time task execution relies on the interaction model that maps the sensed cutting forces into appropriate adaptive motion. The cutting behaviour can be adjusted (offline) by optimising the parameters of the interaction model.

policies with human-like cutting behaviour (Fig. 1.4B). Chapter 6 proposes this behaviour alignment framework for reproducing human-like cutting skills in robots. It relies on the interaction model characterising the cutting behaviour from measured forces, which will be introduced in Chapter 5.

1.2 Problem statement

In this thesis, we study the human skills of cutting soft objects. Our main objective is to model the human-like control of the blade and to reproduce this skill in robots. We approach the problem by a) investigating the role that forces play in shaping the cutting behaviour in humans, b) learning the implicit structure of the constrained cutting motion from demonstrations, and c) constructing the framework for endowing robotic cutting behaviour with human-like features.

We pose the following questions:

- What role does force sensing play in robust cutting observed in humans?
- How can sensed cutting forces be mapped to movement adaptation?
- Can we identify key features of cutting forces characterising human-like cutting?
- How can we endow robotic cutting behaviours with these features?

1.3 Thesis outline

We begin this thesis by formulating and confirming our hypothesis that force feedback plays an important role in human cutting skills. In Chapter 3, we explore the applicability of DMPs for encoding cutting movements, with a hand-engineered control scheme for reactive motion adaptation. Here, we introduce a data-driven model for the desired interaction forces learned from multiple task executions. We follow this work in Chapter 4, where we extend the original DMP formulation to enforce various constraints relevant to cutting, e.g. non-holonomic constraints.

In addition to cutting motions, we study the interaction forces that arise during cutting. Chapter 5 presents a novel sensorised instrument for measuring in situ cutting forces. Using this instrument, we collect a dataset of elliptical excision forces from trials involving professional surgeons and medical students. We explore the characteristics of force measurements capable of identifying the skill and describing the manner of task execution. In this chapter, we propose a generative model that encodes the behaviour using latent features of elliptical excision forces.

This model can be used to align robotic policy with desired human-like behaviour characteristics. In Chapter 6, we employ a Bayesian Optimisation scheme to optimise robotic elliptical excision behaviour with respect to the latent features of the proposed force model. Here, we demonstrate how we can endow the robotic cutting with human-like characteristics of blade-object interaction forces.

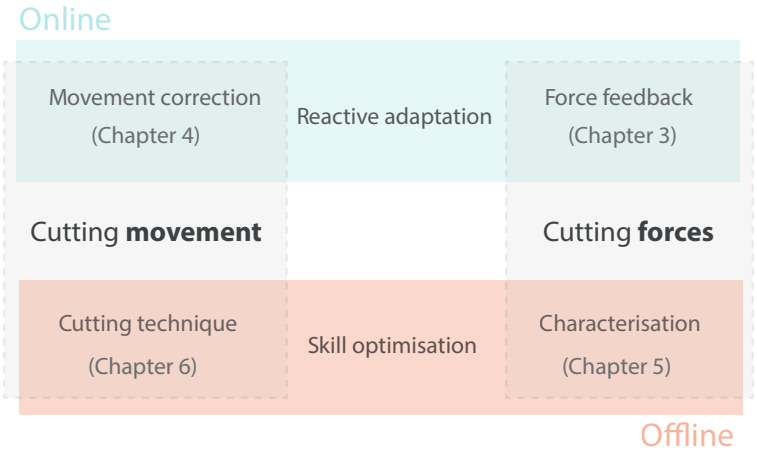

Figure 1.5: Thesis map.

Fig. 1.5 shows the map of this thesis. It can be split into two major themes, as follows:

- Cutting movement and cutting forces: Chapters 4 and 6 focus primarily on the cutting motions, and chapters 3 and 5 on cutting forces.
- Online and offline behaviour adaptation: Chapters 3 and 4 address the online movement adaptation strategies, and chapters 5 and 6 focus on offline behaviour optimisation with respect to the desired blade-object interaction features.

1.4 Major contributions

The key contributions of this thesis can be described as follows:

- Uncertainty-driven control scheme for cutting along the interface between two soft mediums. A novel approach to reactive cutting, with an error signal encoded in the decision boundary of a binary medium classifier trained on torque measurements. This enables robotic cutting along the boundary of two mediums guided by a difference in material properties. (Chapter 3)
- DMP formulation for learning movement primitives subject to a wide range of constraints, including non-holonomic, with guaranteed constraint satisfaction at run time. The proposed approach enables learning human-like reactive blade movement adaptations in cutting tasks characterised by non-holonomic constraints. (Chapter 4)

- Novel design of a low-cost and easy-to-replicate sensorised scalpel capable of measuring cutting forces. This gives us the ability to conduct large-scale field studies on the blade-tissue interaction forces across wide range of surgical procedures. (Chapter 5)
- A generative model of elliptical excision forces capable of characterising excision performance using subject-specific signatures of force measurements. This model lets us decompose the excision behaviour into a set of independent, meaningful features that uniquely describe the manner of task execution. (Chapter 5)
- Method for aligning robotic cutting behaviour with human-like force characteristics. This allows us to learn human-like blade-object interactions in complex cutting tasks. Moreover, the proposed framework opens up opportunities to study the effectiveness of surgical techniques and explore ways for their optimisation with respect to safety and tissue outcomes. (Chapter 6)

Chapter 2

Background

The task of cutting deformable soft objects is an example of quasi-static manipulation, characterized by both kinematics and forces [25]. For example, surgical excisions simultaneously depend on precise motion control along carefully planned trajectories and judicious application of forces while following these trajectories. [26]. Therefore, a comprehensive analysis of the cutting skills must consist of a balanced treatment of these task components.

We begin with a question of the control structure behind the cutting tasks. When humans cut soft objects, they primarily control the motion of the blade to achieve material separation that follows a desired cutting contour. However, increased cutting forces can induce object deformations, altering the intended contour. Additionally, depending on the composition and material properties of the object, increased cutting forces can result in unexpected fractures and tearing at the cutting front, leading to untidy cuts. Because of these factors, cutting relies on adaptation of the blade trajectory in response to fluctuations in cutting forces and object deformations.

Humans use both hands when cutting. While controlling the cutting motion, the guiding hand actively handles object deformations. When slicing a loaf of bread, we grasp it from above and apply pressure to the sides, giving it a firmer texture, which lowers the deformations caused by cutting. Another example is surgery – the following is the quote from the surgical textbook [27]: “Traction of the surrounding area is critical and if no assistants are available, the surgeon must learn how to use the non-dominant hand or must rest the fifth finger of the dominant hand on adjacent skin to apply mild tension on the surgical site”. While this is an important part of human-like cutting behaviour, in this thesis, we only focus on the control of the blade.

When cutting soft objects, humans also control the blade-object interaction forces. In most cases, the goal is to minimise cutting forces, which lead to undesired deformations, cutting resistance, and stress. However, in specific scenarios, the goal can be more complex. For example, professional surgeons exhibit greater cutting forces compared to inexperienced trainees in the task of glioma division [28]. In addition to magnitude, skilful cutting implies the appropriate set of other cutting force features, such as derivatives [29] or temporal structure [2]. Controlling cutting forces involves adjustments to cutting velocity, depth, blade orientation, and surface tension. Throughout the task execution, these variables undergo dynamic changes, adding complexity to the analysis of cutting forces.

While acknowledging the role of feedback in cutting behaviour, it is valuable to study the robustness of feedforward (open-loop) cutting strategies observed in human cutting. As discussed in the Introduction chapter, a significant part of cutting behaviour is predetermined. These nominal cutting trajectories encode the structure underlying the robust cutting behaviours. For example, let us consider a sawing motion executed in an open-loop fashion. The implicit slicing movement makes sawing a robust strategy to cut with minimum deformation. Sawing-like cutting, however, is undesirable in a surgical context where one of the objectives is to prevent uneven and jagged excisions [27]: “In order to avoid a jagged edge, use firm confident strokes”. In these tasks, the desired interaction is often characterised using motion-based [30] or forces-based [29] metrics.

The remaining part of the chapter will lay out the main concepts and principles that underlie cutting motion and its effect on the cutting process. We begin with a brief overview of cutting tasks, the techniques required for task execution, and skills enabling these techniques. We follow with the basics of cutting mechanics and the characteristics of soft objects. We end the chapter with an overview of methodologies for modeling the cutting process and discuss its relevance within the context of task automation.

2.1 Cutting tasks, techniques and skills

Cutting tasks are essential for cooking and surgery. Cutting food can have a significant influence on the taste and plate presentation. In surgery, cutting tasks are performed judiciously and carefully, prioritising patients' safety and post-surgical recovery. Regardless of the task, the objectives are achieved by employing appropriate tools and techniques that maximise the tool's effectiveness. The key, however, is the skill of tool use that embodies both tacit and conceptual knowledge of the task.

2.1.1 Kitchen knife skills

Cutting is the most elemental building block in cookery; hence, knife skills are considered fundamental skills of the chef. Cutting plays a role in the texture and consistency of the dish. It also can affect the taste. For example, finely minced ingredients intensify their flavours, while coarser cuts retain distinct textures, resulting in different tastes.

Cutting skills involve using different knives, each designed to handle specific tasks [31]. For example, a paring knife characterised by a short, narrow, pointed blade is used in delicate tasks, such as trimming or peeling. In contrast, a cleaver is employed in heavy-duty tasks that require significant force and precision. The design of the knife reflects the optimal technique for its use. For instance, the blade of a bread knife features serrations to facilitate sawing motion, promoting the cut through the crust without squashing the bread [32].

The human hand allows for the use of knives with various grips, each influencing cutting performance. The pinch grip [33], for instance, where the thumb and index fingers rest in front of the bolster, amplifies the control and precision and facilitates smooth cutting motions. Conversely, the hammer grip involves a firm grasp of the handle and is used in heavy-duty tasks that demand substantial downward forces.

Cutting techniques can be viewed as optimal strategies for specific tasks. Splitting harder vegetables is typically performed by chopping, where the knife is pressed down with force. Slicing involves an additional horizontal motion component, i.e. parallel to blade travel [34]. There are different variations of a slicing cut [35], e.g., the French slice, in which the blade moves back and forth in a rocking motion, with the blade's tip maintaining contact with the cutting board. In a Japanese slice, the blade glides forward without tilting. These seemingly subtle differences affect both motion

ergonomics and dynamics of the cutting process. The rocking motion of the French slice allows for quick and efficient slicing, mainly when dealing with large quantities of ingredients. The Japanese slicing minimises resistive cutting force, which enables thin and consistent slices of delicate ingredients like fish.

Efficiency and consistency in these tasks rely on precise movement, appropriate rhythm and well-controlled application forces [35]. The guiding hand plays an important role, too - in some cases, it fixes the food in place; in other cases, it dynamically manipulates it as cutting proceeds [36], e.g. feeds the ingredient under the blade or tensions the surface. Cutting skills also involve coordination and smooth transitioning from one cutting style to another. In practice, cutting techniques adapt and change in real-time. For example, a large onion half is likely to be chopped at the start but sliced with a rocking motion towards the end of the task (more ergonomic technique, but not suited for large foods).

Finally, cutting techniques are not constrained to planar motions. Let us consider filleting, an extreme example of an advanced cutting task that relies on the chef's dexterity, precision and power [37]. This task involves a complex composition of cutting motion and an extensive range of blade configurations. During the task, the cutting alternates between using the entire blade length and the tip only. Furthermore, a substantial portion of the cutting is carried out in a scrapping fashion, where the blade's side presses against the flesh as it moves. Filleting demands extreme motion precision - the flesh can be flaky and must be cut at a particular angle. The task also requires precise control of forces, e.g. puncturing through the skin without damaging the flesh. Moreover, coordinated control of precise motion and force application is needed for cutting through a ribcage while preserving the integrity of the underlying skin. Cutting through the skeleton can demand significant force, relying on dynamic and forceful cuts, with the cutting hand leveraging the momentum.

2.1.2 Surgical scalpel skills

Scalpel cutting of soft tissues remains a fundamental surgical skill in clinical practice. Conventional scalpels offer superior precision, more predictable tissue damage, and faster wound healing compared to electrosurgical blades [38, 39].

Scalpel techniques are designed around precision and control of the motion and applied forces. Before cutting, the motion is always carefully planned and, in some cases, outlined to mark the desired cutting contour. The deformation of soft tissues demands precise motion control to incise along the contour. Control of cutting force is paramount - too little and the scalpel will not cut through the tissues; too much, and there is a danger of cutting beyond the desired region and damaging neighbouring tissues. Accordingly, scalpel-cutting tasks depend on excellent hand-eye coordination and visual and tactile guidance.

Let us consider a standard surgical technique called elliptical excision that aims to remove the tumour with a clear margin of healthy tissue around it. This procedure is characterized by continuous skin incisions along a marked contour. Throughout the incision, the non-dominant hand applies continuous tension to the tissues surrounding the cutting contour, while the dominant hand controls the blade's movement. In [27] Hanlon et al. describe the elliptical excision task as follows: "The point of the blade makes the initial cut at the apex, then quickly the sharper belly is used to move along the arc. [...] The incision should be carried down to subcutis on the first pass". The ellipse is dissected using short delicate strokes that cut in the same plane, while avoiding damage to the epidermis [40]. Next, the edges are undermined using scissors before closing the wound using the appropriate suture technique [41]. Finally, after excision, the removed specimen is sent for pathological examination of margins to determine the excision's adequacy.

Even the initial phase of this procedure, making the incision, poses a challenging task of bimanual manipulation of soft tissues. The complex geometry of the workspace severely restricts task kinematics and visibility. The cutting is guided by weak tactile cues in the presence of occlusions. In addition, the behaviour of biological tissues is highly uncertain and unpredictable, which requires continuous adaptation in the applied motions.

Mastering these skills relies on developing the “tactile knowledge” of the task. Given the breadth of conceptual knowledge learned in the classroom, surgical trainees spend years practising this in operation theatres until they reach the required level of bodily control. However, an apparent gap exists in understanding what underlies these skills. For example, despite critical importance, the approaches to objective evaluation of surgical skills remain largely elusive [30]. Surgical textbooks are filled with expressions like “the right kind of pressure” [16] or “firm confident strokes” [27], which emphasize the objective and implicit nature of embodied knowledge.

2.1.3 Cutting techniques and motion primitives

While most studies of cutting soft objects focus on the straight cuts restricted to a plane, such as chopping or slicing [42–46], this is just one of the many manoeuvres involved in real-life cutting tasks. For instance, preparing a grapefruit involves chopping, slicing, curved cutting and scooping (Fig. 2.1).

Each manoeuvre achieves separation differently. The kinematic differences in these cutting types affect the deformation and fracture processes. For example, the curved cut changes the blade’s orientation in 3D, making it significantly harder to perform and analyze than more straightforward planar cuts. The rotations of the blade inside the object introduce shear deformation of the material and change the contact dynamics.

Another example is a scooping cut separating material by pushing the blade longitudinally (as in piercing) while simultaneously lifting the offcut on the side of the blade. Unlike straight cuts that exhibit direct crack propagation, the scooping cut involves a combination of cutting and tearing modes. The analysis of underlying forces is complicated since both tear resistance and compression forces act on the same plane.

Cutting techniques, such as chopping or elliptical excision, can be decomposed into motion components (see Fig. 1.3). Here, we call these components cutting primitives to emphasise their elementary role in constructing complex cutting movements. As discussed in Chapter 1, such decomposition consists of nominal and adaptive components; the former executes the prescribed cutting trajectory that shapes the technique, and the latter assists the execution by engaging the auxiliary cutting modes. For example, when starting chopping, one might adjust the blade’s orientation or slide it across the surface to facilitate crack initiation. This adaptation leverages the principles of the slicing technique, which is known to reduce cutting resistance.

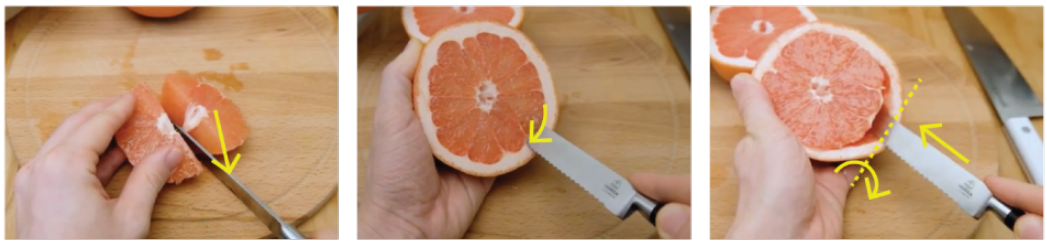

Figure 2.1: The task of preparing a grapefruit involves performing a straight cut (left), a curved cut (center) and a scooping cut (right).

2.2 Basics of cutting

2.2.1 Kinematics of cutting

Blade kinematics in cutting tasks can reveal the structure of cutting techniques, which can be further exploited for task automation. Fig. provides examples of four different cutting techniques. In the chopping technique (Fig. 2.2A), the blade translates downwards without changing blade orientation. This type of cutting is applied when cutting harder ingredients, sometimes with the assistance of a guiding hand that applies force on the back of the blade.

The slicing technique (Fig. 2.2B) balances by resting the knife on its tip and utilizing a rocking motion. This technique introduces the horizontal motion component, which results in the reduction of the cutting effort when compared to the chopping cut. From a user perspective, the rocking motion enables leveraging the point of contact (where the tip is rested), leading to more effortless execution and increased precision.

Fig. 2.2C shows a French slicing motion in which the blade glides forward as it rocks, further increasing the horizontal movement component and reducing the cutting effort. The natural rocking motion helps reduce strain on the wrist and arm during prolonged cutting tasks, contributing to a more comfortable and sustainable cutting experience.

Finally, the drag slice (Fig. 2.2D) moves the blade backwards as it cuts. The technique minimises the cutting resistance by dragging the blade along the ingredient's surface. This is particularly advantageous when cutting delicate ingredients like a boiled egg or tender cuts of meat. The pulling motion enables greater precision and control over the cut. Chefs can easily adjust the cut's depth and speed, achieving consistently uniform slices.

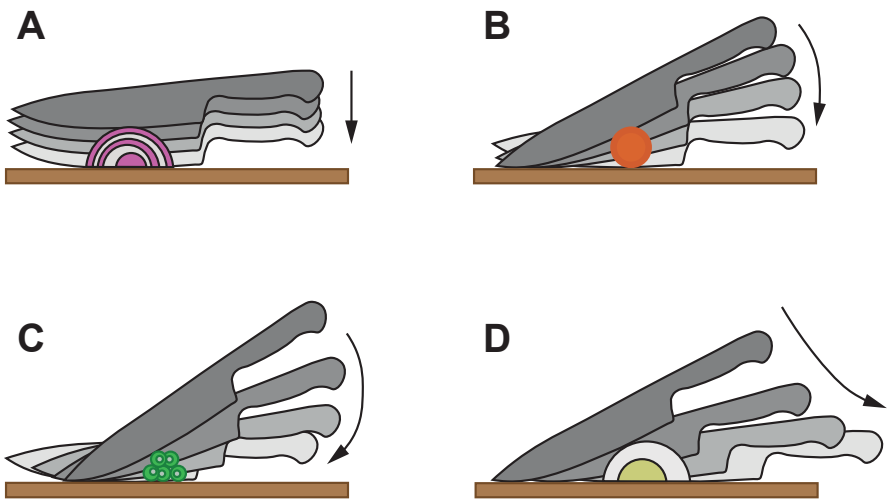

Figure 2.2: A Basic chopping technique, **B** Basic slicing technique, **C** the French slice, and **D** Drag cut.

Constraints

Cutting tasks are inherently constrained. When performing a straight cut, the lateral motion of the blade is negligible. In addition, the medium restricts the inserted blade from rotation on the spot. As the result, the spatial trajectories of the cutting blade are limited by nonholonomic-like constraints [44]. In particular, this is importaint in robotic cutting, as movement adaptation strategies must respect the limits of permissible motion space.

2.2.2 Mechanics of cutting

The process of cutting soft objects involves interplay between complex physical phenomena such as nonlinear deformation, crack propagation and friction. Understanding the mechanisms underlying this process can be helpful in many practical applications, including soft tissue surgery. In this section, we briefly review the basic model of cutting - this will serve as a relevant background for Chapter 5, where we study the cutting forces arising during surgical excisions.

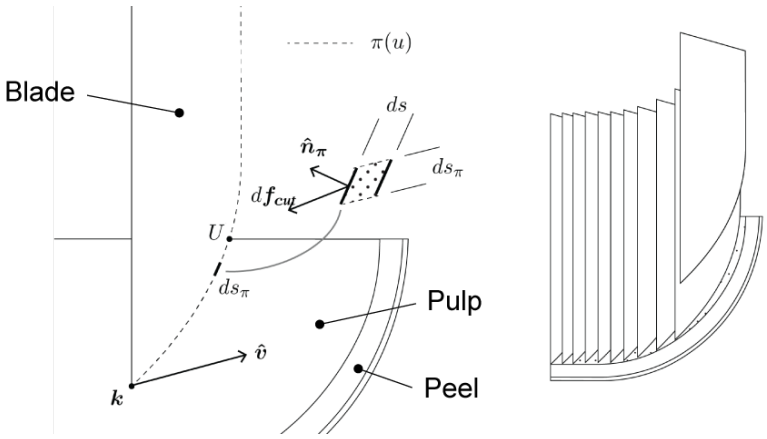

Figure 2.3: (Left) Mechanics of a straight cut in a grapefruit slicing task, (right) trajectory of the blade performing a straight cut.

Here, let us consider the task of slicing a grapefruit with a straight cut, as shown in Fig. 2.3. The cut is performed in the plane restricting the motion of the blade along the desired trajectory. The tip of the blade is marked by a point $\boldsymbol{k}$ that defines the origin of the blade's coordinate frame. Velocity of $\boldsymbol{k}$ is denoted as $\boldsymbol{v}_k$. The curve $\pi(u)$ describes the geometry of the blade's edge, where $u \in [\boldsymbol{k}, U]$ denotes the region of the blade's edge that is inserted in the fruit, and U denotes a point at which the blade's edge and grapefruit's surface intersect.

The mechanics of the task can be formulated as energy balance between cutting, friction and deformation of the material [21]. The total force $\boldsymbol{f}$ impressed upon the blade is a sum of cutting force $\boldsymbol{f}_{cut}$, friction force $\boldsymbol{f}_f$ and deformation resistance $\boldsymbol{f}_u$:

$$\boldsymbol{f} = \boldsymbol{f}_{cut} + \boldsymbol{f}_f + \boldsymbol{f}_u \tag{2.1}$$

The cutting force $\boldsymbol{f}_{cut}$ which is responsible for propagating the fracture. Figure 2.3 illustrates how an infinitesimal length of contact ds_π displaced by an increment ds in the direction of $\hat{\boldsymbol{v}}$ gives rise to the cutting force $d\boldsymbol{f}_{cut}$. By definition, the work done by this force is the dot product of $d\boldsymbol{f}_{cut}$ and displacement vector $\hat{\boldsymbol{v}}\ ds$:

$$dW_c = d\boldsymbol{f}_{cut} \cdot \hat{\boldsymbol{v}}\ ds \tag{2.2}$$

The $d\boldsymbol{f}_{cut}$ is proportional to the length of the contact $\pi(u)$ for u region [$\boldsymbol{k}$, U]:

$$dW_c = R\ (\hat{\boldsymbol{n}}_\pi\ ds_\pi) \cdot (\hat{\boldsymbol{v}}\ ds) = R\ (\hat{\boldsymbol{v}} \cdot \hat{\boldsymbol{n}}_\pi)\ ds_\pi ds \tag{2.3}$$

where R is the fracture toughness and $\hat{\boldsymbol{n}}_\pi$ is the unit vector of length of contact ds_π.

By rearranging equations, the cutting force $d\boldsymbol{f}_{cut}$ can be expressed as:

$$d\boldsymbol{f}_{cut} = R\,(\hat{\boldsymbol{v}} \cdot \hat{\boldsymbol{n}}_\pi)\,\hat{\boldsymbol{v}}\,ds_\pi \tag{2.4}$$

The total cutting force $\boldsymbol{f}_{cut}$ is defined by the integral over the entire blade's edge $\boldsymbol{\pi}(u)$ for $u \in [\boldsymbol{k}, U]$:

$$\boldsymbol{f}_{cut} = \int_\pi d\boldsymbol{f}_{cut} \tag{2.5}$$

Finally, the friction forces $\boldsymbol{f}_f$ can be represented as Coloumb friction model [47] and the deformation forces $\boldsymbol{f}_u$ can be represented by any of the deformation models described in the previous section.

2.2.3 Slice/push ratio

It is well known from everyday experience that cutting tomato or bread involves a slicing movement, where in addition to pushing downwards, the blade is sliding over the surface. When cutting-by-pressing a highly deformable object, the rupture event precedes large deformations beyond the linear region, leading to an untidy cut [48]. Slicing motion enables one to make a well-controlled neat cut with very little downward pushing force [49] [50].

For quantification of this effect, Atkins et al. introduced a "slice to push" ratio [49] [20]. This was further studied in [51], where authors showed that shear loading allows reaching the critical stress required for crack initialization with considerably smaller downward force. The potential role of friction in this phenomenon was first discussed by Chaudhury [52], followed by a study [53] revealing that friction facilitates the build-up of localized tension responsible for fracture initiation. These studies are particularly interesting in the context of robotic cutting with force-based movement adaptation schemes.

In the above discussion, global deformations were handled by adjusting the scalpel movement. However, cutting is a bimanual task, in which the non-dominant hand supports the object and actively controls its deformation. For example, when cutting a grapefruit (Fig. 2.1, center), a supporting hand subtly squishes a fruit to tension the tissues around the edge of the blade. A similar mechanism is exploited in surgery, where the non-dominant hand actively assists in cutting by providing the required tension in the area of the crack.

2.3 Modeling cutting process

The process of cutting soft material can be divided into three distinct phases, namely the deformation phase, the rupture phase and the steady cutting phase [54] [48]. During the deformation phase, the blade compresses the material with increased forces in accordance with material's viscoelastic properties. In addition to fracture characteristics of the object, the extent of deformation before the crack initiation is determined by the sharpness of the blade and its configuration [55]. The rupture phase is characterized by abrupt decrease in cutting forces [56] due to release of the strain energy accumulated in the deformation phase [57]. Following this, is the steady cutting phase, in which the crack propagates continuously. For highly anisotropic and heterogeneous objects, like soft tissues, this phase might consist of a series of localized deformation-rupture events [58].

Depending on the application, cutting phases can play different roles in the task. For example, in surgical incisions it is crucial to precisely control the penetration depth [59], a process guided by tactile cues during the rupture phase. Also, clean cuts require reduction in cutting forces [50], thus control in the cutting phase are important in many applications (e.g. in surgery, or microtome). Finally, as will be discussed in the following sections, the deformation phase of the cutting process plays an important role in guiding blade's configuration and overall cutting envelope.

2.3.1 Properties of soft objects

Foods

Food products that are cut in everyday life have a rich set of peculiar mechanical properties. These properties are determined by food compositions and microstructure. For example, it is known that the stiffness of cheese is determined by the fat to protein ratio [60]. In addition, the deformation and fracture properties of cheese are influenced by the coarseness of its protein network [61]. Other examples are fruits and vegetables, whose tissues are living systems with diverse microstructures and complex cellular mechanics. At a macroscopic level, fruit tissues consist of several layers with distinctly different physical properties, which are influenced by the chemical composition and arrangement of cells, as well as the structure of intercellular spaces. For example, the level of pectin content in tissue cell walls affects the overall stiffness of the fruit's body [62]; combination of cellular arrangement, diameter and wall thickness of cells, their turgidity, as well as degree of cell adhesion influences the fracture properties of a plant [63].

Soft tissues

The macroscopic construction of biological soft tissues consists of cells and an extracellular matrix (ECM). The ECM is a three-dimensional network of collagen, elastic and reticular fibers, that provide cells with structural support and maintain cell communication. Because of the ECM structure, soft tissues are often viewed as complex fiber-reinforced composite materials [64], whose mechanical properties are defined by the spatial arrangement and configuration of collagen and elastin fibers. The former is responsible for the strength and resilience of the tissue, while the latter provides the tissue with elastic properties.

The complex composition of soft tissues causes a non-trivial set of mechanical properties [65]. Biological soft tissues are non-homogeneous due to their complicated structural composition. The spatial distribution of collagen and elastin fibers is responsible for anisotropy (i.e. dependence on direction) in the tissues' mechanical properties. In addition, the soft tissues demonstrate viscoelastic (i.e. time-dependent) behaviour, because of the high content of water. In addition, the combination of the

elastic response of elastin fibers and viscous damping due to high water content in tissue cells, gives rise to viscoelastic (time-dependent) tissue behaviour. As a result, the mechanical response of soft tissues is highly nonlinear over finite strains, with a strong dependence on stress and strain rate.

2.3.2 Modeling deformation

Continuum mechanics and finite element methods

In continuum mechanics, materials are modeled as continuous mediums which obey the fundamental physical laws, such as conservation of energy, in conjunction with constitutive laws that describe complex mechanical behaviour. Since the discrete nature of matter is ignored, all physical quantities in continuum analysis, such as stress or displacement, are considered continuous functions of position within the domain of the problem. This continuum assumption has proven to be valid for a large number of applications with practical importance, where the dimensions of the analyzed body are much larger than the body's underlying microstructure.

The classical elasticity problems of solving for the unknown field variables (e.g. displacement), given the known field variable (e.g. stress) and some boundary and initial conditions, typically involve one of the variational principles such as the principle of minimum potential energy. Generally, the analytical solutions for such problems are not available, unless the geometry and loading conditions are simple and fields are uniform and linear. In practice, the solution is numerically approximated by finite element methods or other computational techniques.

The finite element method (FEM) is a computational technique for the numerical approximation of solutions to field problems, such as described above. The procedure involves subdividing the problem domain Ω into a finite number of non-overlapping subdomains Ω_e, called elements, often using triangular or tetrahedral meshing techniques. The behaviour of each element is characterized by field variables evaluated at the element's boundary points, called nodes. The solution for each of the elements is approximated by interpolating the field variables. The global behaviour of the modeled domain Ω can then be described by assembling the total system of equations in the following matrix form

$$\mathbf{M}\ddot{\boldsymbol{u}} + \mathbf{C}\dot{\boldsymbol{u}} + \mathbf{K}\boldsymbol{u} = \mathbf{f} \tag{2.6}$$

where $\boldsymbol{u}$, $\dot{\boldsymbol{u}}$ and $\ddot{\boldsymbol{u}}$ are vectors of node displacements and its first and second time derivatives, respectively. **M**, **C** and **K** are element mass, damping, and stiffness matrices, respectively. **f** is a vector of total force acting on the element nodes.

Nonlinear hyperelastic models

The theory of nonlinear elasticity addresses the major limitation of linear elastic models, namely the inability to describe the material response over large strains. The foundation of nonlinear elasticity was established in the late 1940s, a period of early work on modeling the mechanical response of rubber. In particular, significant advancements were made by Reiner [66] and Rivlin [67], whose work laid down the general principles of nonlinear constitutive relations. In the 1960s, the newly developed theory of finite elasticity was applied in the field of biomechanics by Fung [68], a notable work that highlights early attempts at soft tissue modeling. Materials that behave according to nonlinear elasticity theory are modeled by hyperelastic constitutive equations.

Heuristic models

The described above physics-based models are mostly implemented using FEM. Heuristic models avoid the complexities associated with FEM, and instead focus on computationally efficient *heuristic*-based techniques that yield plausible tissue behaviour. These models are ubiquitous in interactive surgical simulations, however, they generally lack physical accuracy, and sometimes validity.

For example, deformable splines [69] can model the geometry of the tissue with parameterized curves, such as Bezier or NURBS, whose curvature is defined by a set of control points. Another example is the mass-spring-damper (MSD) model, which was the first deformation model used in the surgical simulator [69] and to this day is the most widely used technique for modeling soft tissue deformation in real-time. In MSD, the tissues are represented as a network of discrete masses linked by springs and dampers. The dynamics of the system obey Newton's laws of motion, where the position of the individual mass point at each time step is defined by the balance of forces that act on the point. However, in addition to inherent stability issues, the conventional MSD implementation lacks the volume preservation mechanism, which is critical for modeling many biological tissues.

Modeling viscoelasticity

The models described above do not account for viscoelastic effects. Viscoelasticity is generally modelled using a linear combination of ideal elastic (Hookean) springs and ideal viscous (Newtonian) dampers. By definition, the Hookean spring obeys the following constitutive law

$$\varepsilon = \frac{1}{k}\,\sigma \tag{2.7}$$

where ε, σ and k are strain, stress and elastic modulus of the material, respectively.

A Newtonian damper responds as follows,

$$\frac{d\varepsilon}{dt} = \frac{1}{\eta}\,\sigma \tag{2.8}$$

where η is viscosity of the material.

In combination, these ideal elastic and viscous elements can be used to describe the transient response of the modeled system. For example, in a series configuration (called the Maxwell model) both elastic and viscous elements are subjected to the same stress but exhibit different strains. In contrast, the parallel arrangement (called th Kelvin-Voigt model) subjects the elements to the same strain, but different stresses. Other models use various combinations of three elements (e.g. Standard Linear Solid model), in addition to more complex models that consist of many elements (e.g. generalized Maxwell model).

It is often convenient to express the stress-strain relationship through a creep compliance function C(t) and relaxation modulus function G(t), respectively.

$$\varepsilon(t) = \sigma_0\, C(t), \quad C(t) = \frac{t}{\eta} + \frac{1}{k} \tag{2.9}$$

$$\sigma(t) = \varepsilon_0\, G(t), \quad G(t) = ke^{-tk/\eta} \tag{2.10}$$

where σ_0 and ε_0 are constant stress and strain, respectively, applied at the initial instant (t = 0).

The *C*(t) and *G*(t) functions are often used in the integral representation for stress-strain relationship. For instance, given the strain history over $[0,t]$, the stress can be evaluated using following convolution integral

$$\sigma(t) = \varepsilon_0\, G(t) + \int_0^t G(t-\tau)\, \frac{d\varepsilon(\tau)}{d\tau} d\tau \tag{2.11}$$

Equivalently, the strain profile $\varepsilon(t)$ can be obtained given the stress profile $\sigma(t)$

$$\varepsilon(t) = \sigma_0\, C(t) + \int_0^t C(t-\tau)\, \frac{d\sigma(\tau)}{d\tau} d\tau \tag{2.12}$$

In practice, the required creep compliance function (or relaxation modulus function) is obtained from the creep recovery (or stress relaxation) test.

The relaxation function $G(t)$ is often expressed in terms of a Prony series in a following form

$$G(t) = G_\infty + \sum_{i=1}^{N} G_i (1 - e^{-t/\tau_i}) \tag{2.13}$$

where G_∞, G_i and τ_i are called equilibrium modulus, *i*-th elastic component and relaxation time.

2.3.3 Modeling fracture

The cutting process has been extensively studied in the field of Fracture Mechanics. The problem of cutting through soft tissues is complicated by the accumulation of large strain in the tissue prior to cracking. The nonlinearity of constitutive relations caused by finite strains invalidates many of the underlying assumptions in the classical Fracture Mechanics, which was originally developed for strong ductile solids such as metals. In addition, the complex friction and crack blunting effects further complicates modeling of cutting process. Finally, cutting introduces the topological changes in the geometry of the tissue, which makes it extremely hard for mesh-based analysis, such as FEM.

Nevertheless, cutting of soft biological tissues remains an active area of research. For example, in [70] authors measured the forces acting on the blade during the cutting of porcine liver. The results revealed a series of local deformation-crack cycles, which were characterized by proposed local elastic modulus quantity. In [71] the numerical model of cutting based on energy approach is described. Generally, the

fracture mechanics formulation considers total work done by cutting as a sum of cutting energy, strain energy and frictional losses. The cutting energy is often measured by "double insertion" technique [71], in which the difference in total measured force at first and second cut yields so-called *fracture toughness*, a crack-resistant or cutting force. Tissue puncture and cutting needle insertion is often modeled using *J integral* that represents the power per unit of crack advance, parameterized by the geometry of the needle and insertion rate. In this model approach, the crack initiates and propagates if the J integral is equal to or exceeds tissue's fracture toughness for given needle displacement [72]. It should be noted, that due to geometrical differences, the needle insertion and cutting with scalpel models demonstrate important qualitative differences. For instance, it is reported that in the needle insertion tasks the fracture toughness is almost independent on the insertion speed, but shows strong dependence on needle diameter [54]. In contrast, the experiments on tissue cutting using scalpel reveal strong dependence of cutting forces on the velocity [70].

2.4 Human-like robotic cutting

Studies on robotic cutting of soft tissues predominantly focus on tasks involving planar cutting motions [12, 21, 73–84], such as chopping or slicing.

Modeling [11,12,51,75] of deformation and fracture is widely applied to hand-engineer [21] or to learn control policies for these robotic cutting behaviours. For example, analytical models are employed for implementing robust robotic cutting of materials via manually-designed planar trajectories [21, 74]. Another example is learning slicing skills via a differentiable simulation that predicts the cutting forces and object deformation given the motion of the blade [73].

These model-centric approaches are motivated by objectives beyond material separation. Indeed, robotic splitting of soft objects using a sharp blade can be achieved by employing position-based control along a straightforward linear path, regardless of cutting forces. If, for example, in addition to splitting we aim to maximise cutting efficiency or to minimise object deformation, a physically-accurate predictive model can be used to optimise the behaviour. The defined objective function then encodes the desired behaviour.

In [73] authors report that optimisation of cutting behavior resulted in a robot policy that implements slicing technique. On the one hand, this shows that by the use of appropriate modeling and policy learning techniques, we can recover the “optimal” cutting strategies that resemble natural cutting behaviour exhibited by humans. On the other hand, this raises the question of whether we should try learning these strategies directly from humans instead.

Intriguingly, humans demonstrate a remarkable robustness at cutting tasks without access to a detailed model. If human-demonstrated behaviour encompasses successful cutting strategies to achieve object separation, we should investigate to what extent these are robust to variations of material properties. Where it succeeds and where does it fail? How do variations in objects’ geometry and materials properties translate into variations of the cutting trajectory?

These questions become particularly relevant when we transition to automation of cutting tasks that involve more complex blade trajectories [44] and blade-object interactions [85, 86], e.g. in grapefruit scooping or elliptical excision tasks. What is the objective function that shapes the cutting behaviour in these tasks? While we cannot answer this question with certainty, we can demonstrate the desired behaviour across various conditions. The consistency and variability inherent to these demonstrations can let us uncover the structure behind the technique and the mechanism that drives the behaviour [87].

These are the ideas from the Learning from Demonstration (LfD) [88], a paradigm for teaching robots to imitate human behaviour. This thesis explores the application of LfD in an attempt to answer the above questions. In chapters 3 and 4, we apply the LfD methods to learn complex cutting skills, such as grapefruit scooping and skin incisions. In chapters 5 and 6 we explore the questions related to the objective function and behaviour optimisation raised above.

2.4.1 Learning from Demonstration

The task of cutting soft objects falls in the category of tasks where the desired behaviour cannot be easily scripted (due to the unpredictable behaviour of deformable objects) and cannot be easily formulated as an optimisation problem (due to an unknown reward function), however, can be easily demonstrated. The LfD paradigm is especially well-suited for these tasks [88].

At its core, the LfD methods assume that expert-demonstrated behaviour consists of all the information required to capture the skill. This brings some unique advantages over other approaches. For example, LfD enables task domain experts with no experience in robot programming to teach complex skills to robots. When compared to Reinforcement Learning (RL) methods, which learn optimal policies via trial and error, the LfD approaches are significantly more efficient, as their policy learning is guided by expert demonstrations. Moreover, RL (and other optimisation-based methods) require the reward function, which is not trivial to specify in many practical cases. The LfD methods, in addition to learning policies, can be used to learn the reward function from demonstrations [89] [90].

Among the policy-learning LfD methods, the ones of particular relevance to this thesis are those focused on learning trajectories from demonstrations. Broadly speaking, these methods can be divided into optimization-based (e.g. [91] and [92]), probabilistic (e.g. [93] and [94]), and dynamical system-based approaches (e.g. [95] and [96]). Specifically, in this thesis we focus on the LfD approach called Dynamic Movement Primitives [96], which models trajectories using dynamical systems. This approach offers some interesting properties that can be leveraged when encoding complex cutting trajectories of the blade. In the following section, we present a brief overview of this elegant method.

While LfD offers numerous advantages compared to other robot learning methods, it also comes with several limitations. For example, the assumption that the provided demonstrations are optimal is often too strong. Even with an expert demonstrator, the recorded demonstration can be corrupted by sensor noise or occlusions. Besides, in situations involving multiple demonstrations, the expert may exhibit ambiguity through inconsistent choices of action for a given state [97]. Moreover, the LfD can suffer from the correspondence problem, characterised by a mismatch between the actuation of the demonstrator and the robot [88]. Although kinesthetic teaching (where the robot arm is physically moved during the demonstration) can alleviate this issue, it is not suitable for many tasks of practical importance. Cutting soft objects is one of these tasks - it requires delicate manipulation skills that involve small-scale movements and weak but highly informative tactile feedback, which renders traditional kinesthetic teaching infeasible.

2.4.2 Dynamic Movement Primitives

Dynamic Movement Primitives (DMPs), is an elegant framework for learning trajectories from demonstration, first introduced by Ijspeert et al. [98] and later extended in [99]. The main idea behind DMPs is that a demonstrated trajectory can be encoded using a stable nonlinear dynamical system. Within the DMP framework, any goal-oriented motion can be represented using a combination of a) linear second-order attractor dynamics, which guarantees the system's convergence to a goal state, and b) nonlinear forcing function f, which shapes the attractor landscape (hence allowing to capture an arbitrary complex motion).

More specifically, a single degree-of-freedom (DoF) trajectory y of a point-to-point movement primitive can be expressed as:

$$\tau\ddot{y} = \alpha_z(\beta_z(g-y)-\dot{y})+f \tag{2.14}$$

where g is a goal position, $\tau > 0$ is a temporal scaling factor, and $\alpha_z > 0$ and $\beta_z > 0$ are time constants. Note that in the above equation, the nonlinear term f modulates the landscape of a global point attractor g. Thus, an arbitrarily complex movement can be represented by appropriately constructing f term.

Typically, the nonlinear function f is represented using a normalized linear combination of basis functions:

$$f(x) = \frac{\sum_{i=1}^{N}\Psi_i(x)w_i}{\sum_{i=1}^{N}\Psi_i(x)}x \tag{2.15}$$

where N is the number of basis functions $\Psi_i(x) = \exp\left(-h_i(x-c_i)^2\right)$ with center c_i, widths h_i and weights w_i. The forcing term does not depend on time, but does depend on phase variable x that monotonically decays from 1 to 0 with a user-specified rate α_x:

$$\tau\dot{x} = -\alpha_x x \tag{2.16}$$

The equation 2.16 is often referred as canonical system. Note that for systems with more than one DoF, the trajectory is encoded with separate DMPs (eq. 2.14) for every DoF, with all DoF sharing the canonical system (eq. 2.16).

The DMP formulation offers a set of unique and attractive properties. First, thanks to the attractor dynamics, the DMPs are intrinsically robust against uncertainties and perturbations. Second, the learning parameters that encode the desired trajectory do not affect the stability and convergence properties of the system. Third, in addition to generalization to new initial and goal states, DMPs are capable of spatial and temporal scaling of learned trajectories. Moreover, the DMP formulation enables straightforward adaptation of trajectory via additional coupling terms (in Chapter 4, we explore this property to enforce a pre-defined set of constraints). Finally, DMPs present an efficient one-shot learning of trajectory from a single demonstration.

Chapter 3

Precision cutting of soft tissue using torque-based medium classification

Precision cutting of soft-tissue remains a challenging problem in robotics, due to the complex and unpredictable mechanical behaviour of tissue under manipulation. Here, we consider the challenge of cutting along the boundary between two soft mediums, a problem that is made extremely difficult due to visibility constraints, which means that the precise location of the cutting trajectory is typically unknown. This chapter introduces a novel strategy to address this task, using a probabilistic binary medium classifier trained using joint torque measurements, and a closed loop control law that relies on an error signal compactly encoded in the decision boundary of the classifier. We illustrate this on a grapefruit cutting task, successfully modulating a nominal trajectory fit using dynamic movement primitives to follow the boundary between grapefruit pulp and peel using torque-based medium classification. Results show that this control strategy is successful in 72% of attempts in contrast to control using a nominal trajectory, which only succeeds in 50% of attempts.

3.1 Introduction

The design of effective learning and adaptive control strategies for precision cutting remains an open problem in robotics [21, 82, 100]. This is particularly true for the case where cutting involves moving between two mediums, and where there is uncertainty in the location of these.

Cutting tasks of this form are regularly encountered in surgery, where tumour extraction is guided by well-established continuum differences between tumours and normal tissue [101, 102]. This chapter is motivated by wide local excision, a surgical procedure that aims to remove a tumour with a clear margin of healthy tissue around it.

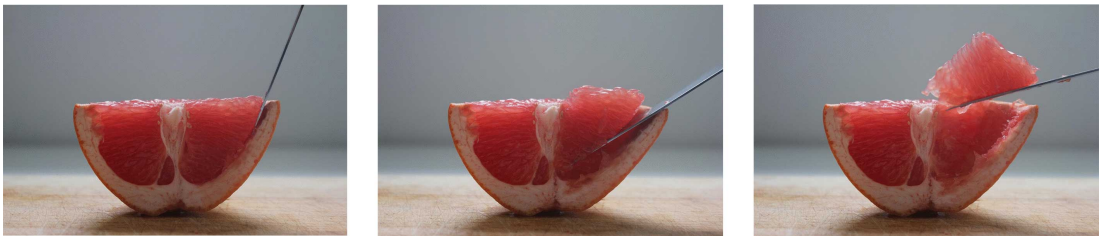

Figure 3.1: Scooping grapefruit with a regular paring knife.

At present, manipulation tasks like these are inconceivable for autonomous robots, for a variety of reasons. First, the constrained operational space of non-trivial geometry restricts an end-effector's maneuverability and is severely limited by visibility constraints. These visibility constraints are a particular challenge, and human surgeons often rely strongly on haptic feedback for cutting, using tactile tissue differences to guide procedures instead of vision. In addition, this task is highly variable and uncertain, due to the unpredictable behaviour of deformable tissue and varied tumour shapes. Finally, and most importantly, this contact-rich task is characterised by safety constraints imposed on the region of operation and allowable applied forces. It is therefore critical to keep an end-effector inside a desired region while executing the task.

In this chapter, we move towards addressing the challenge of autonomous cutting with visibility constraints by 1) employing probabilistic inference to identify the boundary between two mediums using torque sensing, and 2) using the medium classification probability as an error signal for online, closed-loop movement adaptation. As a testbed, we consider fruit processing, and study the task of scooping a grapefruit segment out of the membrane with a regular paring knife (see Fig. 3.1). This manipulation task shares several important characteristics with the surgery problem described above, including the complex geometry of the task space, the need for contact-rich manipulation in a deformable environment and the presence of two mediums with different material properties. Precision food processing is itself an industrially useful skill, and the ability to extract fruit portions without damaging food products is particularly valuable.

A key feature of the grapefruit testbed is an implicit task requirement to keep the knife inside the intermediate region between the peel and pulp boundary, such that most of the pulpy segment is extracted without the knife getting stuck in the peel, or too much grapefruit being left on the membrane. Since the exact shape and location of this boundary curve is unknown, it must be inferred during task execution. The

key insight for the approach proposed in this work comes from observing grapefruit scooping when executed by human. It is clear that humans do not rely on an accurate geometrical model of the fruit, but instead apply a general scooping movement that is continued until *it stops feeling right* (i.e. when the knife starts progressively entering the peel). In these cases, the movement is either adjusted, or completely restarted using a different insertion angle. Our hypothesis is thus that cutting occurs using a rough nominal trajectory that is modulated by torque feedback resulting from the differing tissue characteristics of the two mediums being separated.

This chapter introduces a novel framework to accomplish tasks of this form. Here, we use Dynamic Movement Primitives (DMPs) to learn a nominal scooping motion using kinesthetic demonstration. However, due to the variations in grapefruit's shape and its mechanical properties, we show that generalisation of the learned movement primitive is inadequate. We therefore propose a control scheme in which the corrections to the DMP trajectory reflect the probability of knife being inserted into either of the two mediums. In this formulation, the point of highest uncertainty in this belief (probability of 0.5) serves as a proxy for the desired region of operation (i.e. the boundary between the pulp and peel). This probability is estimated at each time step of task execution by classifying torque readings from the joints of robot arm. We use a logistic regression classifier trained to disambiguate the mediums on a dataset of multiple task executions to demonstrate the feasibility of this method.

3.2 Related work

There is a substantial amount of research on the use of the force feedback in robotic manipulation tasks. However, most work is focused on rigid object manipulation. For example, there is extensive research on the use of force data in the areas of robot door opening [103–105], grasping [104,106,107] and object identification [108,109], where task dynamics are relatively well understood and many mature techniques for motion planning and control are readily available. Unfortunately, many of these techniques are not applicable to the manipulation of deformable objects.

A particularly representative deformable object manipulation task involves food cutting, for example fruits or cheese. This process has time-varying nonlinear dynamics that are extremely difficult to describe analytically [110], although attempts have been made [21, 49, 83]. As a result, learning-based techniques have been proposed to

address this challenge. Lenz et. al [80] use deep learning techniques to model food cutting tasks and further use these in a model-predictive control scheme. Here, robot controls are optimised in real time with respect to the constructed cost function, which penalises the height of the knife and its deviation from a sawing range, thus forcing a cutting movement. This approach was verified on a variety of food objects, such as lemons and potatoes, and showed its ability to adapt to both intra-class and time-varying variations in the physical properties of the objects.

A similar approach to learning the predictive model is described by Tian et. al [111], where the authors demonstrated tactile servoing using high dimensional tactile sensor data. Another use of learning in the latent space is presented in the work of Gemici and Saxena [112], which is concerned with robotic handling of food objects, e.g. grasping or piercing. Here, latent features of objects were learned from force data collected during the manipulation and then used to classify the objects for manipulation planning.

Many manipulation tasks, e.g. scooping, involve nontrivial kinematic trajectories that can be learned from demonstration. In [99], the authors proposed a general framework (Dynamic Movement Primitives, or DMPs) for encoding complex movements as a parameterised policy. This framework, when coupled with feedback enables reactive movement adaptations [106, 113]. Appropriate feedback models that extend the DMP formulation can be learned, e.g. from human demonstrations [114] or through reinforcement learning [115]. Particularly relevant work is presented in [104], where the desired force and torque profile required for successful execution of compliant manipulation tasks was learned through trial and error reinforcement learning. This path integral method successfully optimizes the policy with respect to user-defined smooth cost function over the observable states of the manipulated object.

In this chapter, we focus on the task where the cost function cannot be easily specified and states of the manipulated object are hidden. Although the method described in [104] is applicable to boolean cost functions [116], this approach can only ever learn a globally optimal force profile. In contrast, we present an alternative problem formulation (local adaptation) that does not involve global optimization and allows us to adapt to variations in fruit geometry while cutting. We use a predictive model of the expected sensor trace, that is based on the statistics of multiple task executions. This approach is similar to [117], where the statistics of sensor measurements from the successful task executions were used to construct a predictive model for online failure detection. We apply a similar method to model the region of operation (pulp or peel in

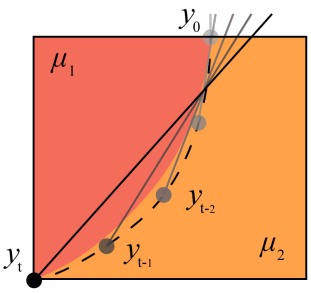

Figure 3.2: Medium separation by following nominal trajectory. μ_1 and μ_2 are stiffness parameters of mediums, y_0 is initial pose and y_t is trajectory of the knife. The dashed line represents the nominal path for tip of the knife.

our grapefruit example) using torque sensor readings. However, a key contribution of this chapter is the use of this classification scheme to perform boundary identification for cutting with visibility constraints, through the introduction of a control scheme for movement adaptation based on the estimated probability of being in a given medium.

3.3 Problem formulation

As discussed previously, this chapter focuses on the task of precision-cutting between two mediums. As our primary interest lies in the development of an adaptive control framework, we do not consider the use of any task-specific cutting equipment or machinery, and instead focus on cutting using a standard kitchen knife. In addition, we allow control of the initial insertion position, and thus, we manually initialise the starting position of the knife.

The task described above can be formulated in a 2D task space. Consider two elastic mediums with different stiffness (μ_1 and μ_2), separated by a curved boundary (see Fig. 3.2). Assume a strong prior over the stiffness and boundary curve (dashed line) is available, but no exact parameters are known. The objective is to steer the tip of the knife along the true boundary such that separation of mediums is maximised, while avoiding excessive deformations imposed to either of mediums by the blade. Since the exact curve of the boundary is unknown, the open loop execution of the prescribed path (based on a prior belief over the curve of the boundary) runs the risk of inserting the knife into the peel (in our grapefruit example), thereby severely restricting the blade's maneuverability.

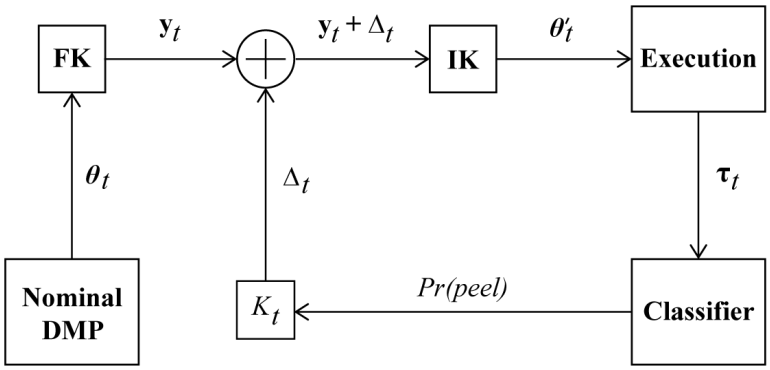

Figure 3.3: Overview of the proposed control scheme.

3.4 Cutting using uncertainty feedback

We address the challenge above using a learning strategy where the desired operational region is compactly encoded in the decision boundary of a probabilistic binary medium classifier. Here, the estimated likelihood of sensor readings associated with either medium guides the movement execution in the form of online trajectory correction. In summary, we 1) use the DMP framework to encode a nominal scooping trajectory, 2) learn probabilistic classification of sensor readings associated with operation in either mediums, and 3) construct a control scheme that corrects the nominal scooping trajectory according to the estimated posterior distribution over either medium, as illustrated in Fig. 3.3.

Here, $\boldsymbol{\theta}_t$ denotes the nominal joint trajectory, $\boldsymbol{\theta}_t^{'}$ the corrected joint trajectory, and $\mathbf{y}_t$ represents the nominal Cartesian trajectory. Δ_t denotes the correction term applied to the Cartesian trajectory, K_t is a gain matrix, $\boldsymbol{\tau}_t$ refers to the sensed torque readings at time step t, and $Pr(peel)$ is the probability of the knife being inserted into the peel. FK and IK are Forward and Inverse Kinematics transformations for the robot arm. Note that gain matrix K_t is time dependent, as the correction direction depends on the position along the nominal trajectory at time t. We briefly discuss each element in the control framework below.

3.4.1 Nominal trajectory modelling using DMPs

In the proposed framework, a nominal scooping trajectory is captured by kinesthetically guiding the robot arm and recording the joint angles. In this study, we encoded the recorded joint trajectory using the DMP model (see section 2.4.2); however, it should be noted that the nominal trajectory can be modelled using any other imitation learning strategy [88].

In our method, at each time step t we add a local correction Δ_t to the current point on the Cartesian path y_t of nominal DMP (see Fig. 3.3). The correction term Δ_t is given by

$$\Delta_t = K_t \Big[Pr(m,t) - 0.5 \Big] \tag{3.1}$$

where K_t is time-varying[1] positive definite gain matrix that defines the sensitivity of task variables and $Pr(m,t) \in [0,1]$ is the probability of the knife being in the medium m at time step t. Note, that the desired region of operation at each time step t lies at the boundary between two mediums, where the probability $Pr(m)$ is assumed to be equal to 0.5.

Thus, our proposed uncertainty-driven control law can be formulated generally as

$$y'_t = y_t + K_t \Big[Pr(m,t) - 0.5 \Big] \tag{3.2}$$

where y'_t is the corrected version of the nominal trajectory y_t.

3.4.2 Logistic regression

In this work, we use logistic regression to model the probability of being in a given medium. In this approach, model parameters w are fit by maximizing the probability of the data under a linear logistic model:

$$\mathscr{L}(w) = \prod_{i=1}^{N} p(y_i | x_i, w) \tag{3.3}$$

where $\mathscr{L}$ is the likelihood, N is the number of training samples of torque readings, y_i is the label (e.g. “Peel” or “Pulp”) of the i th example of torque data, x_i is a vector of torque readings of the i-th example and w is a model parameter.

1. This allow us to vary the direction and amplitude of modulation throughout task execution.

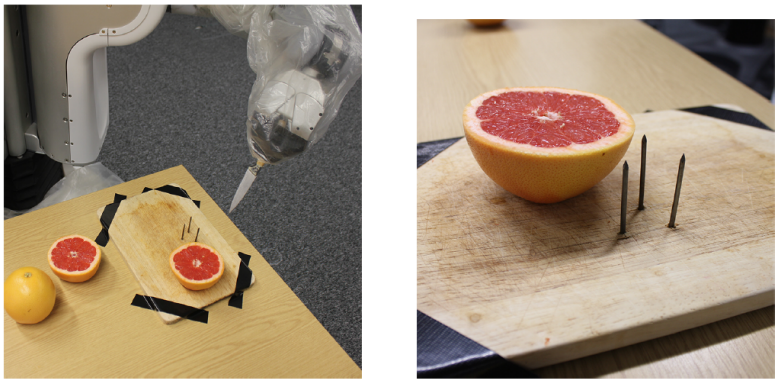

Figure 3.4: Images of securing a grapefruit to a chopping board using nails.

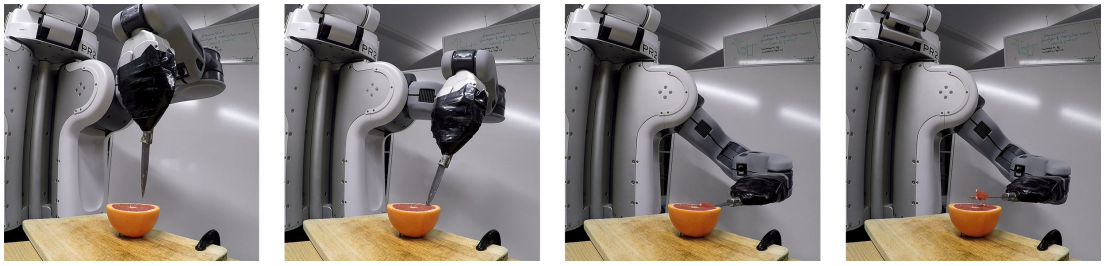

Figure 3.5: Images of the PR2 robot scooping a grapefruit.

If the cost function $J(w)$ is defined as the negative log-likelihood of labels y, then the above expression is equivalent to minimizing:

$$J(w) = \sum_{i=1}^{N} \Big[-y_i \, log(\sigma(w^T x_i)) - (1 - y_i) \, log(1 - \sigma(w^T x_i) \Big] \tag{3.4}$$

where $\sigma(\cdot)$ is a sigmoid function and labels $y \in \{0, 1\}$.

In order to discourage the optimizer from overfitting to the training data, the cost function can include an additional regularization term that penalizes extreme weight coefficients, e.g. $\frac{\lambda}{2}||w||^2$, where λ denotes the regularization strength.

3.4.3 Experimental setup

All experiments were conducted using a 7 degree-of-freedom PR2 robot arm. The PR2 arm is counterbalanced and highly compliant, and is well-suited for kinesthetic demonstrations of flexible and fluid movements. The remaining components of the experimental setup consisted of a chopping board clamped to the table, a halved grapefruit fixed to the chopping board (as shown in Fig. 3.4), and a regular paring knife secured at the gripper (see Fig. 3.5). For registering the torques experienced at the joints of the arm we used standard PR2 joint effort readings (a joint torque estimate based on the joint motor current).

3.4.4 Evaluation of nominal DMP

The learned scooping DMP was evaluated on the 10 randomly chosen segments. Before each trial, a segment was pre-cut along the segment radii and the pose of the knife was manually adjusted, such that the knife begins insertion directly at the pulp/peel interface (as shown in Fig. 3.5, left). Successful task execution implies the complete extraction of the undamaged segment without the knife getting stuck in the peel.

The results of the trials agreed with original expectations, with only 2 successful task executions out of total 10. In 7 of the failed trials, the knife entered the peel and the execution was aborted. Moreover, an instance of tearing apart the segment during the scooping was registered. As anticipated, the main difficulty of the task was avoiding the knife's insertion into the peel, where further knife maneuverability became limited.

3.5 Learning the boundary region using sensed torque

3.5.1 Dataset

The learned DMP was used to accumulate joint torque readings associated with successful (cut through the flesh) and failed task executions (cut into the peel). These traces of torque measurements were analysed and further used for training the logistic regression model to estimate the probability of the knife's deviation from the desired region of operation, i.e. the boundary between pulp and peel, where task executions

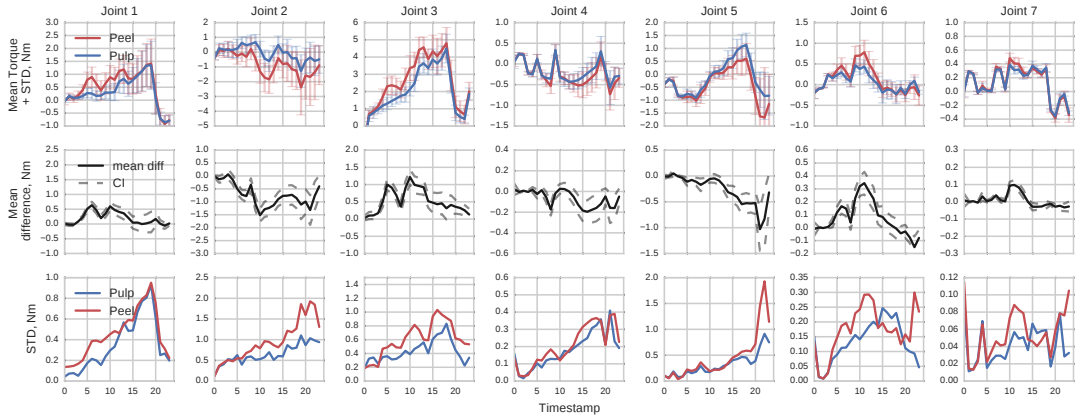

Figure 3.6: Summary statistics for collected torque data. Note: the most dominant joints in the used DMP are joints 1, 2 and 3.

succeed. We used the learned DMP and experimental setup described in the previous section. The criteria for a successful trial remained unchanged from the preliminary evaluation of the DMP. A total of 111 scooping trials were conducted using a number of grapefruit, of which 55 trials were successful and 56 trials failed.

The nominal trajectory comprised 24 segments, at which a single snapshot of torque readings was taken. Thus the recorded data consisted of 24 time-indexed 7-dimensional vectors. Fig. 3.6 shows the descriptive statistics of the collected data.

3.5.2 Classification

The dataset of 111 trials was randomized and split into 90 sensor traces allocated for training and validation and 21 traces held out for testing. The training and validation dataset consisted of 44 examples of “Pulp” torque traces and 46 examples of “Peel”. As discussed, each trace contained of 24 time-indexed samples of torque reading for each of the 7 joints. Thus, in total the training and validation dataset contained 1,056 and 1,104 individual examples of “Pulp” and “Peel” torque readings, respectively. The classifier’s input comprised of an 8-dimensional vector (7 torque readings for each of the joints, plus the time index). The objective of the classification task was to estimate the probability of the measurement being taken inside of either medium given the current torque measurements. In our approach, a desirable property of a classifier is to be robust to the outliers and to handle the ambiguous inputs by reporting the

appropriate levels of uncertainty (i.e. to avoid being overconfident). We used a logistic regression model, which we validated using the K-fold cross-validation technique with 10 folds. Thus, each fold used 81 examples for training and 9 examples for validation. The validation and test results are given in Table 3.1.

It should be noted that the modelling approach has an inherently noisy training process. Since all of the 24 torque samples in the sensor trace share the same label defined by the task outcome, all the intermediate phenomena are disregarded. For instance, if knife was closely following the desired boundary region throughout most of the execution but got stuck in the peel at the very end, all of the 24 torque readings would be labeled as "Peel". In addition, a substantial amount of failed trials were collected, where a stuck knife escaped the peel towards the end of the task execution. The torque profile of such trials show strong similarity to the rest of failed trials, with the exception of torque readings at final time steps where knife escapes the peel. However, the ability to capture the uncertainty demonstrated by Logistic Regression model alleviates this issue (see Fig. 3.7), and in some respects this training process forces a more conservative probabilistic model. It is important to note that despite misclassifying some intermediate samples, the trained model does not commit to any extreme beliefs over the mediums (see Fig. 3.8), unless the test input is strongly representative of a given class (see Fig. 3.7, top row). Finally, in the case of ambiguous test inputs (i.e. where torque levels of the input trace appear uncharacteristic for a given label), the model demonstrates desirable levels of uncertainty, which is extremely important given the fact that we seek to use this for feedback control.

Table 3.1: Logistic regression model evaluation

	Validation		**Test**	
	Predicted Peel	Predicted Pulp	Predicted Peel	Predicted Pulp
Actual Peel	673	431	174	66
Actual Pulp	306	750	65	199
Sensitivity	0.61		0.73	
Specificity	0.71		0.75	
Misclas. rate	34%		26%	

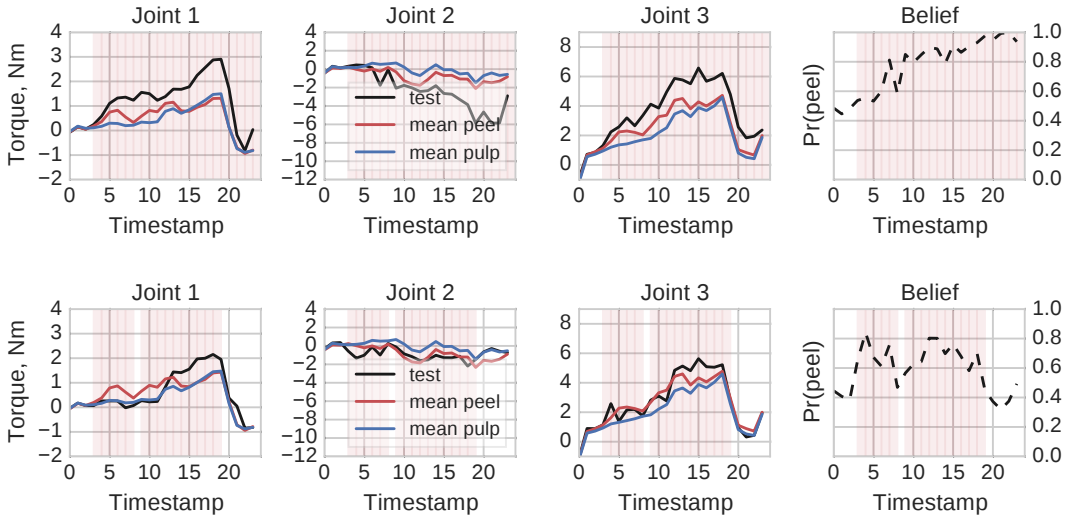

Figure 3.7: Medium classification based on torque readings. Top row: the test trace (black solid line) is a clear example of a trial where the knife got stuck inside the peel. Bottom row: the test trace represents one of the failed trials where the knife enters the peel at the beginning of task execution but escapes towards the end (time step $t = 19$). The red background signifies the classifier's binary decision (red denotes the peel) at time step t. Note, that only 3 most dominant joints are displayed.

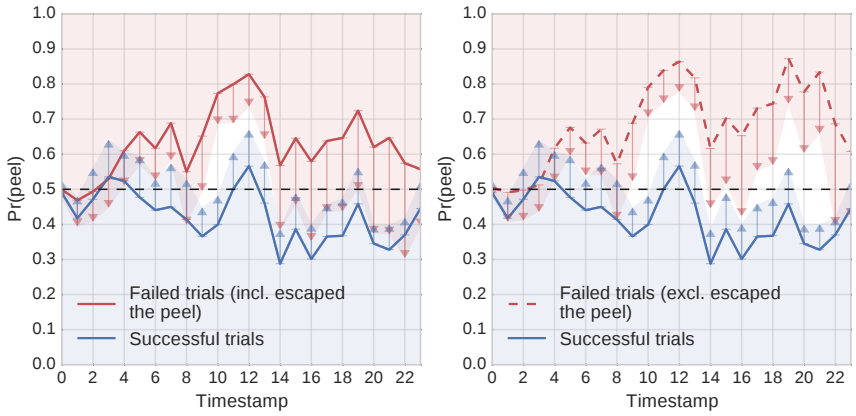

Figure 3.8: Average and standard deviation of *Pr(peel)* belief for successful and failed open loop executions. Throughout the successful trial, on average, our trained medium classifier demonstrates a belief close to or below the desired 0.5 probability score. For the failed trials, where knife gets stuck into the peel, the average belief is above 0.5 probability score. Note: Failed trials, where the knife escaped the peel during the task execution, skew the average belief towards the desired probability score of 0.5 (left); the average belief appears more confident when such trials are excluded (right).

3.6 Online DMP adaptation

We reused the nominal DMP and trained classifier from the previous section and constructed the closed-loop control scheme as shown in Fig. 3.3. First, the nominal joint trajectory associated with learned DMP is transformed into the end-effector's trajectory in the Cartesian space, where all the required corrections are relatively straightforward. As discussed previously, we use the probability of the knife being inserted into the peel for deriving the required motion corrections. We used a simple motion correction scheme for experimentation, in which the first half of the scooping motion (where the most dominant movement component involves pushing the knife downwards) is modulated towards the center of the grapefruit. In the second half of the movement (where the knife slides under the segment), the motion was modulated upwards. Thus, in each of the cases, the knife deviates from the peel region towards the pulp region, when the estimated probability of peel increases. In both cases we used a hand-tuned gain of 0.01 (i.e. 100% probability of peel would translate the movement 10mm away from the nominal trajectory in the prescribed direction). It should be noted that more complex schemes can be applied, e.g. modulation in the direction of the normal to the side of the knife.

For this experiment we conducted 50 trials of grapefruit scooping on randomly chosen segments in a total of 12 different grapefruits. As in the previous section, a successful trial required the complete extraction of an intact segment without the knife getting stuck inside the peel. The results are provided in the Table 3.2. 36 out of 50 trials achieved successful task completion. In all of the 14 failed attempts, the knife entered the peel at the start of the cut and propagated deeply before the peel could be classified. In these cases, the movement corrections towards the center of the grapefruit failed, as the knife could not tear the peel with the side of the blade. Perhaps, in such cases the DMP can be reversed and re-applied with estimated corrections, as the classifier successfully reflected the event of knife being stuck in the peel.

Table 3.2: Method comparison

Control scheme	**Open-loop**	**Closed-loop**
Successful trials	55	36
Failed trials	56	14
Success rate	50%	72%

In the successful trials, the knife visibly responded to the local increase in the resistance throughout the movement execution. It was clear that online movement adaptation improved the segment separation. Since the modulated motion acts in the direction approximately orthogonal to the boundary, it introduces a tearing effect. Similar tearing motions can be observed in human executed grapefruit scooping, where a knife's reorientation lowers movement resistance by tearing through the fibers.

It should also be noted that the described task is strongly dependent on several factors. First, the nominal DMP plays an important role in the success of the task. Since the proposed method relies on torque readings gathered from the execution of the nominal trajectory, a poorly chosen movement can severely impair the medium classification. Second, the experiment is highly sensitive to the sharpness of the knife, as well as the position of the grapefruit relative to the initial pose of the knife. Nevertheless, these experiments highlight the promise of uncertainty driven cutting between mediums with differing stiffness properties.

3.7 Conclusions and next steps

We present an uncertainty-driven feedback control law and demonstrate its performance on the task of grapefruit segmentation. This task is selected because it resembles a common surgical procedure where a hard tumour is extracted from soft tissue, and physical material properties are used to guide human surgeons.

Automating tasks of this form is extremely challenging, as it requires cutting along an uncertain boundary, subject to visibility constraints.

Our experiments show that a simple movement correction scheme, where the movement of a robot arm is modulated along a single Cartesian axis in response to the probability of being in a given medium, significantly improves cutting performance. Although the presented task could be reduced to a planar problem (as discussed in section 3.3), the provided analysis considers a broader case of robot motion in 3D Cartesian space. In the next chapter, we will show how the approach described here can be extended to learn other cutting movements, including those subject to non-holonomic constraints.

Chapter 4

Non-holonomic DMPs using the Udwadia-Kalaba method

Dynamic Movement Primitives (DMPs) offer great versatility for encoding, generating and adapting complex end-effector trajectories. DMPs are also very well suited to learning manipulation skills from human demonstration. However, the reactive nature of DMPs restricts their applicability for tool use and object manipulation tasks involving non-holonomic constraints, such as scalpel cutting or catheter steering. In this chapter, we extend the Cartesian space DMP formulation by adding a coupling term that enforces a pre-defined set of non-holonomic constraints. We obtain the closed-form expression for the constraint forcing term using the Udwadia-Kalaba method. This approach offers a clean and practical solution for *guaranteed* constraint satisfaction at run-time. Further, the proposed analytical form of the constraint forcing term enables efficient trajectory optimization subject to constraints. We demonstrate the usefulness of this approach by showing how we can learn robotic cutting skills from human demonstration.

4.1 Introduction

A characteristic feature of many cutting tasks is the prevalence of non-holonomic constraints (Fig. 4.1). When cutting, it is often unnatural and undesirable to move the blade along the lateral direction, as it can induce uncontrolled material tearing. Instead, one aims at neat and predictable material separation [48]. If we aim to automate the performance of these tasks by a robot, then that autonomous system must account for these types of constraints, especially when precision plays a crucial role such as in surgery.

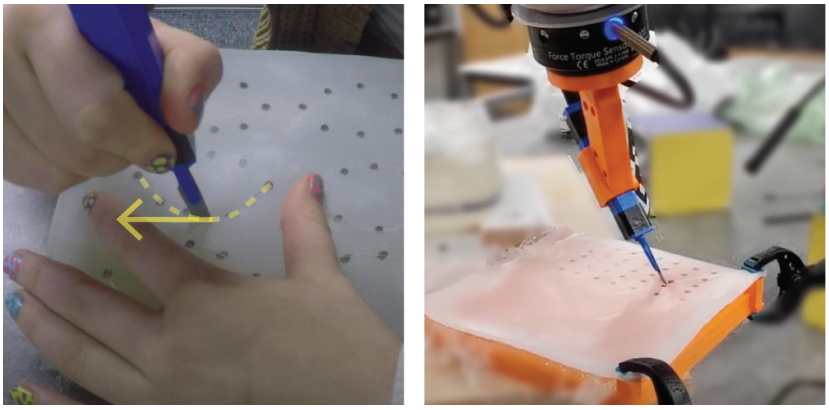

Figure 4.1: Cutting tasks feature non-holonomic constraints that must be considered in automation: a pure lateral movement of the blade is undesired, as it causes unnecessary stress to the material and risks tearing, an unwanted mode of fracture propagation.

Non-holonomic systems attract substantial research interest, especially in the area of mobile robotics [118, 119]. More recently, it has been extensively studied in the context of steerable needles [120, 121], as well as in robotic cutting [122], particularly in the tele-operation setting [44, 123, 124]. In this chapter, we present a novel strategy for *Learning* from Demonstration (LfD) the task of robotic cutting subject to these non-holonomic constraints. As in the previous chapter, we focus on the use of Dynamical Movement Primitives (DMPs) as a representation of the policy. DMPs provide an intuitive way to encode complex kinematic trajectories. The underlying attractor dynamics of DMPs ensure the system's convergence to a goal state, and offer robustness against uncertainties and perturbations. However, the reactive nature of DMPs makes it difficult to encode behaviours subject to non-holonomic constraints. In contrast to systems only under holonomic constraints, such as contact constraints, the non-holonomic systems are path-dependent; therefore, a reactive movement adaptation requires global trajectory re-planning for a non-holonomic system to reach the goal state. Besides, it is challenging to capture faithful end-effector orientation with kinesthetic demonstrations. As a result, this further complicates the application of LfD to non-holonomic systems.

The main contribution of this chapter is a scheme to alleviate these issues, demonstrated in the cutting task, wherein we first encode the pose trajectory using two uncoupled DMPs, a position DMP and an orientation DMP. Generally, such decomposition is not strictly necessary [125]; however, as will become clear in the following sections, it is convenient to structure the motion using distinct position and orientation

components. Next, we extend the position DMP with an analytically-derived coupling term that imposes a non-holonomic equality constraint. As will be discussed in the following sections, the addition of this analytical forcing term establishes the constrained equation of motion, by modifying the acceleration of an unconstrained system at runtime. As a result, if the demonstrated pose trajectory violates the constraint, the Non-holonomic DMP rollout will deviate from the demonstrated position trajectory. Finally, we demonstrate how these deviations from the demonstrated position trajectory can be minimised while satisfying the non-holonomic constraint.

While many researchers have proposed various coupling terms for tackling different types of constraints in DMPs [126], e.g. obstacle [127] or surface [128] constraints, in this chapter, we focus on the "rolling-without-slipping" constraint [129], which is relevant in many practical applications such as cutting or catheter steering. Moreover, we derive a closed-form expression for the constraint coupling term using the Udwadia-Kalaba (UK) theory [130], for the first time in the DMP literature to the best of our knowledge.

4.2 Background

4.2.1 Orientation DMPs

The original DMP formulation described in the 2.4.2 section is best suited to encoding trajectories in joint angle space or position trajectories in Cartesian space. However, orientations belong to the special orthogonal group SO(3), which is a manifold. Thus, the above formulation is not suitable for use in traditional integration schemes that assume flat Euclidean spaces. [106] introduced the orientation DMP, which was later extended by [131] to preserve the SO(3) structure, and further improved by [132]. A formulation of orientation DMPs based on rotation matrix can be described as follows [131]:

$$\begin{aligned} \tau \dot{\boldsymbol{w}} &= \alpha_x(\beta_x \log(\boldsymbol{R}_g \boldsymbol{R}^T) - \boldsymbol{w}) + \boldsymbol{f}_q(s), \\ \tau \dot{\boldsymbol{R}} &= [\boldsymbol{w}]\boldsymbol{R}, \end{aligned} \tag{4.1}$$

where $\dot{\boldsymbol{w}} \in \mathbb{R}^3$ is angular acceleration vector, $\boldsymbol{w} \in \mathbb{R}^3$ is angular velocity vector, $[\boldsymbol{w}] \in \mathbb{R}^{3\times 3}$ is a skew-symmetric matrix of $\boldsymbol{w}$ and $\boldsymbol{f}_q(s) \in \mathbb{R}^3$ is nonlinear forcing function for orientation. $\boldsymbol{R}$ and $\boldsymbol{R}_g \in \mathrm{SO}(3)$ are rotation matrices that uniquely specify the current and goal orientations, respectively.

Assuming constant angular velocity $\boldsymbol{w}$, the above differential equation on $\mathrm{SO}(3)$ has the following closed-form solution:

$$\boldsymbol{R} = \exp([\boldsymbol{w}]\Delta t)\boldsymbol{R}_0, \tag{4.2}$$

where $\boldsymbol{R}_0$ is the initial orientation and $\exp(\cdot)$ is the exponential mapping given by the Rodrigues' formula:

$$\exp([\boldsymbol{w}]\Delta t) = \boldsymbol{I}_3 + \frac{\sin(\theta)}{\theta}[\boldsymbol{w}] + \frac{1-\cos(\theta)}{\theta^2}[\boldsymbol{w}]^2, \tag{4.3}$$

where $\theta = ||\boldsymbol{w}||$.

Its inverse, the logarithmic map from eq. (4.1), is defined as the following:

$$\begin{gathered}\log(\boldsymbol{R}) = \begin{cases}[0,0,0]^T, & \boldsymbol{R} = \boldsymbol{I}_3 \\ \boldsymbol{w} = \theta\boldsymbol{n}, & \text{otherwise.}\end{cases} \\ \theta = \arccos\left(\frac{\mathrm{trace}(\boldsymbol{R})-1}{2}\right), \quad \boldsymbol{n} = \frac{1}{2\sin(\theta)}\begin{bmatrix} r_{32}-r_{23} \\ r_{13}-r_{31} \\ r_{21}-r_{12}\end{bmatrix}.\end{gathered} \tag{4.4}$$

4.2.2 Constrained dynamics

In this section, we describe constrained dynamical systems with an explicit form of constraint forces. First, let us consider an unconstrained dynamical system described by configuration space $\mathscr{Q}$, which is an open subset of $\mathbb{R}^n$ with coordinates $\boldsymbol{\sigma} = [\sigma_1, ..., \sigma_n]^T$, as follows:

$$\boldsymbol{M}(\boldsymbol{\sigma})\ddot{\boldsymbol{\sigma}} = \boldsymbol{f}_{\mathrm{unc}}(\boldsymbol{\sigma}, \dot{\boldsymbol{\sigma}}), \tag{4.5}$$

where $\boldsymbol{M} \in \mathbb{R}^{n\times n}$ is the mass inertia matrix, and $\ddot{\boldsymbol{\sigma}}$, $\dot{\boldsymbol{\sigma}}$ and $\boldsymbol{f}_{\mathrm{unc}}$ denote generalized unconstrained acceleration, velocity and known unconstrained forcing term, respectively.

The motion of the above system can be restricted by introducing a set of $m < n$ Pfaffian velocity constraints [133]:

$$\boldsymbol{\phi}_i^T(\boldsymbol{\sigma})\dot{\boldsymbol{\sigma}} = 0, \quad i = 1, \ldots, m, \tag{4.6}$$

where $\phi_i \in \mathbb{R}^n$ are linearly independent constraint vectors.

If there exist differentiable functions $g_i(\boldsymbol{\sigma}) : \mathbb{R}^n \mapsto \mathbb{R}$, such that $\phi_i(\boldsymbol{\sigma}) = \partial g_i(\boldsymbol{\sigma})/\partial \boldsymbol{\sigma}$ for $i = 1, \ldots, m$, then velocity constraints of the form (4.6) can be reduced to the following constraints on the configuration space:

$$g_i(\boldsymbol{\sigma}) = 0, \quad i = 1, \ldots, m. \tag{4.7}$$

The above constraints restrict the configuration space of the unconstrained system to $n - m$ dimensional submanifold and are called *holonomic*. Constraints, that cannot be reduced to the form of (4.7) are called *non-holonomic*. Note that non-holonomic constraints restrict the instantaneous motion but not the configuration space.

The dynamics of the constrained system can be viewed as a system subjected to constraint forces $\boldsymbol{f}_{\text{con}}$, as follows [129]:

$$\begin{aligned} \boldsymbol{M}(\boldsymbol{\sigma})\ddot{\boldsymbol{\sigma}} &= \boldsymbol{f}_{\text{unc}}(\boldsymbol{\sigma}, \dot{\boldsymbol{\sigma}}) + \boldsymbol{f}_{\text{con}} \\ &= \boldsymbol{f}_{\text{unc}}(\boldsymbol{\sigma}, \dot{\boldsymbol{\sigma}}) + \boldsymbol{A}^T(\boldsymbol{\sigma})\boldsymbol{\lambda} \end{aligned} \tag{4.8}$$

where $\boldsymbol{A} = [\phi_1^T(\boldsymbol{\sigma}) \ \ldots \ \phi_m^T(\boldsymbol{\sigma})]^T \in \mathbb{R}^{m \times n}$ and $\boldsymbol{\lambda} \in \mathbb{R}^m$ is a vector of Lagrange multipliers.

The computation of the Lagrange multipliers $\boldsymbol{\lambda}$ is often a difficult task. Except for the simplest cases, the Lagrange multipliers need to be solved numerically. Moreover, the Lagrange multiplier is generally not unique for a given constraint force [134].

The UK theory, proposed by Firdaus Udwadia and Robert Kalaba in 1992, offers great advantages over many alternative methods for modeling constrained dynamical systems. In comparison to other methods (such as Hamel's equations [135], Kane's formulation [136], Poincarè's equations [137] or Gibbs–Appell method [138]), that rely on Lagrange multipliers or other auxiliary variables, the UK method provides a concise and clear explicit expression of the constraint forces based on the generalized coordinates alone. In the context of constrained DMPs, this significantly simplifies the computation of the constraint accelerations.

In the next section, we present a description of the Udwadia-Kalaba method for deriving an analytical expression of constraint forces $\boldsymbol{f}_{\text{con}}$, which greatly simplifies the task.

4.2.3 Udwadia-Kalaba method

Consider an unconstrained dynamical system (4.5) subjected to a set of m equality constraints (4.6), which could include holonomic or non-holonomic (or a combination of both). A key step in the UK approach is the transformation of the constraint equations into the following second order form:

$$\boldsymbol{A}(\boldsymbol{\sigma})\ddot{\boldsymbol{\sigma}} = \boldsymbol{b}(\boldsymbol{\sigma}, \dot{\boldsymbol{\sigma}}), \tag{4.9}$$

where $\boldsymbol{b} \in \mathbb{R}^m$ is known generalized velocity vector.

In the case of Pfaffian constraints (4.6), this is achieved by taking the time derivative (under the assumption that it is sufficiently smooth), as follows:

$$\frac{\mathrm{d}}{\mathrm{d}t}\boldsymbol{\phi}_i^T(\boldsymbol{\sigma})\dot{\boldsymbol{\sigma}} = \sum_{j=1}^{n} a_{ij}(\boldsymbol{\sigma})\ddot{\sigma}_j + \sum_{j=1}^{n} \frac{\mathrm{d}}{\mathrm{d}t} a_{ij}(\boldsymbol{\sigma})\dot{\sigma}_j = 0, \tag{4.10}$$

where $a_{ij}(\boldsymbol{\sigma})$ is the j element of the constraint vector $\boldsymbol{\phi}_i(\boldsymbol{\sigma})$, and

$$\frac{\mathrm{d}}{\mathrm{d}t} a_{ij}(\boldsymbol{\sigma}) = \sum_{k=1}^{n} \frac{\partial a_{ij}(\boldsymbol{\sigma})}{\partial \sigma_k}\dot{\sigma}_k. \tag{4.11}$$

Let us define b_i as following:

$$b_i(\boldsymbol{\sigma}, \dot{\boldsymbol{\sigma}}) := -\sum_{j=1}^{n} \frac{\mathrm{d}}{\mathrm{d}t} a_{ij}(\boldsymbol{\sigma})\dot{\sigma}_j. \tag{4.12}$$

Finally, we can express eq. (4.10) in the following form:

$$\sum_{j=1}^{n} a_{ij}(\boldsymbol{\sigma})\ddot{\sigma}_j = b_i(\boldsymbol{\sigma}, \dot{\boldsymbol{\sigma}}), \quad i = 1, \ldots, m. \tag{4.13}$$

Note, that the above equation is equivalent to the second order form (4.9).

The main result of the UK approach is the explicit expression of motion under constraints (4.9) as:

$$\boldsymbol{M}(\boldsymbol{\sigma})\ddot{\boldsymbol{\sigma}} = \boldsymbol{f}_{\mathrm{unc}}(\boldsymbol{\sigma}, \dot{\boldsymbol{\sigma}}) + \boldsymbol{f}_{\mathrm{con}}(\boldsymbol{\sigma}, \dot{\boldsymbol{\sigma}}), \tag{4.14}$$

where $\boldsymbol{f}_{\mathrm{con}} \in \mathbb{R}^n$ denotes the constraint forcing term, whose closed-form is provided by the following equation:

$$\boldsymbol{f}_{\text{con}} = \boldsymbol{M}^{\frac{1}{2}}(\boldsymbol{A}\boldsymbol{M}^{-\frac{1}{2}})^{+}(\boldsymbol{b} - \boldsymbol{A}\boldsymbol{f}_{\text{unc}}), \tag{4.15}$$

Here, superscript $^{+}$ indicates the Moore-Penrose pseudoinverse.

It should be noted, that the UK formulation of constrained dynamics assumes that the constraint is satisfied by the initial condition.

4.3 Non-holonomic DMPs

4.3.1 UK-based coupling term for enforcing non-holonomic constraint

Consider a non-holonomic constraint of the following form:

$$\boldsymbol{c}^T \dot{\boldsymbol{p}} = 0, \tag{4.16}$$

where $\boldsymbol{c}$ and $\dot{\boldsymbol{p}} \in \mathbb{R}^3$ are the constraint and instantaneous velocity vectors, respectively, both expressed in the world frame.

We can turn the above constraint equation into second-order form by differentiating it with respect to time:

$$\dot{\boldsymbol{c}}^T \dot{\boldsymbol{p}} + \boldsymbol{c}^T \ddot{\boldsymbol{p}} = 0, \tag{4.17}$$

where $\ddot{\boldsymbol{p}} \in \mathbb{R}^3$ is vector of instantaneous unconstrained acceleration.

By comparison with (4.9), we can identify the generalized velocity vector as $\boldsymbol{b} = -\dot{\boldsymbol{c}}^T \dot{\boldsymbol{p}}$. Assuming the identity mass inertia matrix, i.e. $\boldsymbol{M} = \boldsymbol{I}_n$, we can express the non-holonomic constraint forces using the UK formula (4.15):

$$\boldsymbol{f}_{\text{con}} = \boldsymbol{c}^{+}(\boldsymbol{b} - \boldsymbol{c}^T \ddot{\boldsymbol{p}}) \tag{4.18}$$

The above analytical expression for constraint forces $\boldsymbol{f}_{\text{con}}$ can be incorporated as an additional DMP coupling term. The encoding of the end-effector's pose under constraint (4.16) can be achieved by composition of constrained DMP for position and an unconstrained DMP for orientation, as follows:

$$\begin{aligned}\tau\ddot{\boldsymbol{p}}_{\text{con}} &= \underbrace{\alpha_x(\beta_x(\boldsymbol{p}_g-\boldsymbol{p})-\tau\dot{\boldsymbol{p}})+\boldsymbol{f}_p(s)}_{\ddot{\boldsymbol{p}}} + \boldsymbol{f}_{\text{con}},\\ \tau\dot{\boldsymbol{w}} &= \alpha_x(\beta_x \log(\boldsymbol{R}_g\boldsymbol{R}^T)-\tau\boldsymbol{w})+\boldsymbol{f}_q(s),\end{aligned} \tag{4.19}$$

where $\ddot{\boldsymbol{p}}_{\text{con}} \in \mathbb{R}^3$ is constrained acceleration vector, $\boldsymbol{p}$ and $\boldsymbol{p}_g \in \mathbb{R}^3$ are current and goal position vectors, respectively.

As will become clear in the following section, the above equations are coupled via $\boldsymbol{f}_{\text{con}}$ term, which is a function of angular velocity $\boldsymbol{w}$.

The $\boldsymbol{f}_{\text{con}}$ term guarantees the satisfaction of the constraint eq. (4.16) by modifying the system's acceleration at run-time. In addition, the explicit expression for $\boldsymbol{f}_{\text{con}}$ enables efficient trajectory optimization for $\boldsymbol{f}_{\text{con}} = \boldsymbol{0}$, such that

- the constraint eq. (4.16) is satisfied,
- deviations from the demonstrated position trajectory are minimized.

In the following section, we show how the optimization of the orientation DMPs achieves the above objectives in learning autonomous cutting skills from a demonstration.

4.3.2 Learning cutting skills from demonstration

Consider learning scalpel cutting skills from demonstration using DMPs under the non-holonomic constraint, as described in the previous section. Fig. 4.2 (left) shows the local body-frame of the scalpel with respect to the world frame. Let's denote the coordinates of body-fixed frame as $(\hat{\boldsymbol{x}}_b, \hat{\boldsymbol{y}}_b, \hat{\boldsymbol{z}}_b)$, where $\hat{\boldsymbol{x}}_b = [1,0,0]^T$, $\hat{\boldsymbol{y}}_b = [0,1,0]^T$ and $\hat{\boldsymbol{z}}_b = [0,0,1]^T$. Let the rotation matrix describing the orientation of the body-fixed frame with respect to the world frame be denoted as $\boldsymbol{R}$. In this task, we want to prohibit the lateral motion of the scalpel, thus we define the constraint vector from the non-holonomic equation (4.16) as $\boldsymbol{c} = \boldsymbol{R}\hat{\boldsymbol{y}}_b$. Corresponding $\boldsymbol{b}$ vector from eq. (4.18) is therefore equal to $\boldsymbol{b} = -(\dot{\boldsymbol{R}}\hat{\boldsymbol{y}}_b)^T\dot{\boldsymbol{p}}$. Recall that $\dot{\boldsymbol{R}} = [\boldsymbol{w}]\boldsymbol{R}$, thus the constraint force vector $\boldsymbol{f}_{\text{con}}$ is a function of angular velocity $\boldsymbol{w}$. It is, therefore, possible to optimize the rotation for zero constraint forces, as described in the previous section. Solving for $\boldsymbol{f}_{\text{con}}(\boldsymbol{w}) = \boldsymbol{0}$ is a nonlinear problem, which can be approached numerically. The $\boldsymbol{w}$ solution can be found by minimizing the loss function $\mathscr{L}(\boldsymbol{w}) = ||\boldsymbol{f}_{\text{con}}(\boldsymbol{w})\|_2$.

4.4 Experiments

4.4.1 Numerical example

Here we provide a concise illustration of the proposed non-holonomic DMP formulation used to learn a cutting skill from demonstration. We assume that cutting is required along a desired curved contour on the XY plane. As before, we represent the cutting task with a kinematics model that prohibits lateral motion of the blade (the coordinate system of the scalpel is shown in Fig. 4.2, left). In this example, we apply the position trajectory that matches the desired cutting contour and devise an orientation trajectory that violates the constraint, as illustrated in Fig. 4.3A.

Fig. 4.2 compares the resulting trajectories of the regular DMP (solid lines), the DMP constrained by constraint coupling term $\boldsymbol{f}_{\text{con}}$ (dashed lines) and DMP with an optimized orientation for $\boldsymbol{f}_{\text{con}} = \mathbf{0}$ (dotted lines). As expected, the regular DMP closely follows the demonstration for both position and orientation components. Since the demonstrated pose trajectory violates the constraint, so does the regular DMP. The constrained DMP closely imitates the demonstrated unconstrained orientation trajectory. However, the system deviates from the desired position trajectory as the result of acting constraint forces $\boldsymbol{f}_{\text{con}}$. Finally, the DMP with optimized angular velocity $\boldsymbol{w}$ shows the adjustments in orientation trajectory (note the yaw angle) for maintaining zero constraint forces $\boldsymbol{f}_{\text{con}}$. As the result, the system follows the desired position trajectory without violating the constraint. Fig. 4.3 shows the corresponding poses of the scalpel in 3D.

In this example, the demonstration position trajectories were $x(t) = \sin^2(\pi t)$, $y(t) = \sin^3(\frac{1}{2}\pi t)$ and $z(t) = 0$ for all t. The orientation trajectories were generated with $\alpha(t) = 0$ for roll angle, $\beta(t) = \frac{\pi}{4}$ for pitch angle, and $\gamma(t) = \arctan2(x(t), y(t))$ for yaw angle. The number of radial basis functions in DMPs was set to 100, with $\tau = 1$, $\alpha_x = 25$, $\beta_x = 6.25$ and $\alpha_s = 1$. The DMPs were integrated using the Implicit Euler method, with time step $\Delta t = 0.001$s. For optimization, we used implementation of BFGS algorithm in SciPy [139]. The visualization of the scalpel trajectories in Fig. 4.3 was implemented using pytransform3d library [140]. The code for this example is available at `https://github.com/straizys/nonholonomic-dmp`.

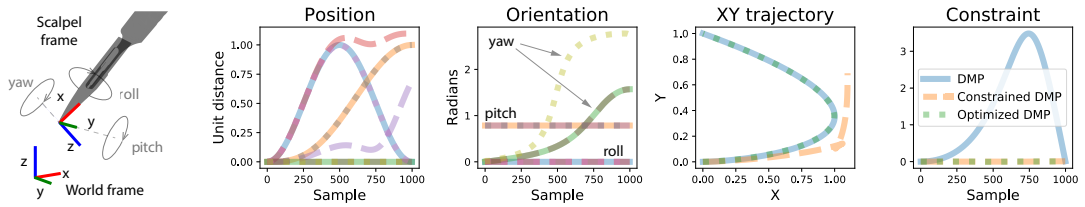

Figure 4.2: (Left) Scalpel frame. (Other) Regular DMP (solid lines) imitates the demonstrated cutting trajectory that closely follows the desired curved contour on the XY plane, but violates the constraint (equation 4.16). The DMP constrained by $\boldsymbol{f}_{\text{con}}$ term (dashed lines) satisfies the constraint and closely follows (unconstrained) orientation trajectory, but deviates from the (constrained) x and y trajectories. The DMP with optimized orientation (dotted lines) closely follows the desired position and orientation trajectories, and satisfies the constraint.

4.4.2 Learning elliptical excision from demonstration under non-holonomic constraints

In this experiment, we apply the proposed approach for learning non-holonomic DMPs from demonstration to the case of elliptical tissue excision (Fig. 4.1, left). The experimental setup consists of a tissue phantom and a cutting tool with a mounted 6DOF electromagnetic (EM) motion tracking sensor (Polhemus VIPER$^{\text{TM}}$ FT-Flatsided), as shown in Fig. 4.4. As suggested by Polhemus VIPER$^{\text{TM}}$ user manual, the sensor is positioned approximately 1 cm or more away from the conductive blade, to avoid EM distortions.

During the experiment, the demonstrator performed a series of eight elliptical excisions on the phantom. The pose trajectory of the sensor was captured at a fixed rate of 120 Hz and converted to a corresponding pose trajectory of the blade, as follows. We define the blade frame with respect to the sensor frame using following homogeneous transformation:

$$\boldsymbol{T}_{sb} = \begin{bmatrix} \boldsymbol{R}_{sb} & \boldsymbol{t}_{sb} \\ \boldsymbol{0}_{1\times 3} & 1 \end{bmatrix} = \begin{bmatrix} 1 & 0 & 0 & 5.2 \\ 0 & 1 & 0 & 0 \\ 0 & 0 & 1 & 1.3 \\ 0 & 0 & 0 & 1 \end{bmatrix}, \tag{4.20}$$

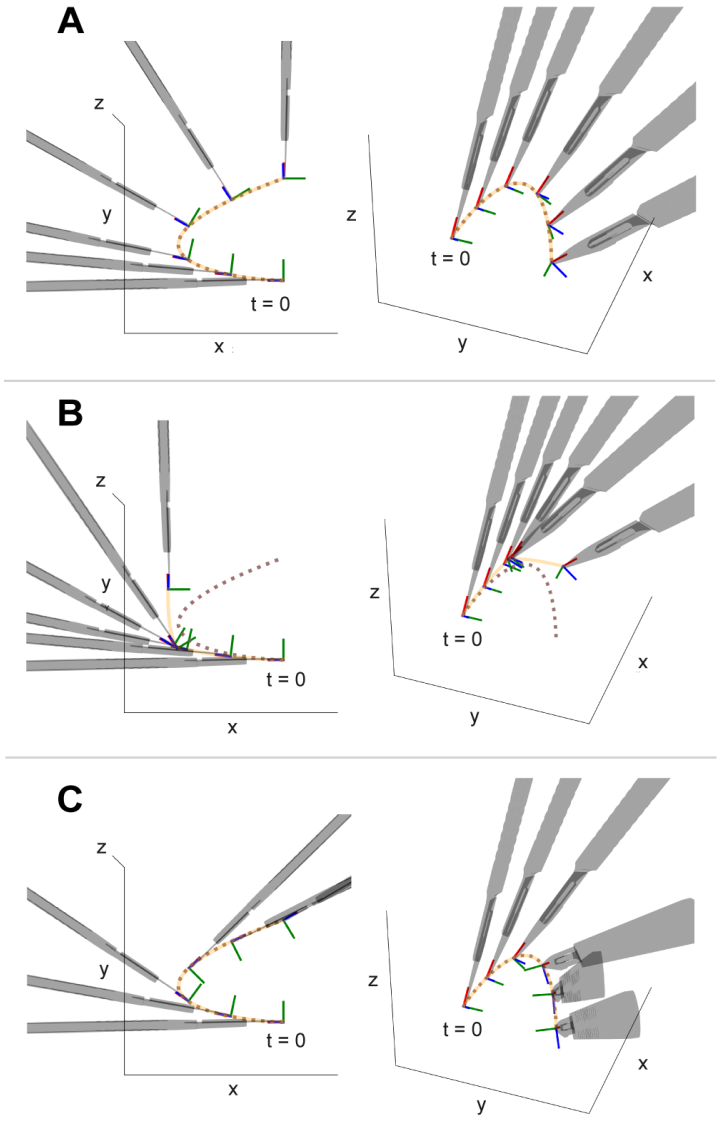

Figure 4.3: Snapshots of scalpel trajectories. **A** Demonstration that violates the non-holonomic constraint. Note, that blade moves in the prohibited lateral direction ($\hat{\boldsymbol{y}}_b$, green) towards the end of task execution. **B** DMP constrained by the coupling term $\boldsymbol{f}_{\text{con}}$. **C** DMP with optimized orientation for $\boldsymbol{f}_{\text{con}} = \boldsymbol{0}$. Note, that the optimized DMP closely follows the desired path on XY plane (marked by dotted line) and $\hat{\boldsymbol{y}}_b$ vector is normal to a contour tangent.

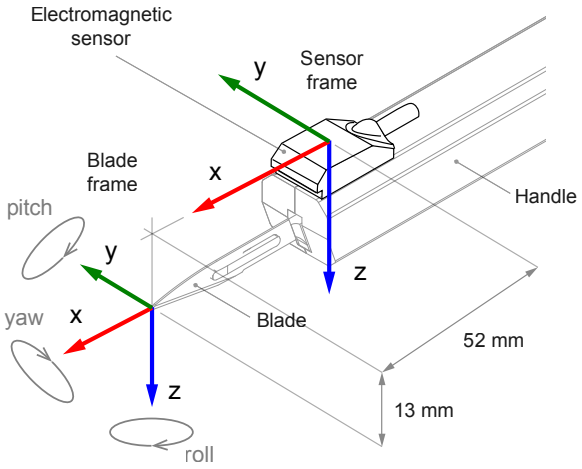

Figure 4.4: Schematic diagram of the cutting tool and sensor configuration, and the coordinate frames used in the experiment.

where $\boldsymbol{R}_{sb} \in \mathrm{SO}(3)$ is the rotation matrix representing the orientation of the blade frame in the sensor reference frame, and vector $\boldsymbol{t}_{sb} \in \mathbb{R}^3$ is the position of the blade frame with respect to the sensor frame, expressed in cm (see Fig. 4.4). The pose trajectory of the blade with respect to the world frame is then simply $\boldsymbol{T}_{wb}(t) = \boldsymbol{T}_{ws}(t)\boldsymbol{T}_{sb}$, where $\boldsymbol{T}_{ws}(t)$ is the time-varying homogeneous transformation representing the original pose trajectory of the sensor.

Eight segments of $\boldsymbol{T}_{wb}(t)$ trajectory corresponding to each elliptical excision were manually extracted. For each segment of the position trajectory, we subtracted the initial positions such that resultant XYZ trajectories start at the origin (i.e. relative to the initial positions of the blade). Finally, the time series were filtered using a 3rd-order Butterworth low-pass filter with a 4.8 Hz cut-off frequency (i.e. the passband is 1/25th of the 120 Hz sampling frequency).

As discussed in section 4.2.3, the UK method requires the initial condition to satisfy the constraint. We enforced this condition by projecting blade's initial velocity vector $\dot{\boldsymbol{p}}_0$ onto the XZ plane of the blade frame, as follows:

$$\dot{\boldsymbol{p}}_0' = \boldsymbol{P}(\boldsymbol{P}^T\boldsymbol{P})^{-1}\boldsymbol{P}^T\dot{\boldsymbol{p}}_0, \tag{4.21}$$

where $\dot{\boldsymbol{p}}_0'$ is the orthogonal projection of $\dot{\boldsymbol{p}}_0$ onto the plane defined by matrix $\boldsymbol{P} = [\boldsymbol{R}_{wb}\hat{\boldsymbol{x}}_b, \boldsymbol{R}_{wb}\hat{\boldsymbol{z}}_b]$. Here, $\boldsymbol{R}_{wb}$ is the rotation matrix representing blade's orientation with respect to the world frame, $\hat{\boldsymbol{x}}_b$ and $\hat{\boldsymbol{z}}_b$ are basis vectors of the blade frame, respectively.

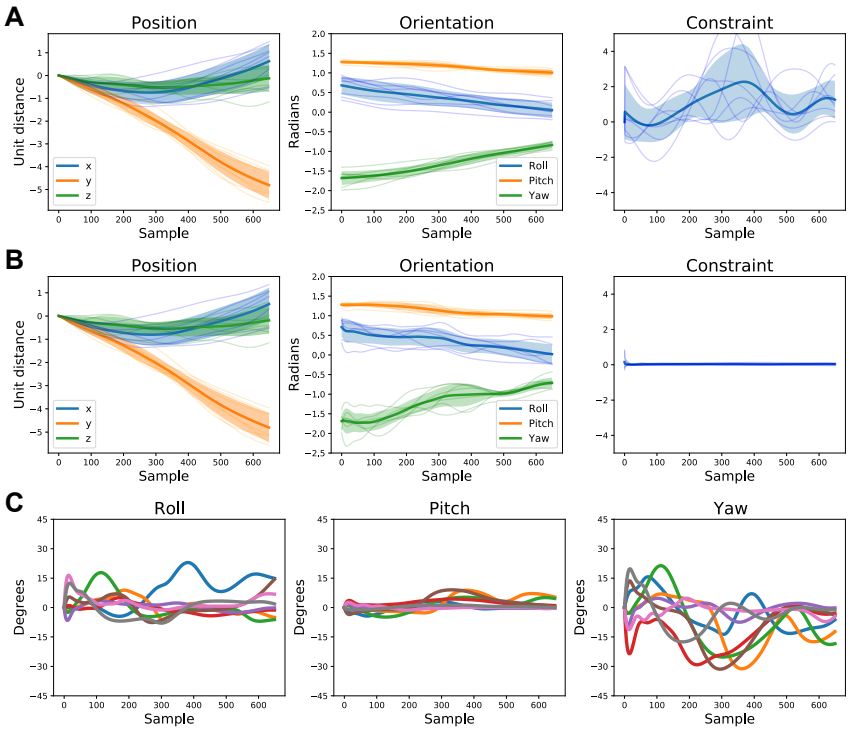

Figure 4.5: A Mean and standard deviation ($N = 8$) of blade trajectories in the elliptical excision task (individual trajectories are shown as thin semi-transparent lines). **B** Trained non-holonomic DMPs with orientation optimized for zero $\boldsymbol{f}_{\text{con}}$. **C** Adjustments to orientation trajectories of the blade. Note: Roll, pitch and yaw angles follow the extrinsic xyz Euler convention.

Finally, the obtained pose trajectories of the blade were used as demonstrations to train the proposed non-holonomic DMPs with optimized orientation (the DMP parameters, i.e. number of RBFs, τ, α_x, β_x and α_s, matched those in the numerical example above). Fig. 4.5A shows the distribution (mean and ± 1 standard deviation) of demonstrations. The evaluated constraint eq. (4.16) shows that, on average, the constraint violation peaks in the middle of task execution. Partially, this can be explained by the velocity variable $\dot{p}$, which reflects the natural acceleration-deceleration motion profile. Alternatively, this can be related to an awkward wrist configuration as the scalpel passes through the peak of the parabola (Fig. 4.1). Interestingly, the constraint curve highlights the systematic violation of the non-holonomic constraint, predominantly along the positive $\hat{\boldsymbol{y}}_b$ vector of the blade frame.

Fig. 4.5B shows the distribution of trained non-holonomic DMPs with optimized orientation. As expected, the position trajectories of the blade match the original demonstrations. However, the orientation trajectories show noticeable adjustments, in particular, to roll and yaw angles of rotation. Most importantly, the optimized non-holonomic

DMPs satisfy the constraint throughout the entire task execution. Fig. 4.5C shows the individual adjustments to roll, pitch and yaw rotations of the demonstrated pose trajectories. With an exception to an outlier (blue line), most orientation adjustments, as expected, are made to yaw rotation (reaching 30 degrees of angle correction).

4.5 Conclusions

In this chapter, we presented a novel approach to constrain DMPs through an additional coupling term deived from an analytical solution derived using the Udwadia-Kalaba method. This approach enables the incorporation of a wide range of equality constraints and their combination, such as holonomic, nonholonomic, scleronomic, rheonomic, catastatic and acatastatic, among others [130]. The analytical expression of the constraint forcing term allows evaluation of the constraint forces at run-time. Our experiments demonstrate the efficacy of the proposed method in learning robotic cutting skills from demonstrations under non-holonomic constraints.

The proposed approach does have several limitations, addressing which is a focus of our current and future work. Firstly, the described Udwadia-Kalaba method for the explicit expression of constraint forces applies to equality constraints only. Therefore, it excludes a highly relevant class of constraints, such as joint limits or collision avoidance. Secondly, the UK approach assumes that the constraint is satisfied by the initial condition already (which need not be the case when the task is initialised arbitrarily in practical applications). Finally, the described approach relies on run-time optimization to ensure that the constrained DMP follows the demonstration - this may need further computational treatment for efficient embedded and real-time implementation.

Chapter 5

Modelling elliptical excision forces to understand surgical skill

Manipulation of soft viscoelastic media is an essential feature of surgical skill. Understanding this skill quantitatively, through generative models, is essential both for accurate quantification of surgical skills, and for eventual automation in robotic platforms. We draw attention to the force modality as a key attribute for in-depth understanding and generative modelling of the manipulation skill, after highlighting some limitations of traditional techniques that relied only on descriptive statistics of force-based measurements. Our study is based on an elliptical excision procedure, a representative manipulation task involving soft viscoelastic material, and we use this to demonstrate that incision forces a) carry valuable information defining the skill, and b) contain revealing temporal structure that is relevant for skill interpretation, but inaccessible via conventional descriptive statistics. We propose a novel sensorised scalpel, along with a generative model, that allow capturing these temporal features and enable a vast array of downstream analysis and data collection, in applications spanning forensics, pathology and surgical skill quantification.

5.1 Introduction

Time and motion studies are frequently used to model, analyse and understand complex human manipulation tasks. This remains the case in the context of deformable tissue handling or manipulation, despite broad acknowledgement of the importance and role of forces in these tasks. For the most part, this reliance on kinematic sensing is due to a limited ability to measure forces at the tool-tissue interface. The ability to capture high-fidelity information at this interface is key to downstream applications and analysis across a broad range of research areas, including pathology, forensics and surgical skill understanding. In this chapter, we introduce a low-cost, easy-to-replicate tool and accompanying models that enable this.

In this chapter, we consider the surgical procedure of elliptical excision, in which skin incisions are made along a parabolic curve before tumour resection. The purpose of this procedure is to remove tumorous tissue within a specified margin. The removed specimen is then sent for examination that evaluates the margin of malignant cells, and in unfortunate cases concludes the risk of tumour recurrence.

As is the case for many important and practical manipulation tasks, the outcome and the quality of task execution directly depends on both the overall amplitude and the temporal characteristics of the applied forces. Throughout an incision, the non-dominant hand applies continuous tension to the tissues surrounding the cutting contour, while the dominant hand controls the scalpel's movement [141]. Successful tissue dissection implies the application of appropriate force levels [26] - sufficient for deliberate and controlled tissue separation, but not too excessive to avoid iatrogenic tissue damage [142]. In addition, cutting forces are continuously modulated by active tissue tensioning and the scalpel's nonholonomic-like movement through viscoelastic tissues.

Despite the central role that forces play in surgery [143–145], the analysis of these remains a novel area of research [26], as the majority of developed methods for analysing these skills are vision-based and mainly focus on instrument motion [30, 146–148]. However, there is some evidence that force-based performance metrics can be superior to metrics that are based on movement alone [29]. In addition, recent studies indicate that tool-tissue interaction forces can uniquely reflect a surgeon's competence [28]. Interestingly, studies show lack of correlation between tool-tissue

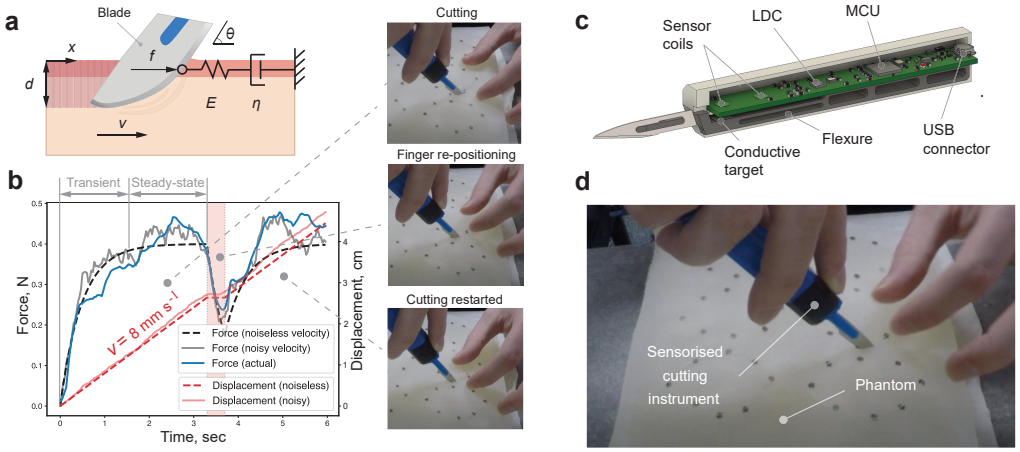

Figure 5.1: Overview of the proposed elliptical excision force model, sensorised scalpel and the experiment. **a** Maxwell model of the cutting process, where x denotes blade's displacement, d is depth of excision, θ is angle of blade insertion, v is blade's velocity, E and η are spring and damping coefficients, respectively. (Pink and ivory colours denote the outer and inner layers of tissue phantom, respectively. The shaded area corresponds to the phantom region separated by the blade.) **b** Generated incision force and blade displacement profiles versus the actual incision force measurement (blue). ($E = 1$ N cm^{-1}, $\eta = 0.5$ N s cm^{-1}, $v \in [0, 8]$ mm s^{-1} with standard deviation of 0.35 mm s^{-1}). **c** Concept design of the sensorised scalpel (here LDC is Inductance-to-Digital converter, MCU is Micro-controller Unit and USB is Universal Serial Bus). **d** The experiment: 12 medical students and two professional surgeons were asked to perform a series of 12 elliptical excisions on a tissue phantom.

forces and motion parameters [149]. Moreover, unlike motion parameters [150, 151], force parameters show no correlation with the execution time of surgical tasks [152, 153]. The above body of evidence indicates that the force modality may offer distinct information that is largely ignored by time and motion studies.

When force sensing is employed, the descriptive statistics applied by most studies disregard the temporal structure of force measurements under stationarity assumptions. This assumption is highly unrealistic for tasks like elliptical excision, where viscoelastic properties of tissues and a set of distinct phases of task execution cause the forces to exhibit strong time-dependent behaviour (Fig. 5.1a, b). Here, we propose and use a generative model of elliptical excision forces to encode the behavioural characteristics of the task execution. In our method, we extend the switching dynamics of a Markov model [154, 155] with a latent continuous dynamical system that captures the viscoelastic properties of scalpel-tissue interaction [156, 157]. Our proposed

elliptical excision force model captures the following components of the observed behaviour: 1) the step-like force profile with distinct transient and steady-state phases, 2) the amplitude and envelope of the force profile, characterised by the upper and the lower force boundaries, 3) the variation of the force magnitude in both transient and steady-state phases, and 4) the smoothness of task execution flow, characterised by the frequency of interruptions due to discrete events of tissue re-tensioning or finger re-positioning.

In this chapter we show that a) these components can compactly describe the execution of elliptical excisions, b) our generative model offers greater insight into analysis of skill when compared to descriptive statistics, and c) the model can quantify the subjective evaluation of excision skills and enable the comparison of expert assessors with differing implicit assessment criteria. In order to apply this model to investigate scalpel cutting skills [16, 158, 159] in an elliptical excision task, we first developed a low-cost sensorised scalpel and an easy-to-replicate multilayered skin-mimicking phantom (Fig. 5.1c, d). We then collected a dataset of 12 incision force profiles from 12 medical students, with video recordings of these incisions evaluated by surgical experts, followed by performance analysis using traditional force-based descriptive statistics. Finally, we contrasted this approach with our generative model and found our model superior to descriptive statistics in terms of its ability to analyze the surgical skill and the implicit criteria employed by experts during evaluation.

To summarize, the core findings of this chapter are as follows:

- Force sensing at the tool-tissue interface enables detailed analysis of manipulation tasks and surgical skill quantification that can be aligned with expert evaluation criteria.
- Commonly considered descriptive statistics that fail to account for non-stationarity are severely limited here, and force-based analysis of manipulation tasks requires a model that explicitly decomposes observations into amplitude and temporal components.

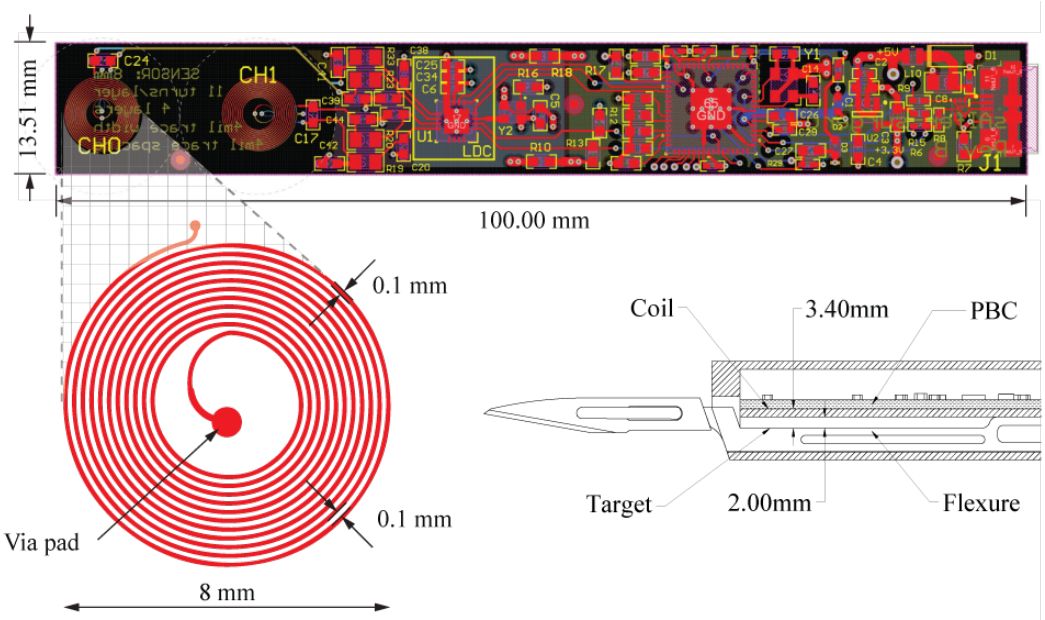

Figure 5.2: (*Top*) PCB layout design of the prototype. (*Bottom left*) Schematic of the planar 8.6 μH inductor: 8 mm diameter, 11 turns per each of four layers, 0.1 mm trace width and 0.1 mm spacing. (*Bottom right*) Schematic of sensor coil and target placement (uniaxial force sensor variant).

5.2 Sensorised cutting instrument

We constructed a uniaxial force sensor based on Texas Instrument's LDC1612 inductance-to-digital converter (or LDC) and a 3D printed flexible element. The LDC provides reliable position measurements at submicron resolution [160], which in combination with a flexible element with a known stress-strain characteristic, enables the construction of displacement-based force sensors. The LDC measures the distance between a conductive target and an inductive coil using the resonant sensing principle. The inductive coil in parallel with the capacitor forms a resonant circuit in which the alternating current flowing through the inductor generates an alternating magnetic field. As a result of Faraday's law, the alternating magnetic field induces eddy currents on the surface of the conductive target as a function of the target displacement. As per Lenz's law, these eddy currents create an opposing magnetic field that reduces the nominal inductance of the resonant circuit, and hence, increases the resonant frequency. The LDC measures this frequency shift and thus provides information about the target's displacement with respect to the inductor. By fixing the target to the free end of the flexure with a known stress-strain characteristic, a displacement measurement can be transformed into a force measurement.

The designed cutting tool consists of two key components, 1) a printed circuit board with an inductive coil, and 2) a flexure with a conductive target. The schematic for the uniaxial force sensor is shown in Fig. 5.2. The inductor is implemented as a circular planar coil of 8 mm diameter. In the rest configuration of the flexure, the effective 8.6 μH inductor (in parallel with 330 pF capacitor) focuses the alternating magnetic of 2.985 MHz frequency into the conductive target located 3.4 mm below. In our design, we used 10 mm square aluminium film of 0.2 mm thickness. The displacement range of the target is restricted to 1.6 mm, with a minimum distance to the inductor of 1.8 mm. When the flexure is at its maximum displacement configuration, the resonant frequency shifts from 2.985 MHz to 3.025 MHz (40 kHz shift, 1.3 % of the nominal resonance at zero displacement). According to [161], the maximum effective resolution achievable with the given frequency variation is 14-15 bits. The dimensions of the printed circuit board are 100 mm x 13.5 mm. The 4-layer board incorporates differential sensor coils, the LDC1612 inductance-to-digital converter, an MSP430F5528 microcontroller, power supply circuitry and a USB connector. The microcontroller configures the LDC via the I2C interface, implements USB Communication Device Class, processes and streams sensor data to a host computer.

The displacement is established by a one-piece 3D printed flexure, in which the free end displaces the conductive target under the presence of external force. As with any displacement-based force sensor, one of the main challenges is to maximize the stiffness of the flexure, while achieving the desired sensitivity. 3D printing provides a relatively easy way of experimenting with various design parameters, such as stiffness, strength, and geometry, as well as printing process parameters, such as material, printing orientation, etc. Importantly, 3D printing facilitates accessibility and reproducibility of the design, while maintaining a cost-effective development process.

In this study, we use a blade flexure with design parameters shown in Fig. 5.2. The flexure was 3D printed with an Ultimaker 3 Extended printer using PLA thermoplastic, 0.2 mm layer height, 20 % infill (triangle pattern) and 0.4 mm nozzle diameter. The extruder temperature was set to 205 C, the travel speed was set to 70 mm per second and the perimeter layers were set to 3. The printing was done at room temperature controlled in a range between 19 and 21 ℃. With these settings, the printed element was approximately 50 microns wider in XY direction.

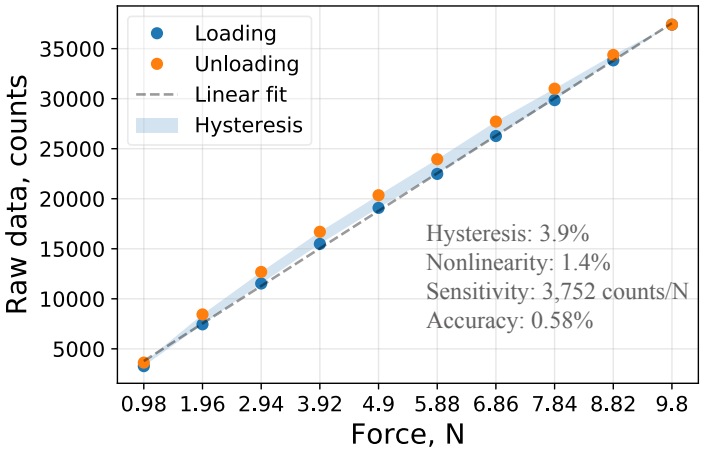

Figure 5.3: Results for the incremental loading test.

Fig. 5.3 shows the results of the incremental load test. During the test, a fully assembled device was incrementally loaded by ten 100 g calibrated weights (i.e. from 0.98 N to 9.8 N). The load was applied at the midpoint of the blade interface. The hysteresis (defined as the maximum difference between loading and unloading samples relative to the full-scale output) is 3.9%. The dotted line on the graph represents the linear least squares fit to the loading curve. The maximum deviation from the linear fit (non-linearity) is 1.4% of the full-scale output and the sensitivity of the sensor is 3,752 counts per newton. Finally, the measured accuracy (maximum standard deviation of sensor output at the maximum measured load and relative to the maximum measured load, i.e. to 9.8 N) is 0.58%.

The above characterisation data is based on the single assembled unit (with $N = 10$ samples for each data point). The exact characteristics are expected to differ from unit to unit, especially in the case of manual unit assembly. The dominant sources of variance are the placement of PCB and flexure inside the enclosure (determine the nominal distance between the sensor and the target), and mechanical properties of the 3D-printed flexure (determine dynamic characteristics, such as hysteresis).

5.3 Elliptical excision force model

The incision forces show temporal features that can characterize the cutting behaviour. We propose a generative model that captures these features in the force profiles and enables the disentanglement of skill from incision force measurements.

Fig. 5.1a shows the approximate model of the task of cutting a viscoelastic phantom as a continuous blade's movement through a Maxwell body. In the context of this approximation, the Maxwell model [162] relates the actual incision force $f(t)$ to a "virtual" velocity of the blade $\dot{x}(t)$, as follows:

$$\eta\dot{x}(t) = f(t) + \frac{\eta}{E}\dot{f}(t) \tag{5.1}$$

where $\dot{f}(t)$ is the time derivative of the force, and η and E are the Maxwell model's damping and spring coefficients, respectively.

By taking the Laplace transform of equation (5.1) and rearranging the terms, we obtain the transfer function $G(s)$, which relates a virtual blade's displacement $X(s)$ and the actual force $F(s)$, as follows:

$$G(s) = \frac{F(s)}{X(s)} = \frac{\eta s}{\frac{\eta}{E}s + 1} \tag{5.2}$$

The above transfer function indicates that the model exhibits high-pass characteristics in the force response to the displacement input. This predicts an exponential decay of force with a time constant $\frac{\eta}{E}$, as a response to a unit step displacement. Importantly, this also predicts a step-like response in the force to a ramp-like displacement input, and therefore, the observed cutting force profiles can be described as a response to a continuous virtual scalpel displacement $x(t)$ at a constant velocity. As such, this model represents an elliptical excision process as a virtual hybrid system with K linear regimes, in which the blade velocity $\dot{x}(t) = v_k$ is feedback-regulated by means of switching between the discrete regimes $v_1, ..., v_K$. In this work, we show that such formulation can bring a greater insight into the analysis of surgical skill when compared to the descriptive statistics approach more commonly applied in this area. In the next section, we focus on the problem of inferring the parameters of our model from force measurements.

5.3.1 Excision as a Switching Linear Dynamical System

The switching linear dynamical system [163–168] is an example of a broader class of hybrid system, in which globally nonlinear dynamics are approximated by a series of linear systems. In the generative model of a switching linear dynamical system, the switching between each of its K linear regimes is described by a discrete hidden state variable $s_t \in \{1, ..., K\}$. The evolution of s_t is characterized by $K \times K$ transition matrix $\mathbf{Q}$ that captures the probabilities of state transitions, i.e. $P(s_t|s_{t-1})$. The continuous hidden state vector $\mathbf{z}_t \in \mathbb{R}^D$ evolves according to a $D \times D$ dynamics matrix $\mathbf{A}$, and the observation vector $\mathbf{y}_t \in \mathbb{R}^L$ is generated according to an $L \times D$ observation matrix $\mathbf{C}$, as follows:

$$\mathbf{z}_t = \mathbf{A}^{(k)}\mathbf{z}_{t-1} + \mathbf{w}_t^{(k)}, \tag{5.3}$$

$$\mathbf{y}_t = \mathbf{C}^{(k)}\mathbf{z}_t + \mathbf{v}_t^{(k)}. \tag{5.4}$$

where $\mathbf{A}^{(k)}$ and $\mathbf{C}^{(k)}$ are associated with a regime $s_t = k$, and $\mathbf{w}_t^{(k)}$ and $\mathbf{v}_t^{(k)}$ are the disturbance and observation noise, respectively.

We model the elliptical excision process with two discrete linear regimes, $k \in \{L, U\}$. Each regime corresponds to a constant virtual velocity of the blade, and satisfies $v_L < v_U$ (we call L — a lower regime, and U — an upper regime). For each of these linear regimes, we model the uncertainty in the constant velocity as $\tilde{v}_k \sim \mathcal{N}\left(v_k, \sigma_k^2\right)$, where σ_k^2 is the variance of the velocity noise in the regime k. The continuous hidden state vector $\mathbf{z}_t = \begin{bmatrix} g_t \\ x_t \\ 1 \end{bmatrix}$, comprises g_t and x_t, the latent cutting force and virtual displacement of the blade at time step t, respectively. Since we only measure the cutting force, the observable y_t is a scalar that represents the force measurement at time step t. The continuous dynamics in the linear regime k is $\mathbf{A}^{(k)} = \begin{bmatrix} \alpha & \beta & 0 \\ 0 & 0 & \tilde{v}_k \\ 0 & 0 & 0 \end{bmatrix}$, where constants α and β define the displacement-to-force relationship of the Maxwell model, and are found by transforming the transfer function, equation (5.2), into the equivalent state space form. The observation matrix in the linear regime k is $\mathbf{C}^{(k)} = \begin{bmatrix} \gamma & \delta & 0 \end{bmatrix}$, where γ and δ are the observation constants from the state space representation of the Maxwell model's transfer function. In this work, we set the spring constant $E = 1$ N cm^{-1} and the damping coefficient $\eta = 0.5$ N s cm^{-1}, which yield $\alpha = -2$, $\beta = 1$,

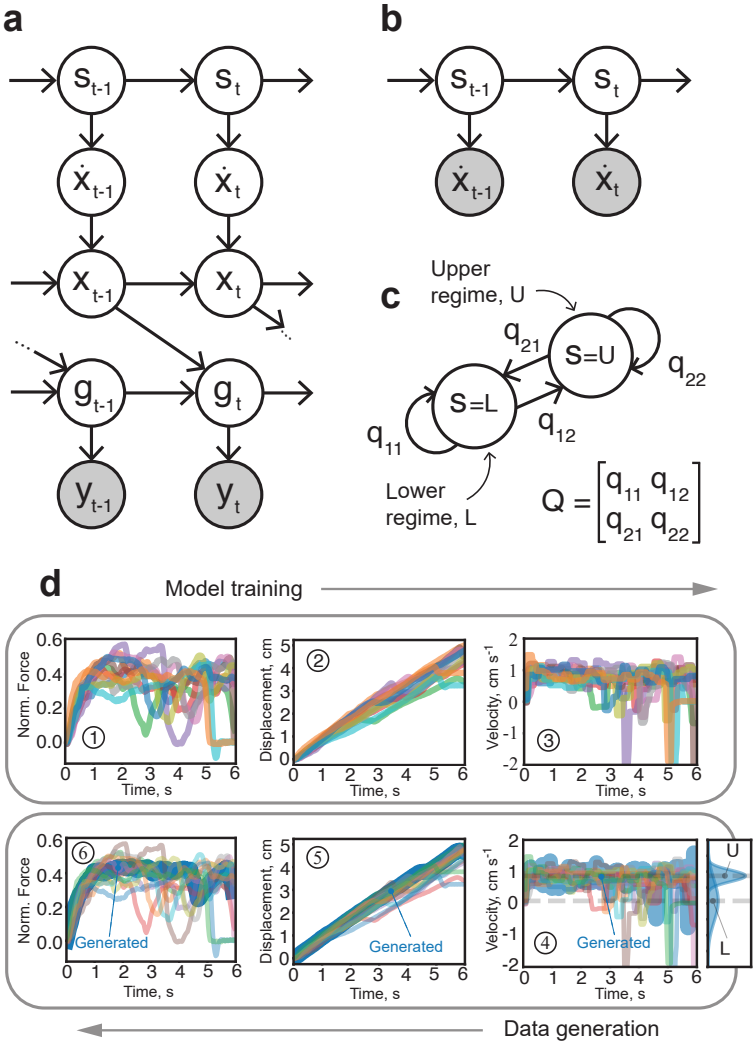

Figure 5.4: The elliptical excision force model. **a** A graphical model representation of the generative model, where s is a discrete state, $\dot{x}$ is blade's velocity, x is blade's displacement, g is excision force, y is force measurement and t is a time step. Shaded nodes represent the observed variables. **b** Hidden Markov Model (HMM) with a hidden discrete state s_t (the cutting regime at time step t), and an observable virtual velocity $\dot{x}_t$. **c** Markov chain with two cutting regimes defined by the transition matrix $\mathbf{Q}$. **d** Model fitting (1, 2 and 3) and data generation processes (4, 5 and 6). (1) Actual measurements of forces collected during the trials. (2) The virtual displacement derived from the force measurements using the Maxwell model. (3) The virtual velocity profiles (finite differences of the displacement profiles) are used to train the HMM. (4) The velocity sampled from the trained HMM (blue line). (5) and (6) The synthetic displacement and force (blue lines), generated by the model.

$\gamma = -2$ and $\delta = 1$ constant values. The parameters were chosen such that estimated displacements approximately match the actual distance travelled by the scalpel. Finally, given the uncertainty captured in the velocity $\tilde{v}_k$, we can further assume the disturbance-free dynamics ($\mathbf{w}_t^{(k)}$ is zero vector) and noise-free observations ($\mathrm{v}_t^{(k)} = 0$).

A graphical representation of this generative model is shown in Fig. 5.4a. There are several ways to infer the parameters of this class of models from observations. For example, the variational approach to learning in switching linear dynamical systems [167] approximates the posterior probabilities of the hidden states by optimizing evidence lower bound. In this study, we bypass the inference of discrete hidden states s_t by assuming that velocities $\dot{x}(t)$ are fully observable under the assumption of the Maxwell model (Fig. 5.4b). This turns the switching linear dynamical system inference into a problem of learning an HMM [169], fully characterized by transition probability matrix $\mathbf{Q}$ (Fig. 5.4c) and the emission probabilities defined by v_k and σ_k^2, for each of the linear regimes k. Given the virtual velocity profiles $\dot{x}(t)$, this model can be easily fit using the Expectation-Maximization algorithm [170].

Fig. 5.4d provides an overview of the model fitting process. First, the virtual displacement profiles are derived from the force measurements using the inverse of the transfer function, specified by Maxwell model parameters, equation (5.2). Then, the obtained displacement profiles are numerically differentiated for estimation of the virtual velocities $\dot{x}(t)$. Finally, the obtained virtual velocity profiles are used to fit an HMM with the Expectation-Maximization algorithm.

5.4 Experiment

Twelve right-handed medical students (four female and eight male) and two professional surgeons (both male) were recruited for this study. We labelled medical students with letters *A* to *L*, and surgeons with"*SA*" and "*SB*" labels (referring to surgeon A and B, respectively). Only three subjects (*A, C* and *D*) repeated the trials (two months after the first trial). Subjects that repeated the trials have a numeral in the label indicating the trial order (e.g. "*A2*" means the second trial of subject *A*). None of the student participants had any prior experience in surgical cutting tasks. The study was approved by the University of Edinburgh, School of Informatics, Informatics Ethics panel. All participants provided written informed consent to participate in this study.

The participants were asked to perform a series of 6 elliptical excisions on the phantom using the developed sensorised cutting tool (Fig. 5.1d). The use of a phantom model instead of animal tissues allowed us to minimise the force variability caused by the differences in tissue properties. Before each trial, a new blade (Swann-Morton No. 10)

was mounted to the cutting tool. After receiving the task instructions, participants were familiarized with the experimental setup, cutting tool ergonomics, phantom mechanical properties, etc. Next, each subject was asked to rehearse the described task using a dedicated sacrificial phantom. During the trials, the cutting forces that act on the blade in the direction of cutting were recorded at a fixed frequency of 30 Hz. Finally, at the end of the trials, each participant was asked to complete a post-study questionnaire.

5.4.1 Data measurement

Each participant performed 6 elliptical excisions as a part of the task, yielding 12 force profiles per trial (each excision consists of upper and lower cuts). The recorded profiles were time-aligned and cropped to a fixed length of 120 samples (i.e. 4 seconds duration). Finally, the samples were normalized to the maximum force value in the entire dataset.

Given the normalized force profiles $f(t)$ (Fig. 5.5a), the virtual displacement profiles $x(t)$ (Fig. 5.5b) were obtained by solving the differential equation for the Maxwell model, equation (5.1), as follows:

$$x(t) = \frac{f(t)}{E} + \frac{1}{\eta}\int_0^T f(t)\,\mathrm{d}t \tag{5.5}$$

where $f(t)$ is the corresponding force profile, T is the duration of the force profile, $\eta = 0.5$ N s cm^{-1} and $E = 1$ N cm^{-1} are Maxwell model's damping and spring coefficients, respectively. As discussed in section 5.3.1, these parameters were chosen such that estimated displacements approximately match the actual distance travelled by the scalpel.

The corresponding virtual velocity profiles $\dot{x}(t)$ (Fig. 5.5c) were obtained by approximating the time derivative of $x(t)$ using the finite difference method with a step size $\mathrm{d}t = 0.033$.

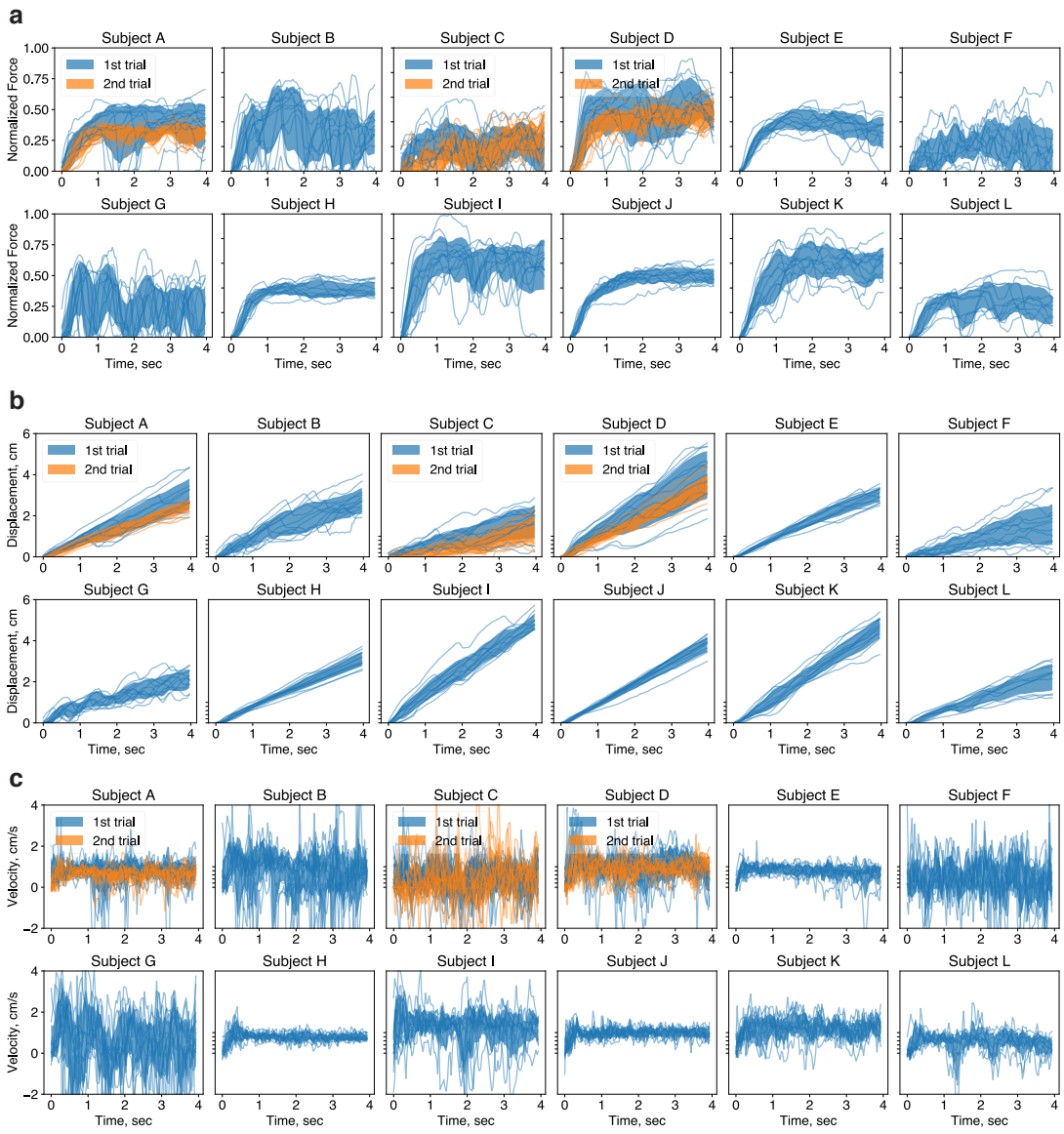

Figure 5.5: Data used for training the elliptical excision force model. **a** Normalised measurements of excision forces. **b** Blade's virtual displacement traces. **c** Blade's virtual velocity traces. Note: the individual traces are shown as semi-transparent lines and their distribution (one standard deviation) is shown as coloured areas. For each distribution, there is $N = 12$ independent trials.

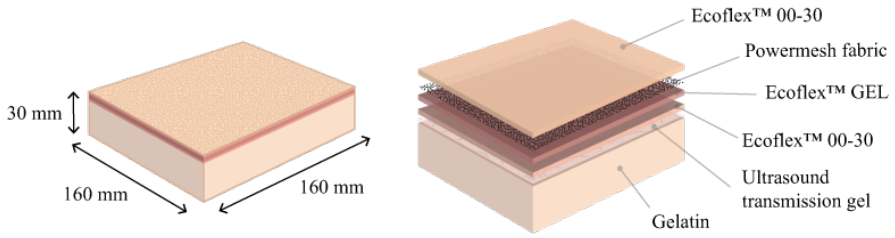

Figure 5.6: The design and construction of the multilayered skin-mimicking phantom.

5.4.2 Tissue phantom

Fig. 5.6 illustrates the design and material composition of the multilayered phantom used in this study. The design consists of a gelatin base that simulates the recoil of subcutaneous tissues, and a stack of three silicone layers that mimic the mechanical properties of human skin. The outer silicon layer is reinforced by pre-tensioned power mesh fabric that increases the tear strength of a sample. The gelatin base and silicon layers are coupled through a thin layer of an ultrasound gel. The fully assembled phantom has dimensions of 160 mm x 160 mm x 30 mm.

The fabrication of each phantom comprised of the following procedure. 64 g of gelatin powder (240 Bloom) was spread across 640 ml of cold water and left unstirred for 20 min, then simmered and stirred until fully dissolved. The liquid was poured into a 3D printed mould (160 mm x 160 mm x 25 mm volume container) wrapped in cellophane film and was left to solidify overnight in a refrigerator.

Next, a square piece of power mesh fabric (180 mm x 180 mm) was secured to the working surface under a slight amount of tension. 20 ml of two-part silicone rubber (Smooth-On Ecoflex^{TM} 00-30, shore hardness 30) was thoroughly mixed in a 1:1 ratio for 2 min and poured onto the center of stretched fabric in the series of three pours. The silicone-saturated mesh was then left for 45 min to cure. When cured, the next layer of 20 ml silicone (Smooth-On Ecoflex^{TM} GEL with shore hardness 000-35) was mixed and poured over. Finally, the second batch of 25 ml Smooth-On Ecoflex^{TM} 00-30 was poured over the pre-cured silicone layers. The silicone sample was left to cure for 4 hours.

The cured silicone sample was placed on the full set gelatin base with a power mesh-reinforced layer presenting the skin surface. The remaining edges of the power mesh are trimmed to match the surface area of the phantom. The fully assembled phantom is stored in a refrigerator prior to each experiment.

Table 5.1: Expert grading of phantom realism (from least to most realistic. H - Hard, S - Soft and VS - Very soft)

Realism	Bottom layer	Middle layer	Top layer	Comments
1	H (20 ml)	N/A	H (25 ml)	Not very realistic
2	S (20 ml)	N/A	S (25 ml)	N/A
3	S (20 ml)	N/A	H (25 ml)	N/A
4	S (20 ml)	VS (20 ml)	H (20 ml)	Child-like skin
5	H (25 ml)	VS (20 ml)	H (20 ml)	An older adult's skin
6	S (25 ml)	VS (50 ml)	S (20 ml)	Realistic
7	S (25 ml)	VS (20 ml)	S (20 ml)	Very realistic

The design of the phantom was selected after extensive validation with a single experienced surgeon, and selected for its realistic viscoelastic properties. A total of seven phantom designs were evaluated according to the perceived realism of pressing, stretching, pinching and cutting the phantom surface. All evaluated designs consisted of a gelatin base with 100g per litre concentration and varying combinations of silicone layers. We have chosen Smooth-On Ecoflex^{TM} Gel, Smooth-On Ecoflex^{TM} 00-30 and Smooth-On Dragon Skin^{TM} (shore hardness 10A) silicone rubbers to represent very soft, soft and hard phantom layers, respectively. Table 5.1 shows the phantom design ranking (from least to most realistic). A few summary points:

- Softer silicone rubbers (shore hardness < 30) appear more realistic.
- The combination of silicone layers with varying hardness increases realism. Single-layer designs were scored lowest, while three-layer designs were rated as most realistic.
- The hardness gradient (with a harder outer layer) plays a role in the realism of shear loads (e.g. stretching the skin).
- The hardness of the bottom layer plays role in pressing load and can mimic the age of the skin.

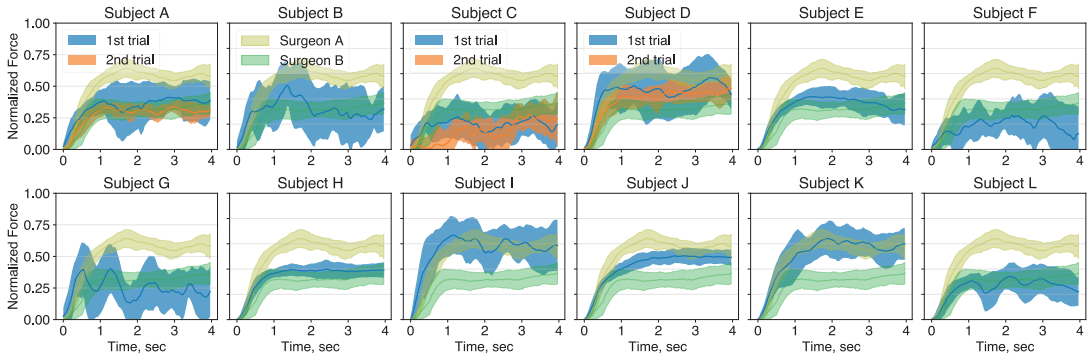

Figure 5.7: Subject-specific distributions of the excision force profiles. Mean and standard deviation (N = 12) of normalized force profiles for each of the medical students (blue) and practicing surgeons (dark yellow and green). Subjects *A*, *C* and *D* have repeated the trials after two months (orange). Fig. 5.5a shows individual force profiles for each subject.

5.5 Results

Fig. 5.7 shows the distribution of force profiles (mean and standard deviation) for each of the 12 medical students (blue), compared with force profiles of two practising surgeons - consultant neurosurgeon (dark yellow) and plastic surgeon (green), each with 5 years of experience. There is a considerable difference in the mean, variability (standard deviation) and overall shape (envelope) of the incision force profiles across the subjects. For example, force profiles of subjects *H* and *J* resemble an overdamped step-like response with a smooth and even force level in the steady-state phase of the excision, whereas force profiles of surgeon *A* (dark yellow) show noticeable force modulation (e.g. dip in the force at t = 3 s). The narrow envelope of the profile distribution (i.e. force profile variability) in the surgeon's trials indicate that such modulation is consistent, and hence, is likely to be a part of the cutting behaviour.

Subjective evaluation of the incision skills

Four surgical experts (two plastic surgeons and two neurosurgeons) subjectively evaluated all 15 trials (12 original trials plus 3 repeated, see Methods section for details) independently, based on trial videos. The experts were asked to group the trials according to their perceived proficiency (i.e. experts were free to evaluate the performance according to the criteria of their own choice) and provide comments to support their judgement (Appendix A). Fig. 5.8 shows the boxplots of the grouped subjects based on proficiency ratings from 0 to 3 (where 0 is the poorest performance).

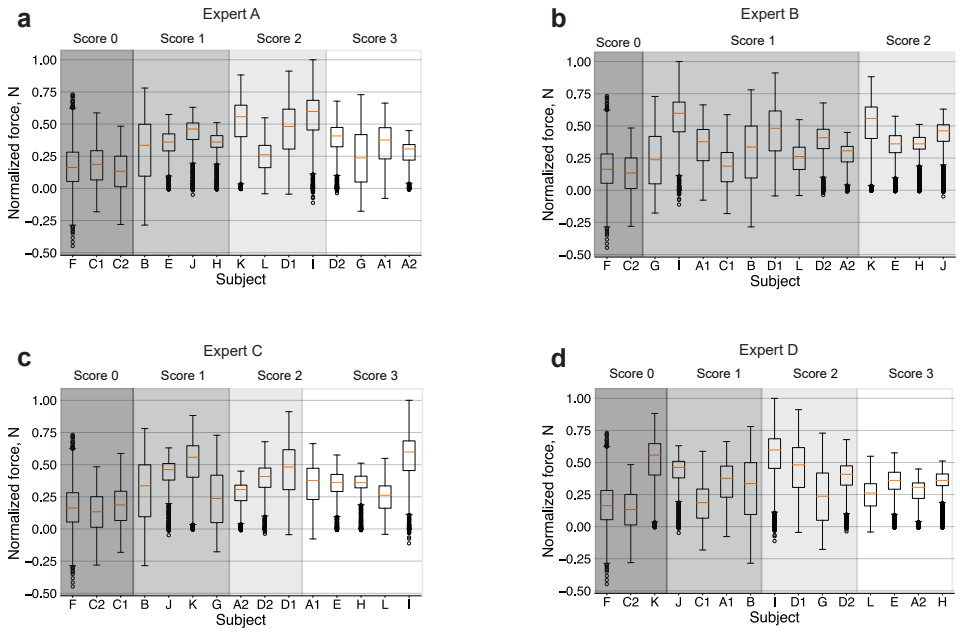

Figure 5.8: Box plots of force samples (N = 1,440) sorted by expert evaluation scores. Subjective evaluation by surgical experts (Appendix A). Proficiency is scored from lowest (0, darkest region) to highest (3, lightest region).

The assessment showed poor inter-rated agreement [171] among the experts, with an intraclass correlation coefficient (two-way random, single measures) of 0.45. Despite agreeing in their assessments of the poorest performances (both subject *F* and the second trial of subject *C* were rated the worst by each of the experts), experts showed a noticeable difference in rating the average and top performers. For example, Expert A rated subject *G* with the highest score of 3, while both experts B and C rated it as the second poorest performer (score 1). In addition, subjects *E* and *H* were rated with the highest score by experts C and D, but only with a second-lowest score by expert A. Finally, experts A and C rated the first trial of subject *A* with the highest score, but it was rated as the second poorest by experts B and D.

The discrepancies in subjective assessment of the overall proficiency perceived by the experts highlight the challenges in teaching and assessing skills that are typically mastered through apprenticeship. These differences in assessment might reflect the different specialities, schools or experience levels of the experts. In this study, we treat each expert assessment as an equally valid evaluation.

Below, we investigate the characteristics of elliptical excision performance that drive each expert's perception of skill. Specifically, we study the relationships between the measured incision forces and the subjective assessments of skill based on motion alone. In the following sections, we perform the analysis using the conventional force-based metrics and introduce a generative model for elliptical excision forces that decomposes force measurements into a set of independent components that uniquely describe the manner of the excision. Finally, we provide an analysis of how these components can explain the subjective criteria employed by each expert.

Traditional performance analysis

In this section, we analyzed the relationships between the subjective evaluations by experts and the following objective force-based metrics: mean force, force variability (standard deviation), peak force, scaled force (mean force divided by the peak force value, an indication of force overshoot), derivative of force with respect to time [29] (indication of the aggressiveness) and force integral (indication of cutting energy).

Levene's test showed that the variance of incision force samples has a statistically significant difference across the subjects (p-value < 0.05). Therefore, the omnibus Welch's ANOVA (analysis of variance) and Games-Howell post-hoc tests with a family-wise error rate of 0.05 were used. Subjective evaluation by expert A showed no

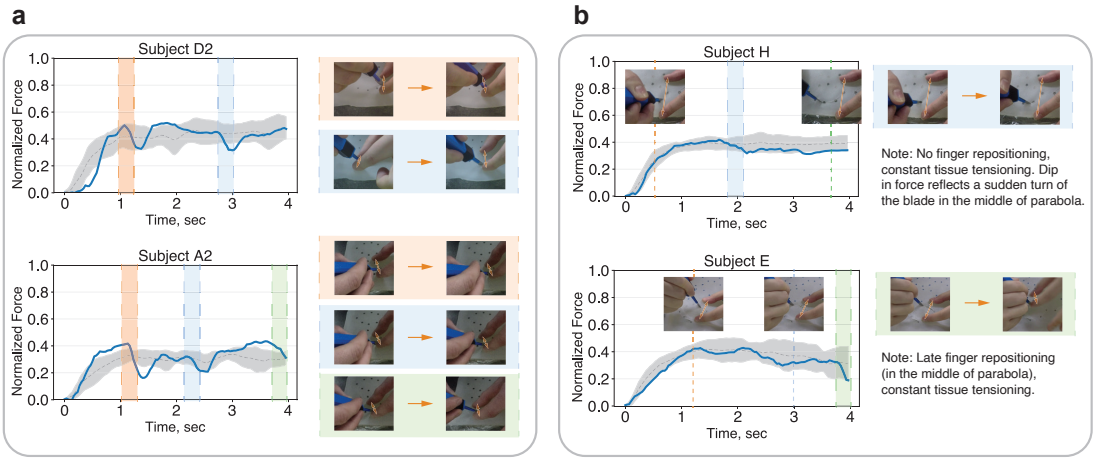

Figure 5.9: Comparison of high scorers from expert evaluations. **a** High scorers from expert A evaluation (second trials of subjects *D* and *A*) performed incisions with frequent tissue re-tensioning. **b** High scorers from expert B evaluation (subjects *H* and *E*) executed incisions with constant tissue tensioning. The blue lines are the individual force profiles (depicted on the images), and the grey dotted lines and shaded regions are the mean and standard deviations of force profiles from high scorers' trials.

monotonic relationship with any of the described above force-based metrics. On the other hand, expert B ratings showed positive monotonic relationship with the mean force, peak force, scaled force and force integral metrics. Expert C ratings showed a positive monotonic relationship with the mean force, scaled force and force integral metrics. In the peak force metric, the middle rated groups (with scores 1 and 2) by expert B showed no significant difference. For expert C, no significant difference is registered between groups with scores 1, 2 and 3 in the mean force and force integral metrics, and groups 2 and 3 in the scaled force metric. In addition, ratings from experts B and C show negative monotonic relationship with the time derivative of force (groups rated with scores 0, 1 by expert B, as well as groups rated with scores 2 and 3 by expert C show no significant difference). Expert D shows a positive monotonic relationship with scaled force, with groups scored 1 and 2 showing no significant difference. No monotonic relationship between the subjective assessment of experts and force variability is registered.

The analysis above suggests that experts B and C reward the incisions that are executed with smooth (i.e. uninterrupted) force profiles of larger amplitude and low overshoot. This observation is in agreement with an intuitive interpretation of the force-based metrics - higher force integral (larger incision forces with longer duration)

along with lower force derivative corresponds to “confident” incisions with consistent application of forces throughout the task execution. In the case of expert D, there is an indication that the expert penalizes the excisions with an overshoot in the force profile.

However, the above analysis fails at explaining the implicit criteria of expert A. Fig. 5.9 compares the high scorers from the experts’ evaluations. The top scorers from expert A evaluation executed the incisions with distinct frequency of tissue re-tensioning. In contrast, the top scorers from evaluation by experts B and C show noticeable passivity of the non-dominant hand - the surrounded tissues held in constant tension with occasional finger re-positioning in the later stages of task execution. The inspection of the commentary from expert A (Appendix Table A.2) further suggests that active re-positioning of fingers (or tissue re-tensioning) might be one of the dominant performance criteria employed by the expert. Nevertheless, the traditional force-based metrics fail to identify this rating dimension. In the following section, we show how this problem can be addressed by exploring the parameter space of our probabilistic generative model.

Elliptical excision force model parameters and behaviour analysis

The proposed elliptical excision force model encodes the observed cutting behaviour using the following set of parameters with meaningful and intuitive interpretation:

- v_L and v_U, which determine the lower and upper excision force levels and characterise the overall amplitude and the spread of the force profile distribution.
- σ_L^2 and σ_U^2, which capture the uncertainty of the upper and lower excision force levels and reflect sample-to-sample variability within the force profile.
- transition probability matrix $\mathbf{Q} = \begin{bmatrix} q_{11} & q_{12} \\ q_{21} & q_{22} \end{bmatrix}$, which determines the temporal characteristics of the incision force profile, i.e. the modulation of forces observed in the experiment. Here, q_{12} is the probability of switching from the lower to the upper force level, q_{21} is the probability of switching from the upper to the lower force level, q_{11} and q_{22} are probabilities of remaining in the lower and upper force levels, respectively.

Fig. 5.10 illustrates the effect of the above parameters on the learned behaviour for subjects *H* and *D*. Note that actual incision forces exerted by the subjects have similar mean amplitude (approx. 0.4), but differ in the force envelope - subject *H* shows a tighter distribution in force profiles compared to subject *D*, which is reflected in

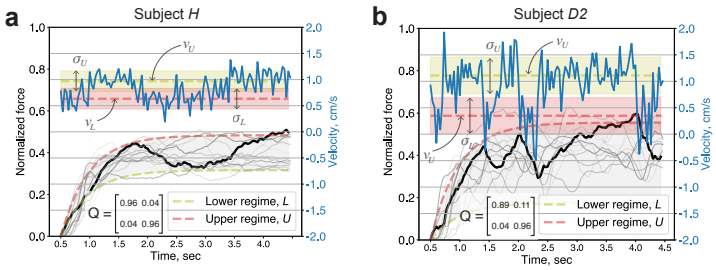

Figure 5.10: Excision forces and model parameters. Learned model parameters ($v_L, v_U, \sigma_L^2, \sigma_U^2$ and $\mathbf{Q}$) from (**a**) subject *H* and (**b**) second trial of subject *D*, respectively. Thick black lines are synthetic force profiles (generated by the trained model), blue lines are corresponding generated velocity profiles, and semi-transparent grey lines are the actual force profiles used in model training. Note: The pink and green shading corresponds to the standard deviation of velocity at the lower and the upper regimes (σ_L and σ_U), respectively. The grey shading denotes the envelope of the excision forces, defined by the lower and the upper regimes (v_L and v_U).

the corresponding v_L and v_U parameters. In addition, the subjects differ in temporal characteristics of the excision forces - subject *H* shows slow varying modulation between the upper and the lower force levels, whereas subject *D* shows occasional losses in the excision forces followed by rapid recovery to the upper force level. These characteristics are captured by the transition probability matrix $\mathbf{Q}$ (Fig. 5.10).

Fig. 5.11a shows the scatter plot of v_L versus v_U parameters across the subjects (including the surgeons *SA* and *SB*), and the corresponding distributions of forces for each cluster along the amplitude axis (higher the v_L and v_U parameter values correspond to the higher mean forces). Note that subjects *H* and *D* are well aligned along the amplitude axis, as expected. In addition, it should be noted that the axis orthogonal to the amplitude axis describes the width of force envelope, e.g. simultaneous increase in v_L and reduction in v_U corresponds to narrower force profiles, and vice versa (see the effect of v_L and v_U parameters on the force envelope in Fig. 5.10). As expected, subjects *H* and *J*, as well as surgeons *SA* and *SB* are located in the bottom right corner of Fig. 5.11a plot, reflecting highly consistent force application with a narrow envelope (Fig. 5.7).

The proposed model implicitly encodes the descriptive statistics of the excision forces and provides a compact representation of a range of heuristic metrics previously considered in the literature, such as mean forces or force variability. However, our model extends the analysis by explicitly capturing the temporal structure of the behaviour, which is typically lost when descriptive statistics are computed directly. For instance,

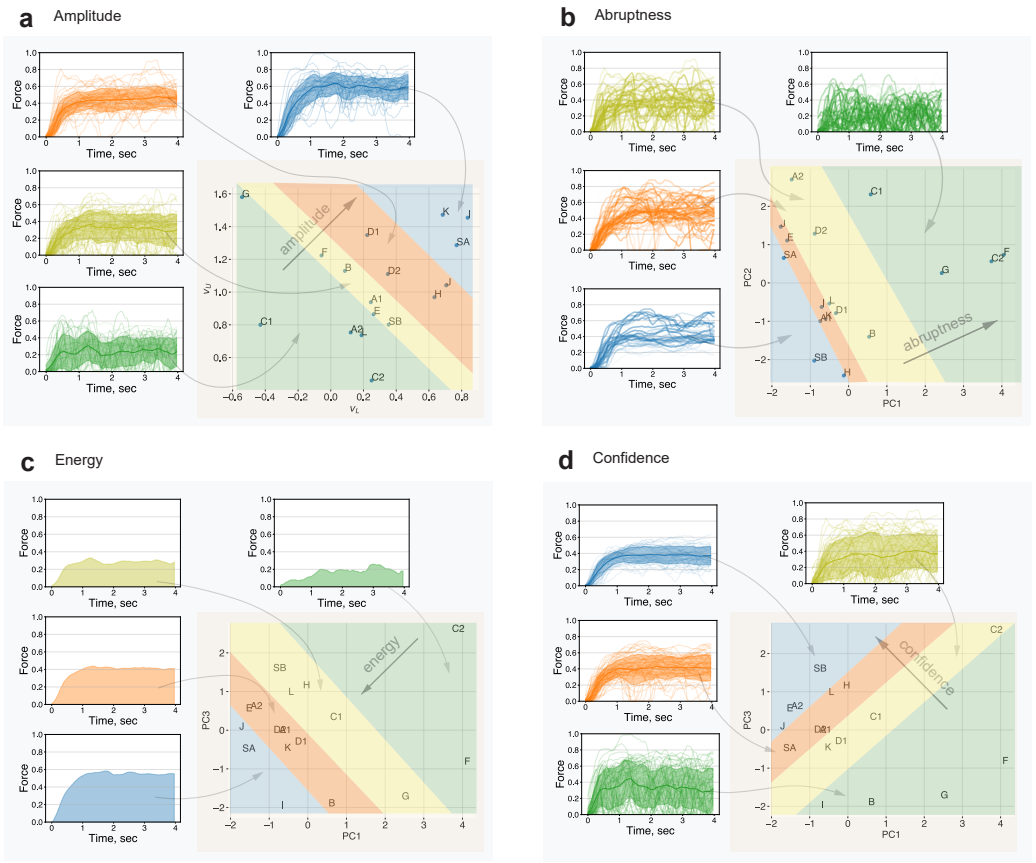

Figure 5.11: Performance analysis using model parameters. **a** Parameters v_L and v_U encode the amplitude information of the excision forces (the mean, the standard deviation and the individual force profiles for each highlighted group are shown as solid lines, shaded region and semi-transparent lines, respectively). **b**-**d** The Principal Component Analysis representation of parameter space encodes meaningful features that can characterise the task execution. **b** The diagonal axis on the Principal Component 1 (PC1) vs Principal Component 2 (PC2) plot captures the excision abruptness, characterised by increased probabilities of sudden rises and falls in the applied forces. **c** The PC1 vs Principal Component 3 (PC3) plot captures the Energy feature, characterised by the amplitude and steadiness of the excision forces (the integrals of the mean force profiles for each of the groups is shown here). **d** Orthogonal to the Energy axis is the Confidence feature reflecting the consistent and steady force application (the mean, the standard deviation and the individual force profiles of the highlighted groups are shown as solid lines, shaded region and semi-transparent lines, respectively). Note: Letters *A* to *L* correspond to medical students (where numeral indicates the trial), "*SA*" and "*SB*" correspond to surgeon A and B, respectively.

a close inspection of incision force profiles from subjects *J* and *H* (Fig. 5.5a) reveals that subject *J* executes the incision with a lower amount of modulation of the force amplitude. However, the standard deviation of normalized force profiles (the width of the force envelope) for *J* and *H* subjects is identical, 0.056 $\pm$ 0.031 vs 0.056 $\pm$ 0.036 (N = 12, excision profiles), respectively. In addition, the force profiles from subject *J* trials exhibit a higher force derivative metric score [29] (3.7 $\pm$ 0.37 vs 3.2 $\pm$ 0.53, N = 1,440 force samples), which might lead to an incorrect conclusion. Our model correctly captures this temporal characteristic with the transition probability matrix $\mathbf{Q}$: the smooth and slowly varying force profile modulation shown by subject *H* is reflected in the equal and low transition probabilities $q_{21} = q_{12} = 0.037$. In contrast, the imbalance in the transition probabilities for subject *J* ($q_{12} = 0.124$ and $q_{21} = 0.028$) yields a considerably higher long-term probability of application of a steady excision force ($\pi_U = 0.819$) compared to subject *H* ($\pi_U = 0.496$).

The Principal Component Analysis (PCA) of model parameters allows the extraction of meaningful features that characterise the performance. Fig. 5.11b shows the PCA projection of model parameters for each subject on the 2D plot, with highlighted groups along the diagonal axis. The principal component PC1 reflects a simultaneous reduction in the lower force level v_L (Fig. 5.12a) and an increase in the probability of a sudden drop of applied forces q_{21} (Fig. 5.12b). In other words, the higher end of the PC1 axis corresponds to a more frequent and drastic loss of applied force throughout the task execution. The PC2 component reflects the increase in the probability of a sharp rise of excision forces (Fig. 5.12c), i.e. the higher end of the PC2 axis corresponds to a more aggressive brush stroke-like application of excision forces. We call the diagonal axis on PC1 vs PC2 plot an Abruptness feature, as it reflects a degree of discontinuity of the task execution.

The third principal component PC3 corresponds to a reduction of the upper force level v_U (Fig. 5.12d). Note that model parameters whose projection lies on the high ends of PC1 and PC3 would correspond to low overall excision forces (due to low values for v_L and v_U parameters) with frequent switching to a lower force level (due to high probability q_{21}). Conversely, the model parameters that are projected to the lower regions of the PC1 and PC3 axes would correspond to high excision forces with rare loss of the applied forces. We call this diagonal axis of the PC1 vs PC3 plot an Energy feature (the higher excision forces applied for a longer duration, the greater the energy of task execution). Fig. 5.11c shows the PC1 vs PC3 plot and groups of subjects aligned along the Energy axis.

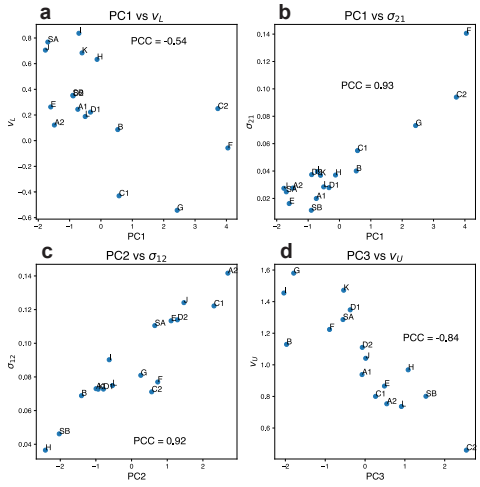

Figure 5.12: Correlation between principal components PC1, PC2 and PC3 and model parameters v_L, v_U, σ_{12} and σ_{21} (N = 17 independent trials). Note: PCC - Pearson Correlation Coefficient. Letters *A* to *L* correspond to medical students (where numeral indicates the trial), "*SA*" and "*SB*" correspond to surgeon A and B, respectively.

Finally, the model parameters that are simultaneously projected on the lower end of the PC1 and on the higher end of the PC3, correspond to highly uniform (due to low probability of q_21) and highly consistent excision forces with narrow envelope (due to high values of v_L and low values of v_U parameters). We call this diagonal of PC1 vs PC3 plot a Confidence feature. Note that the Confidence axis is orthogonal to the Energy feature, i.e. equally confident excisions can be executed at different energy levels (e.g. subject *J* and surgeon *SB*), and vice versa (e.g. subject *I* and surgeon *SA*).

Beyond traditional performance analysis

We performed correlation analysis to identify whether the inferred parameters of the proposed elliptical excision force model reflect the evaluation score provided by each of the experts. The expert B evaluation scores showed significant (p-value < 0.05) Spearman rank-order correlation with v_L, σ_L^2, q_{11} and q_{22} model parameters. The performance evaluation by experts C and D showed significant Spearman's rank correlation with parameters σ_U^2 and q_{22}. In the above analysis, the critical value of 0.446 was used for $N = 15$ observations [172].

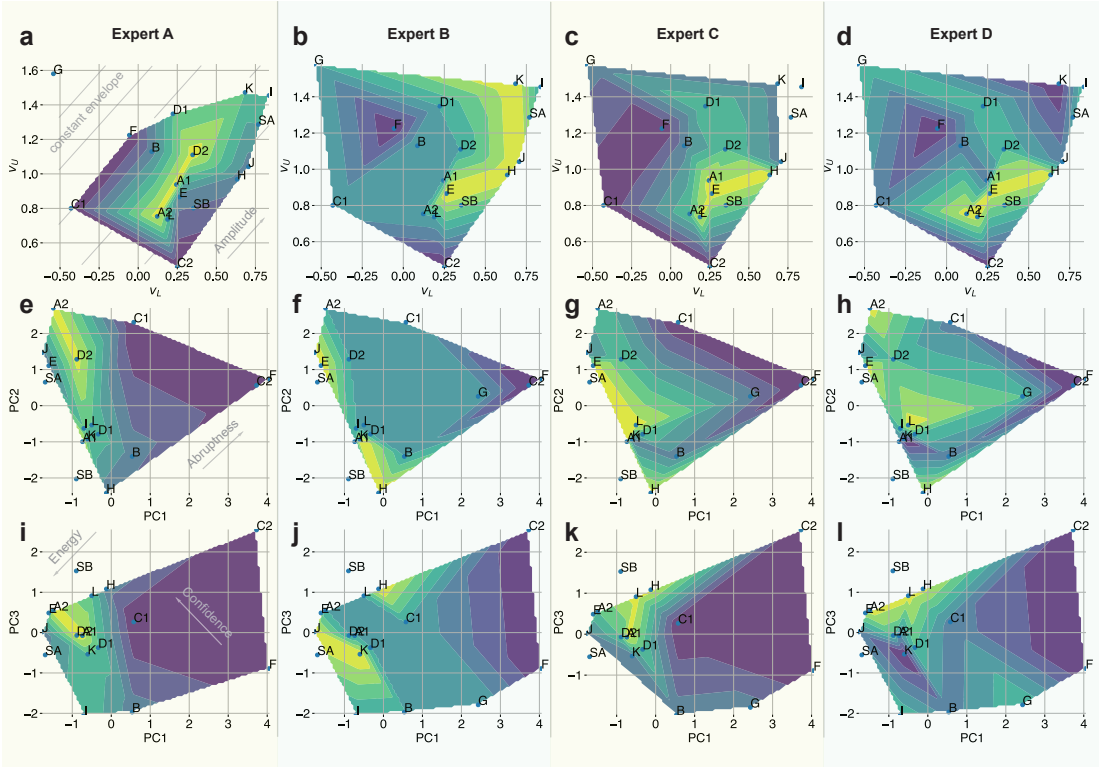

Figure 5.13: Analysis of experts' evaluation criteria with model parameters. **a**-**d** Scatter plot of parameters v_L and v_U with linearly interpolated expert evaluation score (with the brighter region corresponding to the higher score). **e**-**h** and **i**-**l** PCA plots of model parameters with linearly interpolated expert evaluation score. Note the subjects *G* and *I* were excluded as outliers from the analysis of experts A and C. Note: Letters *A* to *L* correspond to medical students (where numeral indicates the trial), "*SA*" and "*SB*" correspond to surgeon A and B, respectively.

Fig. 5.13 (top row) shows the scatter plot of v_L and v_U parameters with a contour plot of linearly interpolated evaluation score provided by each of the experts. The plot suggests that evaluation by expert A is approximately invariant to the overall amplitude of the force profiles, however, it is well aligned with an axis that defines the width of the force envelope. In addition, it can be seen that the top scorers from the evaluation of expert A cut with higher force envelope width compared to the top scorers from other experts. Note that the top scorers by expert B cut with higher mean force (i.e. subjects are located higher along the v_L and v_U axes) compared to other experts.

Fig. 5.13 (middle row) shows the PCA projection of model parameters across the expert evaluations with highlighted Abruptness feature. It can be seen from the plot, that interpolated evaluations of experts A, B and C are well aligned with the Abruptness axis. Note that the top scorers evaluated by expert A are located further along the axis

compared to evaluations from experts B and C, which indicates that expert A rewards task executions with highly pronounced modulation of the excision forces. In contrast, the top scorers from experts B and C are located on the lowest side of the Abruptness feature, suggesting that the experts penalise discontinuous application of excision forces. Finally, expert D showed no distinctive alignment with the defined axis, which suggests that the Abruptness feature does not reflect the expert's evaluation criteria.

Fig. 5.13 (bottom row) shows the PC1 vs PC3 plot, with corresponding Energy and Confidence features. It can be seen from the PCA plots that expert A rewarded the performers that scored highly along the axis of the Energy feature, as well as moderately along the Confidence axis. This agrees with previous conclusions that expert A values a certain degree of force modulation. In addition, it can be noted that expert B rewarded the performers that executed the task with high energy and high confidence (with an exception of subject *K*). Finally, the evaluation of expert D appears invariant to the Energy axis, however, it is well aligned with the Confidence axis (the top scorers are clustered in the region of the highest confidence score).

The above analysis suggests that, in contrast to other experts, expert A rewards the incisions that are executed with a wider force envelope and an increased amount of switching between the distinct force levels. In the elliptical excision task, such behaviour corresponds to an explicit force modulation due to well-pronounced tissue re-tensioning or finger re-positioning events (Fig. 5.9). This conclusion agrees with both the additional commentary from the expert (Appendix Table A.2), as well as with the qualitative assessment of force profiles from the distribution of high scorers (Fig. 5.5a).

In summary, the analysis indicates that expert B rewards confident incisions executed with higher energy. Expert C rewards excisions with consistent force application (i.e. narrow envelope of the force profiles). Both experts B and C penalise interrupted incisions. Finally, according to the analysis, expert D rewards the Confidence feature, but is invariant to the Energy feature, which suggests that overall force amplitude is not part of the expert's evaluation criteria. Importantly, the above analysis is in agreement with conclusions derived from the traditional force-based metrics, yet it offers an additional insight by introducing temporal features into the analysis.

5.6 Discussion

The contributions of this chapter are threefold. Firstly, we have developed a low-cost easy-to-replicate cutting instrument with an integrated force sensor. Secondly, our experiments using this instrument revealed that the time series of incision forces consists of subject-specific signatures that can reflect the subjective expert evaluation, and can be used for downstream performance analysis and objective surgeon comparisons. Thirdly, we compare the traditional force-based analysis techniques with the proposed superior method of analyzing incision forces.

The collected dataset of elliptical incisions shows a distinct pattern of a step-like response in the cutting force, with noticeable amplitude modulation in the steady-state phase. We found that incision force profiles encode the characteristics relevant to the perceived quality of task execution, and therefore can map the subjective criteria of an expert. The proposed model extends traditional descriptive statistics through a rigorous treatment of the temporal dependency of force measurements and conveniently decomposes the cutting behaviour into amplitude and temporal components. Analysis showed that this decomposition offers greater flexibility and brings deeper insight into the complex behaviours of surgeons, which are characterized by strong temporal structure.

We intentionally limited the scope of this study to the analysis of incision forces alone. We acknowledge the importance of motion analysis, and regard the role of force measurements as complementary. Nevertheless, it is critical to highlight the practical implications of force-based skill quantification. As accurate motion capture remains prohibitively expensive and difficult to deploy in realistic settings [173, 174], the tools and analysis approach described in this work offer an opportunity to explore the composition of surgical skills at a considerably larger scale.

This chapter opens up a number of opportunities for future work. Firstly, a comprehensive analysis of the utility of objective performance characterisation using a greater number of participants would be valuable, alongside work investigating skill requirements for different tasks and procedures. A small cohort of trainees with no prior experience in the studied procedure is a limitation that we aim to address in future work. Our study would also benefit from a comprehensive analysis of the learning curve, with a series of repeated trials across the entire cohort. The mapping between these objective measurements and downstream patient outcomes would also be particularly interesting. Moreover, an analysis of the variations in criteria

underpinning subjective evaluations of surgeons would be valuable, and it would be interesting to determine if there are specialisation-specific nuances or preferences present using the techniques introduced here. Finally, with minor modifications to sensing hardware, the described method can be applied to studying other complex manipulation skills, such as tissue characterization through palpation, or gentle grasping, where the force modality and its temporal components are also likely to play a dominant role. Finally, the proposed model is particularly promising for the analysis of highly procedural surgical tasks with multiple distinct execution phases, such as suturing. Although we found that two regimes are sufficient for modeling the force measurements in the elliptical excision task, the number of states can be increased for modeling more complex data. Being a hybrid system, our model enables modeling complex nonlinear behaviours with multiple linear dynamical systems. In practice, however, the inference of large number of parameters for switching linear dynamical system can be challenging given limited and noisy measurements.

In the next chapter, we show how the proposed model can be used to align robotic elliptical excision with desired characteristics of cutting forces.

Chapter 6

Learning robotic elliptical excision with human-like tool-tissue interactions

In surgery, the application of appropriate force levels is critical for the success and safety of a given procedure. While many studies are focused on measuring in situ forces, little attention has been devoted to relating these observed forces to surgical techniques. Answering questions like "Can certain changes to a surgical technique result in lower forces and increased safety margins?" could lead to improved surgical practice, and importantly, patient outcomes. However, such studies would require a large number of trials and professional surgeons, which is generally impractical to arrange. Instead, we show how robots can learn several variations of a surgical technique from a smaller number of surgical demonstrations and interpolate learnt behaviour via a parameterised skill model. This enables a large number of trials to be performed by a robotic system and the analysis of surgical techniques and their downstream effects on tissue. Here, we introduce a parameterised model of the elliptical excision skill and apply a Bayesian optimisation scheme to optimise the excision behaviour with respect to expert ratings, as well as individual characteristics of excision forces. Results show that the proposed framework can successfully align the generated robot behaviour with subjects across varying levels of proficiency in terms of excision forces.

6.1 Introduction

Surgical excision implies the application of physical forces necessary for tissue separation [85]. A successful procedure requires appropriate levels of excision forces - sufficient for cutting, yet conservative to avoid damaging tissue (excessive force can account for more than half of the medical errors committed by surgical trainees [175]). Cutting forces, on the other hand, strongly depend on the configuration of the blade [11, 24, 176], and therefore on the excision technique. In order to derive optimal surgical techniques, in the context of surgical training or autonomous surgery, tool-tissue interaction forces and their downstream effect on the tissues must be studied in a controlled manner. A comprehensive analysis of a wide range of behaviours across different levels of expertise is needed to identify good and bad practices and to measure their benefit or harm.

Unfortunately, such studies require a large number of participants at different stages of their professional development, which is extremely time-consuming and challenging in terms of logistics. As an alternative, we can use a considerably smaller number of subjects to teach a robot performing the excisions from various levels of proficiency and apply machine learning techniques to interpolate the behaviour between the demonstrations. A suitably parameterised behaviour model would let us generate a large number of trials with tight control over the process parameters, such as excision velocity, blade insertion angle, etc. Such a robotic setup would facilitate the exploration of the downstream effects of the cutting technique on the tissues, and therefore provide a deeper insight into its efficacy and safety. Importantly, this gives us the ability to align robotic cutting behaviour with the desired characteristics of excision forces to analyse various techniques and their influence on tissue outcome.

A standard approach to accomplish this relies on imitation learning techniques [177], such as the Dynamic Movement Primitive (DMP) [96], to learn excision behaviours directly from demonstrations. In the case of the classical DMP formulation, the encoded policy can be generalised via hyper-parameters, such as the goal state and temporal scaling, as well as the coupling terms [127]. Unfortunately, although this allows exploration around the demonstrated trajectories, the parameterised policies are restricted to individual demonstrations with no relation to one another. Alternatively, one could apply DMP formulations that leverage multiple demonstrations to capture behaviour variability as a separate task parameter [178, 179], which can be interpolated to synthesise unseen behaviours [180]. In the context of learning surgical

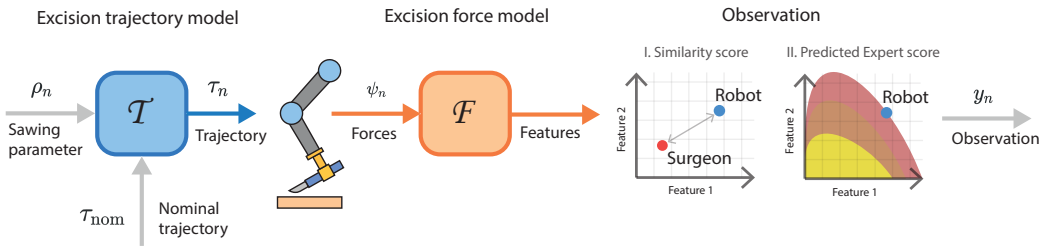

Figure 6.1: The proposed framework to generate human-like excision behaviours operates as follows. At a high level, an objective function takes in the sawing parameter ρ and outputs an observation similarity score y. The goal of the optimiser is to find the value for ρ that maximises the observation variable y. The inner structure of the proposed objective function consists of the proposed trajectory generator ($\mathscr{T}$) that given the scalar $\rho \in [1, 10]$ and a nominal trajectory τ_{nom}, generates the pose trajectory of the blade τ. Next, the robot executes the trajectory τ, and collected forces ψ are converted to a set of performance features by model $\mathscr{F}$. The obtained features are then used to define the final objective function, e.g. the similarity score between the robot-executed task and the performance of an actual surgeon, which updates the optimiser and generates a new excision behaviour.

excisions, these methods allow explicit capture of different "styles" of cutting tissues, which is particularly relevant for our task. However, these methods are unsuitable to encode the end-effector's pose trajectory in Cartesian space, as the orientation component requires special treatment of the SO(3) structure [181]. This presents challenges to apply the above methods to learn cutting skills, as the position and orientation trajectories of a blade are inherently coupled due to the nonholonomic nature of the cutting motion [3, 182].

As an alternative, in this chapter we introduce a simple parametric model of elliptical excision that decomposes the skill into nominal and behaviour-driven components, each of which can be learned from demonstrations. Here, we focus on modelling a sawing movement as the most dominant characteristic of the elliptical excision technique [183] observed in human trials [2], with less experienced trainees showing more pronounced sawing behaviour. Our model encodes the behaviour with a single real-valued parameter ρ that determines the amount of sawing movement applied during excision. We then show how this model can generate a variety of human-like excision trajectories, and apply Bayesian optimisation to align the generated behaviour with expert ratings.

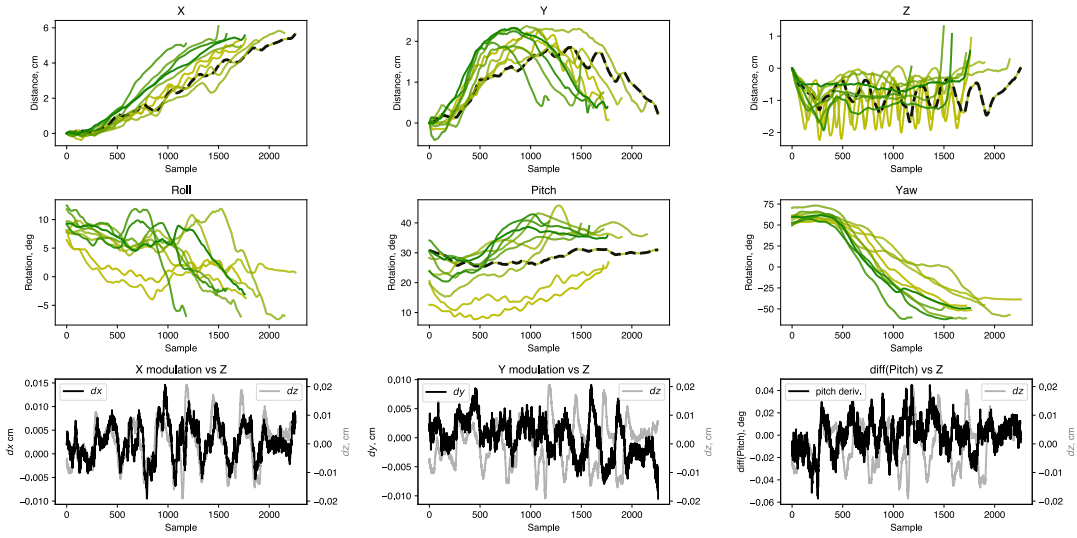

Figure 6.2: Measured individual position (top row) and orientation (middle row) trajectories of the blade for each of the demonstrated behaviour (the darker green lines correspond to smoother excisions). (Bottom row) Differenced measurements of x, y and pitch versus differenced measurements of z. Note: the original measured trajectories are shown as black dashed lines in the above plots.

Finally, as the core contribution of this chapter, we propose a framework for aligning human-like robotic elliptical excisions with the desired characteristics of excision forces and demonstrate its applicability for analysing excision skills. In this framework (Fig. 6.1), we generate an elliptical excision behaviour using the parametric model described above, which generates the pose trajectory of the blade, specified by a behaviour parameter ρ and a nominal cutting trajectory. The robot executes the generated trajectory in a real-world experiment. A suitable model characterising the excision behaviour from the excision force measurements [2, 184, 185] allows us to 1) calibrate the robotic behaviours to match the desired characteristics of tool-tissue interaction, and 2) use the aligned robotic behaviour to analyse the excision techniques in a well-controlled and repeatable manner. Here, we propose a Bayesian Optimisation scheme to minimise the number of phantom excisions required for behaviour tuning.

6.2 Parametric generation of human-like excision trajectories

The primary objective of our excision trajectory generator is to produce realistic pose trajectories of the blade, mirroring those typically observed during an elliptical excision procedure. In particular, we are interested in learning the auxiliary sawing movement of the blade, which can play a role in assisting the excision by lowering the cutting forces required for the task [11]. In this section, we introduce a generative model of blade trajectories with a single parameter ρ that specifies the amount of sawing movement applied to any desired elliptical excision motion.

Our central hypothesis is that elliptical excision comprises two movement components: a nominal smooth cutting motion along the ellipse and an adaptive sawing motion that assists the excision. To better understand the interplay between these two components, we recorded ten elliptical excisions with varying amounts of sawing behaviour, from a highly pronounced sawing movement to an extremely smooth excision. Fig. 6.2 (top and middle rows) shows the measured position and orientation trajectories of the blade in each trial. Notice the back-and-forth oscillation of the blade on the XY plane, a distinct feature of the sawing movement. It should be noted that sawing is executed at a noticeably different pitch when compared to smoother executions. Unsurprisingly, smoother excisions result in a much lower spread of the pose trajectories, which highlights the challenge of maintaining consistent motion when sawing. As expected, the sawing motion is most dominant along the z axis, i.e. the cutting depth. However, the sawing is also reflected in the blade's x, y and pitch trajectories.

Fig. 6.2 (bottom row) shows the trajectories of differenced x, y and pitch motion components, compared to a differenced z trace, all from one of the observed sawing behaviours. The entire trace of x, and the first half of the parabola in y trajectory, are noticeably in-phase with the z. In contrast, the whole trace of the pitch, and the second half of the parabola in y trajectory, are noticeably out-of-phase with the z trajectory. The relationship between z and xy trajectories indicates that sawing movement is achieved by propagating the blade forward on the ascent, with residual backward motion on the blade's descent. The relation between z and pitch trajectories suggests that consistent modulation of the insertion angle is also a part of the slicing motion.

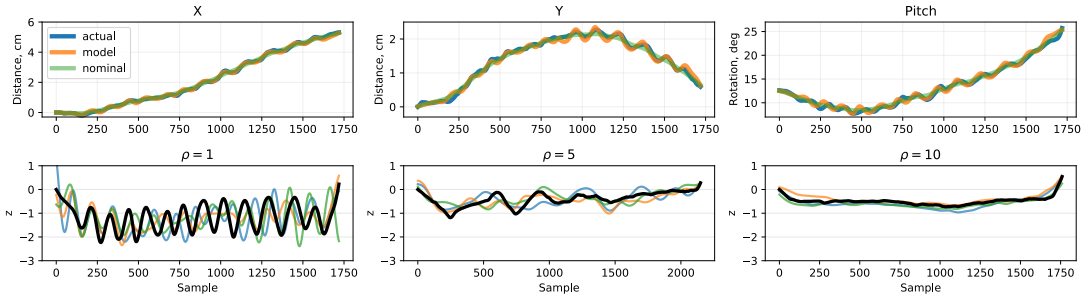

Figure 6.3: (Top row) Comparison of measured x, y and pitch trajectories (blue lines) with model predictions (orange lines). The nominal trajectories obtained by low-pass filtering raw measurements are denoted with green. (Bottom row) Comparison of measured z trajectories for three different sawing behaviours (black lines) and corresponding synthetic trajectories generated by the model (coloured semi-transparent lines).

6.2.1 Modeling blade trajectories for elliptical excisions

Given the above insights, we model the elliptical excision behaviour as follows. First, we decompose the cutting motion into a *nominal* movement component that follows the desired smooth cutting contour, and a *behaviour* component that characterises the manner of task execution (e.g. sawing vs smooth excisions). For the z trajectory, this is written as

$$z_m = z_n + z_b \tag{6.1}$$

where z_m, z_n and z_b are the measured, nominal and behaviour trajectories along the z axis, respectively.

Next, we assume that a nominal movement component can be approximated by low-pass filtering of the measurements, and therefore the behaviour component can be computed as $z_b = z_m - z_n$. The obtained behaviour component z_b can be used to model the observed x, y and pitch trajectories of the blade, as follows:

$$\begin{aligned} x_m &= x_n + c_x z_b \\ y_m &= y_n + c_y z_b \\ \beta_m &= \beta_n + c_\beta z_b \end{aligned} \tag{6.2}$$

Here x_m, y_m and β_m are the measured x, y and pitch trajectories, respectively, and x_n, y_n and β_n are their corresponding nominal trajectories. c_x, c_y and c_β are the scaling coefficients. (We invert the sign of c_y in the second half of the y_m parabola to correctly represent the modulation of parabolic nominal trajectories on the XY plane - here the ascent of the blade corresponds to propagation along the negative Y slope.)

As a result, we model the x, y and pitch trajectories as a function of z_b. According to this model, any modulation along the cutting depth is reflected in the x, y and pitch trajectories. Fig. 6.3 (top row) compares the actual trajectories with those predicted by our model for one of the observed sawing behaviours. Here, we used a first-order Butterworth filter with a cutoff frequency of 0.6 Hz to obtain the nominal trajectories from the raw measurements. Finally, parameters c_x, c_y and c_β were manually selected as 0.2, 0.13 and -1.2, respectively.

6.2.2 Learning cutting behaviour

The movement component z_b, which defines the excision behaviour, can be learned using one of many supervised learning techniques. In this work, we first apply the following function approximation to encode the behaviour component z_b:

$$z_b(t) \approx \frac{\sum_{i=1}^{N} \psi_i(t)\theta_i}{\sum_{i=1}^{N} \psi_i(t)}, \tag{6.3}$$

where $\psi_i(t) = \exp(-h_i(t-c_i)^2)$ are Gaussian basis functions, N is the number of basis functions, t is the timestep, c_i and h_i are the centres and widths of the basis functions, and θ_i are the weights of the basis functions.

The vector of learned weights $\boldsymbol{\theta} = [\theta_1, ..., \theta_N]$ can be viewed as a compressed representation of the z_b time series. We fit a second-order autoregression model to vector $\boldsymbol{\theta}$:

$$\theta_i = c + a_1\theta_{i-1} + a_2\theta_{i-2} + \varepsilon_i \tag{6.4}$$

where a_k and c are the autoregression coefficients and bias constant, respectively; ε_i is the white noise term.

Finally, given the excision behaviour label (1 to 10, where 1 represents the distinct sawing cuts, and 10 denotes smooth excisions), we fit a linear model to predict the a_1 and a_2 coefficients. Thus, given a real number $\rho \in [1, 10]$, our model generates the behaviour component z_b, which along with a nominal cutting trajectory can be used to produce a human-like pose trajectory of the blade with desired sawing behaviour to be executed by a robot. Fig. 6.3 (bottom row) compares the z trajectories sampled from our model with the actual measurements z_m for different sawing behaviours.

6.3 Optimisation of elliptical excision technique

Optimisation of the robotic behaviour with respect to the excision force characteristics can offer interesting prospects for studies on the effects of surgical procedures. For example, the alignment of robot behaviour with excision forces that match those of expert surgeons is particularly promising for robotic surgery applications. Equally important is the ability to faithfully recreate sub-standard excision techniques and study the common mistakes observed in less experienced surgeons or trainees. In addition, technique optimisation concerning force characteristics critical to the procedure's safety could positively contribute to the existing surgical training and practice.

In this work, we use an excision force model described in [2], characterising the excision performance from force measurements; however, other force-based characterisation approaches can be readily applied in the proposed framework. Below, we provide a brief overview of the force-based characterisation of elliptical excision used in this study, followed by descriptions of the objective function and the proposed method for technique optimisation.

6.3.1 Performance characterisation from force measurements

A model of excision forces introduced in [2] allows characterising the performance of the generated excision behaviours directly from the measurements of the excision forces. Alongside descriptive statistics of excision forces, this model parameterises task-related characteristics correlated with elliptical excision performance, such as abruptness of task execution flow. This approach models the elliptical excision process as a hybrid system, with underlying continuous dynamics of viscoelastic interaction between tissues and the blade, as well as discrete event dynamics, typically associated with tissue re-tensioning or blade re-orientation.

First, the model approximates the process of cutting a viscoelastic object as a continuous blade's movement through Maxwell material using the following constitutive law:

$$\frac{\eta}{E}\dot{f} + f = \eta\dot{x} \tag{6.5}$$

with f is the excision force, $\dot{f}$ the time derivative of the excision force, $\dot{x}$ is the blade's velocity, E and η the Maxwell model's spring and damper coefficients, respectively.

The model assumes that an excision is executed using K cutting regimes, where each regime k corresponds to a constant velocity of the blade v_k. System uncertainty is modelled using white Gaussian noise with variance σ_k, $\tilde{v}_k \sim \mathcal{N}(v_k, \sigma_k^2)$. Cutting regimes are switched according to $K \times K$ transition matrix $\mathbf{Q}$, which along with v_k and σ_k^2, can be learned by fitting a Hidden Markov Model (HMM) to $\dot{x}$. Under the assumption of the Maxwell model, v_k can be obtained directly from force measurements f, captured using a suitably instrumented scalpel.

The learned model parameters encode the amplitude and temporal features of the excision forces that characterise the manner of task execution. For instance, parameters $\{v_1 ... v_K\}$ describe the dominant force levels of the excision forces, and thus the overall magnitude and spread of forces applied during the excision. Along with transition probability matrix $\mathbf{Q}$, which captures the temporal characteristics of the excision forces, these parameters can encode meaningful features, such as Energy (where increased energy reflects higher cutting forces applied for a longer duration) or Smoothness (where increased smoothness reflects the lower probability of sudden rise and fall of excision forces).

6.3.2 Objective function

Fig. 6.1 shows a diagram of the proposed framework for aligning robotic cutting behaviour with desired characteristics of excision forces, typically observed in human trials. At every n-th iteration, the robot executes the excision trajectory τ_n generated by the proposed trajectory model ($\mathscr{T}$) using candidate behaviour parameter ρ_n and a fixed nominal trajectory τ_{nom}. After the execution, the recorded excision force profile ψ_n is provided to the force-based characterisation model ($\mathscr{F}$), which encodes the characteristics of the excision forces, as described in the previous section. The features extracted by model $\mathscr{F}$ are then used to evaluate the objective function $g(\rho_n)$. Two scoring methods are used to evaluate the proposed objective function:

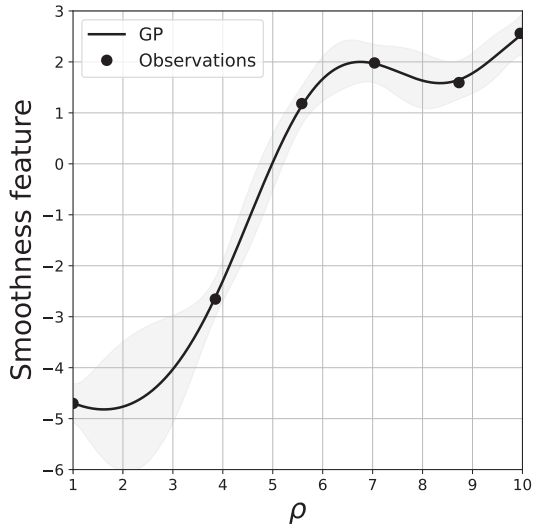

Figure 6.4: Gaussian process model fit to six datapoints (black dots) collected by optimising ρ with respect to the Smoothness feature. (The black line is the posterior mean, and the shaded region is 95% confidence interval).

A single characteristic of excision forces

is used for aligning the generated robot behaviour with respect to a certain characteristic of the excision forces, e.g. amplitude or smoothness evaluated by model $\mathscr{F}$.

Expert rating

This objective function is used to optimise the robot behaviour with respect to a predicted expert score. [2] evaluated the magnitude-based characteristics of the excision forces (the Amplitude and Consistency features, captured by model $\mathscr{F}$) using 15 expert-labelled excision trials. Here, we apply k-nearest neighbour regression (with $k = 1$) to predict the expert rating given the excision features.

6.3.3 Bayesian optimisation of excision behaviour

We apply Bayesian Optimisation (BO) [186] to reduce the number of cutting experiments required to generate a given human-like excision behaviour. At each iteration, BO optimises an acquisition function α to choose the next candidate sawing parameter ρ for trajectory generation in order to evaluate the objective function g (as described above). We model the mapping between trajectory parameter ρ and the

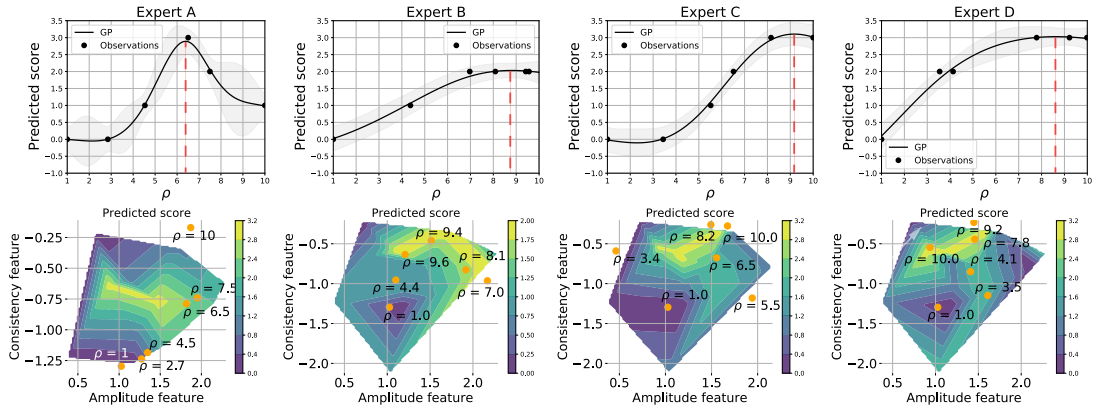

Figure 6.5: Results for behaviour (ρ) optimisation with respect to the interpolated performance score from four experts. (Top row) Gaussian process models fit to six observations (black dots) obtained during optimisation. The black lines show the posterior, the shaded regions illustrate the 95% confidence intervals, and the red dashed lines highlight the optimal ρ parameters for each of the experiments. (Bottom row) Contour plot of the interpolated expert scores over the feature space of the excision force model $\mathscr{F}$. The orange dots are the individual sample points ρ used during optimisation.

objective function using a Gaussian process (GP) [187]:

$$g(\rho) \sim \mathscr{GP}\left(m(\rho), \kappa(\rho, \rho')\right) \tag{6.6}$$

where $m(\rho)$ and $\kappa(\rho, \rho')$ are the mean and kernel functions.

For α, we use the Expected Improvement acquisition function with the following closed-form expression [188]:

$$\alpha(\rho) = (m(\rho) - g(\rho^+) - \varepsilon)\,\Phi(Z) + \sigma(\rho)\phi(Z), \tag{6.7}$$

where

$$Z = \begin{cases} \frac{m(\rho) - g(\rho^+) - \varepsilon}{\sigma(\rho)}, & \text{if } \sigma(\rho) > 0 \\ 0, & \text{if } \sigma(\rho) = 0 \end{cases}$$

Above, $m(\rho)$ and $\sigma(\rho)$ are the mean and the standard deviation of the GP posterior, and Φ and ϕ are the cumulative probability function and the probability density function, respectively. ρ^+ is the current optimal choice of sawing parameter, and ε is a scalar that sets the tradeoff between exploration and exploitation during optimisation.

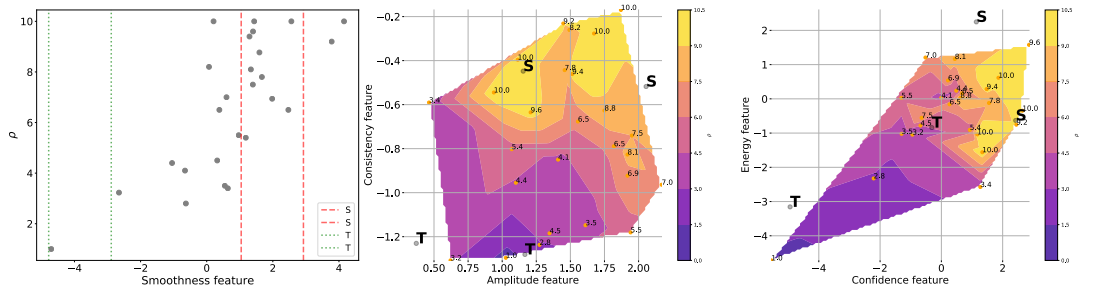

Figure 6.6: (Left) ρ parameter vs evaluated smoothness feature. (Middle and right) Contour plots of the ρ parameter values obtained during experiments. The orange dots are the individual datapoints with shown values for ρ parameter. Note: **T** and **S** denote medical trainee and professional surgeon, respectively.

We use a Matérn kernel [189] function $\kappa(\rho,\rho')$ with the following analytical expression:

$$\kappa(\rho_i,\rho_j) = \frac{1}{\Gamma(\nu)2^{\nu-1}}\left(\frac{\sqrt{2\nu}}{l}r\right)^{\nu} K_\nu\left(\frac{\sqrt{2\nu}}{l}r\right) \tag{6.8}$$

where $r = |\rho_i - \rho_j|$, $\Gamma(\cdot)$ is the gamma function, K_ν the Bessel function, ν and l kernel hyperparameters. We choose this kernel because of its flexibility - Matérn kernel is a generalization of the Gaussian radial basis function and can be reduced to the exponential kernel by controlling the smoothness [190]. In our experiments, we set $\varepsilon = 2$, $\nu = 2.5$ and $l = 1$. These parameters were chosen manually during setup calibration.

6.4 Experiments and Results

We performed two sets of experiments with the following objectives: 1) to find the excision technique that maximises the smoothness feature of the applied cutting forces, and 2) to find the excision technique whose excision forces predict the highest expert ratings.

Fig. 6.4 shows the optimisation results for six iterations of smoothness feature optimisation. The first trial was initialised with a sample $\{\rho_1 = 1, y_1\}$, where y_1 is the force smoothness feature evaluated by model $\mathscr{F}$. Optimisation results confirmed our expectations that smoother excision trajectories (e.g. generated by model $\mathscr{T}$ using larger values of ρ parameter) result in smoother excision forces.

Fig. 6.5 shows the results for six iterations of expert score optimisation, for each of the four experts. As before, we initialised the optimisation with $\{\rho_1 = 1, y_1\}$ pair (this time, y_1 is the predicted expert score, as described in section 6.3.2). The obtained mean of the posterior GP predicts higher expert scores for the excision behaviours generated using larger ρ values (i.e. smoother trajectories). In other words, the results suggest that the sawing movement is more likely to be penalised by experts. In addition, the experiment demonstrates that the sawing behaviour parameterised by ρ can achieve different modulations of excision forces. For example, the score from Expert A highlights the rater's preference towards excisions with a more pronounced force modulation, as reflected by the Consistency feature. Notice that the posterior GP successfully captures this preference with the optimal sawing parameter $\rho \approx 6$.

6.4.1 Excision force characteristics versus ρ parameter

We analysed the $\{\rho, y\}$ datapoints collected in the above experiments to explore the relationships between the sawing parameter ρ and characteristics of the excision forces. Fig. 6.6 (left) shows a scatter plot of the ρ parameter values vs the smoothness feature of the excision forces evaluated by model $\mathscr{F}$. As in the first experiment, the sawing behaviour shows a strong positive correlation with the Smoothness feature (Pearson's $r = 0.74,\ p < 0.05$). This relationship has an intuitive interpretation that smoother excision trajectories must result in a more uniform application of excision forces. The smoothness of the excision forces achieved by two medical students (dotted green lines) and two practising surgeons (dashed red lines) suggest that more experienced surgeons are likely to apply more uniform blade trajectories.

Fig. 6.6 (middle) shows the contour plots of the Amplitude and Consistency features of excision forces against the sawing parameter ρ. The results show that ρ has no significant correlation with the excision force amplitude - both smooth and sawing excision trajectories can yield equally low or high cutting forces. On the other hand, the consistency of excision forces (a feature that reflects the inverse of the spread of force levels during excision), highlights a strong correlation with sawing parameter ρ (Pearson's $r = 0.82,\ p < 0.05$). This relationship is explained by Fig. 6.3 (bottom row), where larger ρ values correspond to the noticeably lower variations of z_b, and as the result, to lower variations along x, y and pitch components of the excision trajectories. This observation agrees with a general intuition that it is more difficult to apply excision forces consistently when sawing.

The Confidence feature (Fig. 6.6 right), which characterises both the uniformity and consistency of the excision forces, shows a significant alignment with sawing parameter ρ (Pearson's $r = 0.78$, $p < 0.05$). Similar to the Amplitude feature, the experiment results show a weak relationship (Pearson's $r = 0.58$, $p < 0.05$) between ρ and the Energy feature. Finally, Fig. 6.6 shows the model $\mathscr{F}$ characterisation of excision forces from two professional surgeons (denoted as **S**) and two medical trainees with no experience at elliptical excision task (denoted as **T**). Notice that model characterisation of surgeon excisions is aligned with the higher sawing parameter ρ values, whereas the performance of trainees matches the region of lower ρ values. Again, this indicates that surgeons are likely to exhibit smoother excision trajectories when compared to less experienced medical students.

6.5 Discussion and conclusions

In this study, we used a model of excision forces to optimise the pose trajectories of a blade in an elliptical excision task. We proposed an excision trajectory generator capable of producing human-like elliptical excision behaviours parameterised by a single parameter ρ that defines the amount of sawing motion applied during excision. These models can be used to efficiently optimise the excision technique with desired excision characteristics using Bayesian optimisation. More specifically, we show how to align robotic excision behaviours with features that satisfy the criteria of surgical experts and behaviours that resemble the performance characteristics of surgeons at various experience levels. Experimental results indicate that the proposed ρ-parameterisation can successfully produce cutting force modulation that maximises the performance assessment of experts.

Our analysis suggests that professional surgeons are more likely to apply smoother excision trajectories, whereas less experienced medical trainees exhibit greater sawing behaviour. It is well known that sawing movement assists the cutting process by lowering the forces required to separate the material [11]. We hypothesise that inexperienced trainees employ this strategy to overcome the need to apply excessive excision forces to perform a controlled cut. Although this study is limited to scalpel trajectories only, the cutting forces are strongly affected by the tissue tensioning controlled by the non-dominant hand. Hence, we hypothesise that experienced surgeons, while applying the smooth excision trajectories, actively tension the tissues to assist

the excision. This combination of excision and tissue tensioning strategies is an interesting line of future work to better understand the dexterous manipulation skills underlying the elliptical excision task. Finally, we want to emphasise the promising prospect of using the proposed framework for studying surgical techniques at various levels of expertise, analysing common mistakes and their effects on the tissues.

Chapter 7

Conclusions

7.1 Discussion of results

In this thesis, we explored three major themes, namely 1) the role of force sensing in the robust cutting behaviours exhibited by humans, 2) the composition of cutting motion applied by humans in various cutting tasks, and 3) robot learning to perform these tasks in a human-like fashion.

We formulated the need for human-like robotic cutting soft objects for the first time in the robotics field. This need is motivated by two key factors. First, an important class of robotic cutting applications – autonomous surgery – needs to comply with a wide range of task specifications that are implicit by nature. We aim to leverage learning these from human demonstrations. Second, the harmonious coexistence of robots and humans in the shared workspace implies a thoughtful approach to constructing robotic behaviours. Humans must perceive these as predictable and familiar. For these reasons, we draw our attention to human cutting skills and ask questions about its underlying structure and how we can capture and reproduce it in robots.

The insights gained by observing the humans at cutting tasks point to the force modality as a potential ingredient to robustness. The role of tactile feedback in the broad context of manipulation tasks is well understood [191]. Earlier works on modelling the dynamics of cutting soft objects highlight curious mechanisms that relate the motion of the blade to the cutting efficiency, e.g. the relation of slice-to-push ratio to overall cutting forces [11, 20]. Interestingly, these mechanisms appear encoded in human cutting skills and give a specific structure to cutting techniques shown by humans. In this thesis, we aim to reverse the discussion and ask whether we can learn these force-driven mechanisms that shape the cutting techniques.

Another observation of human-performed cutting tasks is that the motion envelope has a well-defined structure despite the complexity of the kinematic trajectories observed in practical cutting examples. Chapter 1 introduced the decomposition of cutting movement into two independent components – nominal and adaptive motions. These constraint motions, in general, operate in different degrees of freedom. This dissertation explored how this structure can be exploited and how these components can be learned from human observation.

For example, Chapter 3 described the approach of learning a nominal blade trajectory in the grapefruit scooping task using kinesthetic teaching. The trajectory was encoded as a Dynamic Movement Primitive (DMP), which offers excellent flexibility regarding the composition of behaviours with reactive adaptation, among other advantages. Chapter 4 further explored the applicability of these Dynamic System-based methods in learning cutting skills and identified their significant limitations for a large class of cutting tasks characterised by non-holonomic constraints (e.g. in the task of elliptical excision). The proposed formulation for non-holonomic DMPs enables incorporating a broad range of highly relevant constraints for cutting tasks while benefiting from advantages offered by Dynamical Systems.

A key question about the role of forces in the robustness of cutting tasks, formulated in the opening chapter of this thesis, is closely related to the other motion component – adaptive motion. In Chapter 3, we formulate and confirm the hypothesis that cutting movement guided by force feedback has a fundamental role in the cutting skills of humans. The chapter proposes a probabilistic control law that modulates the nominal trajectory according to the probability of desired blade-object interaction. The insight behind this formulation is based on observation of how humans scoop a grapefruit – a nominal scooping trajectory of the blade is skilfully adjusted in response to a rough judgement of whether the blade is getting stuck in the peel.

This leads us to two interrelated sub-topics, namely, the question of feature representations (the error signal) and the question of feature mapping into movement adaptation (the controller). In Chapter 3, the former problem was approached by learning the desired sensory trace from multiple executions of nominal trajectories. This particular example is analogous to humans learning how it must feel to successfully scoop a grapefruit versus how it feels when the blade gets stuck in the peel.

Chapter 5 and Chapter 6 take a step further by raising the question of whether this approach applies to learning the desired force features in situ (e.g. in surgical training with labelled performances). However, the variability of human-demonstrated cutting motions complicates this matter considerably.

The latter problem of mapping force-based features into the movement adaptation in this dissertation was approached by hand-constructing a control law based on the available knowledge of task geometry. While this approach is feasible, given the convenient decomposition of the cutting motion described above, there is a strong motivation to learn this controller from human data. While the incorporation of structured knowledge in motion decomposition is welcomed – given the available theory of constrained mechanical systems [192], our priors on mapping sensed forces to motion in human cutting behaviour are weak.

This invites us to question how to learn these human-like force-based movement adaptations in cutting tasks. Chapter 5 explores the idea of leveraging the structured environment of surgical training (e.g. carefully curated, well-defined tasks and procedures, cohorts of trainees organised by experience level, labelled performance in the form of scoring, etc.) for developing deeper insights into inner workings of this phenomena. Here, we capture latent characteristics of excision forces that encode subject-specific features and let us quantitatively compare the individual performances from force measurements. In Chapter 6 we shows how these characteristic features of human-like blade-tissue interaction forces can be used to synthesise human-like cutting behaviours.

Human-like motions of the blade, which may or may not reproduce the desired (human-like) blade-object interaction forces (Fig. 1.4). This hinders our ability to learn faithful human-like interactions in a fully autonomous setting (such as the approach used in Chapter 3 to learn latent force-based features of the desired grapefruit scooping behaviour). This thesis proposes to align robotic behaviour with humans by optimising learned human-like cutting motions with respect to the desired (human-like) characteristics of cutting forces. This implies the existence of a model capable of evaluating whether cutting forces resemble the blade-object interactions from human cutting.

Chapter 5 proposes a model capable of characterising the cutting skill and the manner of task execution. A significant contribution to this line of work was the development of a novel low-cost sensorised instrument for measuring cutting forces. The dataset of excision forces collected using the instrument in the elliptical excision task

revealed subject-specific temporal and amplitude signatures in cutting forces, which allow detailed performance analysis and subject-to-subject comparison. In addition to analysing trainee versus surgeon performance, the chapter explores the latent feature space of the model and identifies its relation to expert scoring.

In the context of behaviour alignment, this model lets us evaluate the similarity between robotic and human cutting skills. Chapter 6 proposes the framework for skill optimisation with respect to an objective function defined over the parameter space of the proposed model. This enables the exploration of human-like cutting behaviours around the nominal cutting trajectory while ensuring that the sampled interaction force trace remains within the distribution of human-like interactions.

7.2 Future work

This thesis provides a foundation for a better understanding of the cutting skills in humans and takes a step closer to robust automation of this complex manipulation skill. This work emphasised the importance of drawing our attention to human cutting behaviour for insight and inspiration, but also as a “gold standard” reference. Future studies of robotic cutting can explore various directions in achieving human-level skills.

The composition of the cutting motions discussed in this thesis was engineered based on our intuitive understanding of the task. It is, however, important to explore the techniques for learning this decomposition from data. This could help discover interesting geometrical interdependencies that our intuition can overlook. Besides, the taxonomy of cutting techniques discussed in Chapter 1 is artificial. Practical cutting tasks used by humans will likely involve a mixture of these techniques applied simultaneously. It is possible that the structure extracted from cutting motion data may significantly differ from the canonical techniques discussed in this thesis.

The proposed method for reproducing human-like cutting skills in robots relies on 1) human-like cutting motions learned from demonstrations, 2) a model that evaluates characteristics of blade-object interaction and its similarity to interactions observed in cutting by humans, 3) optimisation of learned human-like cutting motions with respect to these characteristics, and 4) learning the interaction model that maps the sensed cutting forces into an appropriate adaptation of cutting motion. A promising avenue

for future research could look into learning this interaction model direction from pose and forces data. However, collecting such datasets can be challenging – accurate measurement of instrument pose requires expensive equipment with an elaborate setup.

One promising immediate extension of work presented in this thesis is considering the configuration of a robotic arm in achieving organic-looking cutting motions. Redundant articulated manipulators offer the flexibility of planning human-like motions of the entire kinematic chain.

A bimanual robotic setup in which the cutting process is assisted by controlling the local deformation around the cutting front is highly relevant to bringing the performance of autonomous cutting closer to the human level. An exciting application is surgery. Here, in addition to robotic cutting, a model of human-like cutting skills can be used as a predictive model for robot assistants.

The vision modality is a natural extension of the primarily force-based approach to adaptive cutting behaviours considered in this work. The role of vision in dexterous manipulation tasks is undeniable. Deformation tracking and motion re-planning based on visual cues can be among the most impactful additions to this research.

Finally, it is interesting to consider the applicability of the approach presented in this thesis to other manipulation tasks where human-like behaviour is essential. This could be any manual task in surgery, such as palpation, tissue retraction or suture. An exciting line of work could be using the proposed framework to analyse the effectiveness and safety of surgical techniques in these tasks. Here, a robot capable of reproducing human-like surgical skills could simulate the task executions under various scenarios, which opens up opportunities for in-depth analysis of techniques and their downstream effect on the tissues. Importantly, robot learning constrained to human-like trajectories and interaction can lead to the fascinating subject of synthesis of new surgical techniques.

Bibliography

[1] A. Straizys, M. Burke, and S. Ramamoorthy, "Generating robotic elliptical excisions with human-like tool-tissue interactions," in *2024 IEEE International Conference on Robotics and Automation (ICRA)*. IEEE, 2024.

[2] A. Straižys, M. Burke, P. M. Brennan, and S. Ramamoorthy, "A generative force model for surgical skill quantification using sensorised instruments," *Communications Engineering*, vol. 2, no. 1, p. 36, 2023.

[3] A. Straižys, M. Burke, and S. Ramamoorthy, "Learning robotic cutting from demonstration: Non-holonomic dmps using the udwadia-kalaba method," in *2023 IEEE International Conference on Robotics and Automation (ICRA)*. IEEE, 2023, pp. 5034–5040.

[4] A. Straižys, M. Burke, and S. Ramamoorthy, "Surfing on an uncertain edge: Precision cutting of soft tissue using torque-based medium classification," in *2020 IEEE International Conference on Robotics and Automation (ICRA)*. IEEE, 2020, pp. 4623–4629.

[5] EPICURIOUS, "How To Use Every Japanese Knife," https://youtu.be/FDNNG9doFe4?si=zjgrCvAuNuSdiq4u, 2020, [Online; accessed 23-August-2023].

[6] EPICURIOUS, "How To Cut Every Cheese," https://youtu.be/fTgm36y884c, 2022, [Online; accessed 24-August-2022].

[7] A. J. Key and S. J. Lycett, "Technology based evolution? a biometric test of the effects of handsize versus tool form on efficiency in an experimental cutting task," *Journal of Archaeological Science*, vol. 38, no. 7, pp. 1663–1670, 2011. [Online]. Available: https://www.sciencedirect.com/science/article/pii/S0305440311000719

[8] L. Frink, B. Hoffman, and R. Shaw, "Ulu knife use in western alaska: a comparative ethnoarchaeological study," *Current Anthropology*, vol. 44, no. 1, pp. 116–122, 2003.

[9] R. J. Weber and D. N. Perkins, *Inventive minds: Creativity in technology*. Oxford University Press, USA, 1992, vol. 10.

[10] F. Osiurak and A. Badets, "Tool use and affordance: Manipulation-based versus reasoning-based approaches." *Psychological review*, vol. 123, no. 5, p. 534, 2016.

[11] A. G. Atkins, X. Xu, and G. Jeronimidis, “Cutting, by ‘pressing and slicing,’of thin floppy slices of materials illustrated by experiments on cheddar cheese and salami,” *Journal of Materials Science*, vol. 39, pp. 2761–2766, 2004.

[12] P. Jamdagni and Y.-B. Jia, “Robotic slicing of fruits and vegetables: modeling the effects of fracture toughness and knife geometry,” in *2021 IEEE International Conference on Robotics and Automation (ICRA)*. IEEE, 2021, pp. 6607–6613.

[13] R. C. Arkin and L. Moshkina, “Affect in human-robot interaction,” 2014.

[14] Y. He, B. Zhao, X. Hou, P. Gao, Y. Hu, and P. Zhang, “An assistant robot system for sinus surgery,” *Journal of Medical Devices*, vol. 10, no. 3, p. 030925, 2016.

[15] M. J. Zeestraten, I. Havoutis, and S. Calinon, “Programming by demonstration for shared control with an application in teleoperation,” *IEEE Robotics and Automation Letters*, vol. 3, no. 3, pp. 1848–1855, 2018.

[16] T. Schlich, “‘the days of brilliancy are past’: Skill, styles and the changing rules of surgical performance, ca. 1820–1920,” *Medical History*, vol. 59, no. 3, pp. 379–403, Jun. 2015. [Online]. Available: https://doi.org/10.1017/mdh.2015.26

[17] S. Schaal, “Dynamic movement primitives-a framework for motor control in humans and humanoid robotics,” in *Adaptive motion of animals and machines*. Springer, 2006, pp. 261–280.

[18] M. H. Raibert and J. J. Craig, “Hybrid position/force control of manipulators,” 1981.

[19] B. Siciliano and L. Villani, *Robot force control*. Springer Science & Business Media, 1999.

[20] A. Atkins and X. Xu, “Slicing of soft flexible solids with industrial applications,” *International Journal of Mechanical Sciences*, vol. 47, no. 4-5, pp. 479–492, 2005.

[21] X. Mu, Y. Xue, and Y. Jia, “Robotic cutting: Mechanics and control of knife motion,” in *2019 International Conference on Robotics and Automation (ICRA)*, May 2019, pp. 3066–3072.

[22] T. Chanthasopeephan, J. P. Desai, and A. C. Lau, “Modeling soft-tissue deformation prior to cutting for surgical simulation: finite element analysis and study of cutting parameters,” *IEEE transactions on biomedical engineering*, vol. 54, no. 3, pp. 349–359, 2007.

[23] A. G. Atkins and Y.-W. Mai, “Elastic and plastic fracture: metals, polymers, ceramics, composites, biological materials,” *(No Title)*, 1985.

[24] Z. Liu, C. Wang, Z. Chen, and J. Sui, "The advance of surgical blades in cutting soft biological tissue: A review," *The International Journal of Advanced Manufacturing Technology*, vol. 113, pp. 1817–1832, 2021.

[25] M. T. Mason and K. M. Lynch, "Dynamic manipulation," in *Proceedings of 1993 IEEE/RSJ International Conference on Intelligent Robots and Systems (IROS'93)*, vol. 1. IEEE, 1993, pp. 152–159.

[26] A. K. Golahmadi, D. Z. Khan, G. P. Mylonas, and H. J. Marcus, "Tool-tissue forces in surgery: A systematic review," *Annals of Medicine and Surgery*, vol. 65, p. 102268, 2021. [Online]. Available: https://www.sciencedirect.com/science/article/pii/S2049080121002181

[27] S. E. Book, S. Z. Aasi, and D. J. Leffell, "Ellipse, ellipse variations, and dog-ear repairs," in *Surgery of the Skin*. Elsevier, 2010, pp. 239–250. [Online]. Available: https://doi.org/10.1016/b978-0-323-06575-7.00016-x

[28] T. Sugiyama, S. Lama, L. S. Gan, Y. Maddahi, K. Zareinia, and G. R. Sutherland, "Forces of tool-tissue interaction to assess surgical skill level," *JAMA Surgery*, vol. 153, no. 3, p. 234, Mar. 2018. [Online]. Available: https://doi.org/10.1001/jamasurg.2017.4516

[29] A. L. Trejos, R. V. Patel, R. A. Malthaner, and C. M. Schlachta, "Development of force-based metrics for skills assessment in minimally invasive surgery," *Surgical Endoscopy*, vol. 28, no. 7, pp. 2106–2119, Jul 2014. [Online]. Available: https://doi.org/10.1007/s00464-014-3442-9

[30] C. E. Reiley, H. C. Lin, D. D. Yuh, and G. D. Hager, "Review of methods for objective surgical skill evaluation," *Surgical Endoscopy*, vol. 25, no. 2, pp. 356–366, Jul. 2010. [Online]. Available: https://doi.org/10.1007/s00464-010-1190-z

[31] P. Hertzmann, "The Knife Edge - Introduction Knife History," https://www.hertzmann.com/techniques/videos/The_Edge_of_Knife_01.mp4, 2024, [Online; accessed 19-February-2024].

[32] P. Hertzmann, "The Knife Edge - The Serrated Knife," https://www.hertzmann.com/techniques/videos/The_Edge_of_Knife_10.mp4, 2024, [Online; accessed 19-February-2024].

[33] P. Hertzmann, "The Knife Edge - The Chef's Knife," https://www.hertzmann.com/techniques/videos/The_Edge_of_Knife_06.mp4, 2024, [Online; accessed 19-February-2024].

[34] P. Hertzmann, "The Knife Edge - The Slicer," https://www.hertzmann.com/techniques/videos/The_Edge_of_Knife_09.mp4, 2024, [Online; accessed 19-February-2024].

[35] P. Hertzmann, “The Knife Edge - Knife Skills Review,” https://www.hertzmann.com/techniques/videos/The_Edge_of_Knife_13.mp4, 2024, [Online; accessed 19-February-2024].

[36] P. Hertzmann, “The Knife Edge - The Paring Knife,” https://www.hertzmann.com/techniques/videos/The_Edge_of_Knife_08.mp4, 2024, [Online; accessed 19-February-2024].

[37] EPICURIOUS, “How To Fillet Every Fish,” https://youtu.be/wcueSXGueJs?si=B6jnmO6CtPuB0oIS, 2019, [Online; accessed 24-August-2022].

[38] S. G. Kumagai, R. F. Rosales, G. C. Hunter, W. D. Rappaport, D. B. Witzke, T. A. Chvapil, M. Chvapil, and J. C. Sutherland, “Effects of electrocautery on midline laparotomy wound infection,” *The American Journal of Surgery*, vol. 162, no. 6, pp. 620–623, Dec. 1991. [Online]. Available: https://doi.org/10.1016/0002-9610(91)90122-t

[39] W. D. Rappaport, G. C. Hunter, R. Allen, S. Lick, A. Halldorsson, T. Chvapil, M. Holcomb, and M. Chvapil, “Effect of electrocautery on wound healing in midline laparotomy incisions,” *The American Journal of Surgery*, vol. 160, no. 6, pp. 618–620, Dec. 1990. [Online]. Available: https://doi.org/10.1016/s0002-9610(05)80757-3

[40] R. Denadai, R. Saad-Hossne, and L. R. M. Souto, “Simulation-based cutaneous surgical-skill training on a chicken-skin bench model in a medical undergraduate program,” *Indian journal of dermatology*, vol. 58, no. 3, p. 200, 2013.

[41] J. D. Boyer, J. A. Zitelli, and D. G. Brodland, “Undermining in cutaneous surgery,” *Dermatologic surgery*, vol. 27, no. 1, pp. 75–78, 2001.

[42] D. Zhou and G. McMurray, “Modeling of blade sharpness and compression cut of biomaterials,” *Robotica*, vol. 28, no. 2, pp. 311–319, 2010.

[43] T. Chanthasopeephan, J. P. Desai, and A. C. Lau, “Study of soft tissue cutting forces and cutting speeds,” in *Medicine Meets Virtual Reality 12*. IOS press, 2004, pp. 56–62.

[44] R. Rahal, F. Abi-Farraj, P. R. Giordano, and C. Pacchierotti, “Haptic shared-control methods for robotic cutting under nonholonomic constraints,” in *2019 IEEE/RSJ International Conference on Intelligent Robots and Systems (IROS)*, 2019, pp. 8151–8157.

[45] M. Mahvash and V. Hayward, “Haptic rendering of cutting: A fracture mechanics approach,” 2001.

[46] A. Spagnoli, M. Terzano, R. Brighenti, F. Artoni, and P. Ståhle, “The fracture mechanics in cutting: A comparative study on hard and soft polymeric materials,” *International Journal of Mechanical Sciences*, vol. 148, pp. 554–564, 2018.

[47] J. G. Williams, “Friction and plasticity effects in wedge splitting and cutting fracture tests,” *Journal of Materials Science*, vol. 33, pp. 5351–5357, 1998.

[48] Z. Liu, Z. Liao, D. Wang, C. Wang, C. Song, H. Li, and Y. Liu, “Recent advances in soft biological tissue manipulating technologies,” *Chinese journal of mechanical engineering*, vol. 35, no. 1, pp. 1–34, 2022.

[49] A. G. Atkins, X. Xu, and G. Jeronimidis, “Cutting, by ‘pressing and slicing,’ of thin floppy slices of materials illustrated by experiments on cheddar cheese and salami,” *Journal of Materials Science*, vol. 39, no. 8, pp. 2761–2766, Apr 2004.

[50] T. Atkins, “Optimum blade configurations for the cutting of soft solids,” *Engineering fracture mechanics*, vol. 73, no. 16, pp. 2523–2531, 2006.

[51] E. Reyssat, T. Tallinen, M. Le Merrer, and L. Mahadevan, “Slicing softly with shear,” *Physical review letters*, vol. 109, no. 24, p. 244301, 2012.

[52] M. K. Chaudhury, “A cut above the rest,” *Physics*, vol. 5, p. 139, 2012.

[53] Y. Liu, C.-Y. Hui, and W. Hong, “A clean cut,” *Extreme Mechanics Letters*, vol. 46, p. 101343, 2021. [Online]. Available: https://www.sciencedirect.com/science/article/pii/S2352431621001024

[54] M. Khadem, C. Rossa, R. Sloboda, N. Usmani, and M. Tavakoli, “Mechanics of tissue cutting during needle insertion in biological tissue,” *Robotics and Automation Letters, IEEE*, vol. PP, pp. 1–1, 07 2016.

[55] C. McCarthy, M. Hussey, and M. Gilchrist, “On the sharpness of straight edge blades in cutting soft solids: Part i – indentation experiments,” *Engineering Fracture Mechanics*, vol. 74, no. 14, pp. 2205–2224, 2007. [Online]. Available: https://www.sciencedirect.com/science/article/pii/S0013794406004073

[56] Z. Hu, B. Zhang, and W. Sun, “Cutting characteristics of biological soft tissues,” *CIRP annals*, vol. 61, no. 1, pp. 135–138, 2012.

[57] Z. Hu, W. Sun, and B. Zhang, “Characterization of aortic tissue cutting process: Experimental investigation using porcine ascending aorta,” *Journal of the Mechanical Behavior of Biomedical Materials*, vol. 18, pp. 81–89, 2013. [Online]. Available: https://www.sciencedirect.com/science/article/pii/S1751616112002780

[58] T. Chanthasopeephan, J. Desai, and A. Lau, "Deformation resistance in soft tissue cutting: a parametric study," in *12th International Symposium on Haptic Interfaces for Virtual Environment and Teleoperator Systems, 2004. HAPTICS '04. Proceedings.*, 2004, pp. 323–330.

[59] J. A. Auer, "Chapter 12 - surgical techniques," in *Equine Surgery (Fourth Edition)*, fourth edition ed., J. A. Auer and J. A. Stick, Eds. Saint Louis: W.B. Saunders, 2012, pp. 138–149. [Online]. Available: https://www.sciencedirect.com/science/article/pii/B9781437708677000120

[60] M. E. Johnson and C. M. Chen, *Technology of Manufacturing Reduced-Fat Cheddar Cheese*. Boston, MA: Springer US, 1995, pp. 331–337. [Online]. Available: https://doi.org/10.1007/978-1-4615-1913-3_21

[61] M. Green, K. Langley, R. Marshall, B. Brooker, A. Willis, and J. Vincent, "Mechanical properties of cheese, cheese analogues and protein gels in relation to composition and microstructure," *Food Structure*, vol. 5, no. 1, p. 19, 1986.

[62] Z. Li, H. Yang, P. Li, J. Liu, J. Wang, and Y. Xu, "Fruit biomechanics based on anatomy: a review," *International Agrophysics*, vol. 27, no. 1, pp. 97–106, 2013. [Online]. Available: https://doi.org/10.2478/v10247-012-0073-z

[63] J. Vincent, "Fracture properties of plants," ser. Advances in Botanical Research, J. Callow, Ed. Academic Press, 1990, vol. 17, pp. 235–287. [Online]. Available: https://www.sciencedirect.com/science/article/pii/S0065229608601354

[64] G. Holzapfel, "Biomechanics of soft tissue," *The Handbook of Materials Behavior Models*, vol. 3, pp. 1049–1063, 12 2001.

[65] J. Humphrey, "Continuum biomechanics of soft biological tissues," *Proceedings of The Royal Society A: Mathematical, Physical and Engineering Sciences*, vol. 459, pp. 3–46, 01 2003.

[66] M. Reiner, "Elasticity beyond the elastic limit," *American Journal of Mathematics*, vol. 70, no. 2, pp. 433–446, 1948. [Online]. Available: http://www.jstor.org/stable/2372342

[67] R. S. Rivlin, "Large elastic deformations of isotropic materials. vi. further results in the theory of torsion, shear and flexure," *Philosophical Transactions of the Royal Society of London. Series A, Mathematical and Physical Sciences*, vol. 242, no. 845, pp. 173–195, 1949. [Online]. Available: http://www.jstor.org/stable/91457

[68] Y. Fung, “Elasticity of soft tissues in simple elongation,” *American Journal of Physiology-Legacy Content*, vol. 213, no. 6, pp. 1532–1544, 1967, pMID: 6075755. [Online]. Available: https://doi.org/10.1152/ajplegacy.1967.213.6.1532

[69] S. Cover, N. Ezquerra, J. O’Brien, R. Rowe, T. Gadacz, and E. Palm, “Interactively deformable models for surgery simulation,” *IEEE Computer Graphics and Applications*, vol. 13, no. 6, pp. 68–75, Nov. 1993.

[70] T. Chanthasopeephan, J. P. Desai, and A. C. W. Lau, “Study of soft tissue cutting forces and cutting speeds.” *Studies in health technology and informatics*, vol. 98, pp. 56–62, 2004.

[71] T. Azar and V. Hayward, “Estimation of the fracture toughness of soft tissue from needle insertion,” 07 2008, pp. 166–175.

[72] B. Takabi and B. Tai, “A review of cutting mechanics and modeling techniques for biological materials,” *Medical Engineering Physics*, vol. 45, 04 2017.

[73] E. Heiden, M. Macklin, Y. Narang, D. Fox, A. Garg, and F. Ramos, “Disect: A differentiable simulation engine for autonomous robotic cutting,” *arXiv preprint arXiv:2105.12244*, 2021.

[74] X. Mu and Y.-B. Jia, “Physical property estimation and knife trajectory optimization during robotic cutting,” in *2022 International Conference on Robotics and Automation (ICRA)*. IEEE, 2022, pp. 2700–2706.

[75] D. Zhou, M. R. Claffee, K.-M. Lee, and G. V. McMurray, “Cutting," by pressing and slicing", applied to robotic cutting bio-materials. i. modeling of stress distribution,” in *Proceedings 2006 IEEE International Conference on Robotics and Automation, 2006. ICRA 2006.* IEEE, 2006, pp. 2896–2901.

[76] I. Mitsioni, Y. Karayiannidis, and D. Kragic, “Modelling and learning dynamics for robotic food-cutting,” in *2021 IEEE 17th International Conference on Automation Science and Engineering (CASE)*. IEEE, 2021, pp. 1194–1200.

[77] I. Mitsioni, Y. Karayiannidis, J. A. Stork, and D. Kragic, “Data-driven model predictive control for the contact-rich task of food cutting,” in *2019 IEEE-RAS 19th International Conference on Humanoid Robots (Humanoids)*. IEEE, 2019, pp. 244–250.

[78] P. Jamdagni and Y.-B. Jia, “Robotic cutting of solids based on fracture mechanics and fem,” in *2019 IEEE/RSJ International Conference on Intelligent Robots and Systems (IROS)*. IEEE, 2019, pp. 8252–8257.

[79] K. Zhang, M. Sharma, M. Veloso, and O. Kroemer, "Leveraging multimodal haptic sensory data for robust cutting," in *2019 IEEE-RAS 19th International Conference on Humanoid Robots (Humanoids)*. IEEE, 2019, pp. 409–416.

[80] I. Lenz, R. Knepper, and A. Saxena, "DeepMPC: Learning deep latent features for model predictive control," in *Robotics: Science and Systems XI*, 2015.

[81] P. Long, W. Khalil, and P. Martinet, "Force/vision control for robotic cutting of soft materials," in *2014 IEEE/RSJ international conference on intelligent robots and systems*. IEEE, 2014, pp. 4716–4721.

[82] A. Yamaguchi and C. Atkeson, "Combining finger vision and optical tactile sensing: Reducing and handling errors while cutting vegetables," in *IEEE-RAS International Conference on Humanoid Robots*. IEEE Computer Society, 2016, pp. 1045–1051.

[83] G. Zeng and A. Hemami, "An adaptive control strategy for robotic cutting," in *Proceedings of International Conference on Robotics and Automation*, vol. 1, April 1997, pp. 22–27 vol.1.

[84] R. Wu and A. Billard, "Learning from demonstration and interactive control of variable-impedance to cut soft tissues," *IEEE/ASME Transactions on Mechatronics*, vol. 27, no. 5, pp. 2740–2751, 2021.

[85] A. K. Golahmadi, D. Z. Khan, G. P. Mylonas, and H. J. Marcus, "Tool-tissue forces in surgery: A systematic review," *Annals of Medicine and Surgery*, vol. 65, p. 102268, 2021.

[86] S. Misra, K. Ramesh, and A. Okamura, "Modeling of tool-tissue interactions for computer-based surgical simulation: A literature review," *Presence (Cambridge, Mass.)*, vol. 17, p. 463, 10 2008.

[87] A. Billard, S. Calinon, R. Dillmann, and S. Schaal, "Survey: Robot programming by demonstration," Springrer, Tech. Rep., 2008.

[88] H. Ravichandar, A. S. Polydoros, S. Chernova, and A. Billard, "Recent advances in robot learning from demonstration," *Annual review of control, robotics, and autonomous systems*, vol. 3, pp. 297–330, 2020.

[89] A. Y. Ng, S. Russell *et al.*, "Algorithms for inverse reinforcement learning." in *Icml*, vol. 1, 2000, p. 2.

[90] M. Kalakrishnan, P. Pastor, L. Righetti, and S. Schaal, "Learning objective functions for manipulation," in *2013 IEEE International Conference on Robotics and Automation*. IEEE, 2013, pp. 1331–1336.

[91] Y. Meirovitch, D. Bennequin, and T. Flash, "Geometrical invariance and smoothness maximization for task-space movement generation," *IEEE Transactions on Robotics*, vol. 32, no. 4, pp. 837–853, 2016.

[92] M. Vochten, T. De Laet, and J. De Schutter, "Generalizing demonstrated motion trajectories using coordinate-free shape descriptors," *Robotics and Autonomous Systems*, vol. 122, p. 103291, 2019.

[93] A. Paraschos, C. Daniel, J. R. Peters, and G. Neumann, "Probabilistic movement primitives," *Advances in neural information processing systems*, vol. 26, 2013.

[94] S. Kim, R. Haschke, and H. Ritter, "Gaussian mixture model for 3-dof orientations," *Robotics and Autonomous Systems*, vol. 87, pp. 28–37, 2017.

[95] E. Gribovskaya and A. Billard, "Learning nonlinear multi-variate motion dynamics for real-time position and orientation control of robotic manipulators," in *2009 9th IEEE-RAS International Conference on Humanoid Robots*. IEEE, 2009, pp. 472–477.

[96] A. J. Ijspeert, J. Nakanishi, H. Hoffmann, P. Pastor, and S. Schaal, "Dynamical movement primitives: learning attractor models for motor behaviors," *Neural computation*, vol. 25, no. 2, pp. 328–373, 2013.

[97] A. Correia and L. A. Alexandre, "A survey of demonstration learning," *arXiv preprint arXiv:2303.11191*, 2023.

[98] A. J. Ijspeert, J. Nakanishi, and S. Schaal, "Trajectory formation for imitation with nonlinear dynamical systems," in *Proceedings 2001 IEEE/RSJ International Conference on Intelligent Robots and Systems. Expanding the Societal Role of Robotics in the the Next Millennium (Cat. No. 01CH37180)*, vol. 2. IEEE, 2001, pp. 752–757.

[99] A. J. Ijspeert, J. Nakanishi, H. Hoffmann, P. Pastor, and S. Schaal, "Dynamical movement primitives: Learning attractor models for motor behaviors," *Neural Computation*, vol. 25, no. 2, pp. 328–373, 2013.

[100] P. Long, W. Khalil, and P. Martinet, "Robotic deformable object cutting : From simulation to experimental validation," in *European Workshop on Deformable Object Manipulation (EWDOM)*., 2014.

[101] V. Cristini and J. Lowengrub, *Multiscale Modeling of Cancer: An Integrated Experimental and Mathematical Modeling Approach*. Cambridge University Press, 2010.

[102] A. L. McKnight, J. L. Kugel, P. J. Rossman, A. Manduca, L. C. Hartmann, and R. L. Ehman, "MR elastography of breast cancer: preliminary results," *American journal of roentgenology*, vol. 178, no. 6, pp. 1411–1417, 2002.

[103] A. Jain, H. Nguyen, M. Rath, J. Okerman, and C. C. Kemp, "The complex structure of simple devices: A survey of trajectories and forces that open doors and drawers," in *2010 3rd IEEE RAS & EMBS International Conference on Biomedical Robotics and Biomechatronics*. IEEE, 2010, pp. 184–190.

[104] M. Kalakrishnan, L. Righetti, P. Pastor, and S. Schaal, "Learning force control policies for compliant manipulation," in *2011 IEEE/RSJ International Conference on Intelligent Robots and Systems*, Sep. 2011, pp. 4639–4644.

[105] A. Jain and C. Kemp, "Improving robot manipulation with data-driven object-centric models of everyday forces," *Autonomous Robots*, vol. 35, no. 2-3, pp. 143–159, 2013.

[106] P. Pastor, L. Righetti, M. Kalakrishnan, and S. Schaal, "Online movement adaptation based on previous sensor experiences," in *IEEE International Conference on Intelligent Robots and Systems*, 2011, pp. 365–371.

[107] J. M. Romano, K. Hsiao, G. Niemeyer, S. Chitta, and K. J. Kuchenbecker, "Human-inspired robotic grasp control with tactile sensing," *IEEE Transactions on Robotics*, vol. 27, no. 6, pp. 1067–1079, Dec 2011.

[108] A. Schneider, J. Sturm, C. Stachniss, M. Reisert, H. Burkhardt, and W. Burgard, "Object identification with tactile sensors using bag-of-features," in *2009 IEEE/RSJ International Conference on Intelligent Robots and Systems*. IEEE, 2009, pp. 243–248.

[109] J. A. Fishel and G. E. Loeb, "Bayesian exploration for intelligent identification of textures," *Frontiers in Neurorobotics*, vol. 6, no. JUNE, 2012.

[110] F. C. Moon and T. Kalmár-Nagy, "Nonlinear models for complex dynamics in cutting materials," *Philosophical Transactions: Mathematical, Physical and Engineering Sciences*, vol. 359, no. 1781, pp. 695–711, 2001.

[111] S. Tian, F. Ebert, D. Jayaraman, M. Mudigonda, C. Finn, R. Calandra, and S. Levine, "Manipulation by feel: Touch-based control with deep predictive models," in *2019 International Conference on Robotics and Automation (ICRA)*, 2019.

[112] M. C. Gemici and A. Saxena, "Learning haptic representation for manipulating deformable food objects," in *2014 IEEE/RSJ International Conference on Intelligent Robots and Systems*, Sep. 2014, pp. 638–645.

[113] P. Pastor, H. Hoffmann, T. Asfour, and S. Schaal, "Learning and generalization of motor skills by learning from demonstration," in *2009 IEEE International Conference on Robotics and Automation*, May 2009, pp. 763–768.

[114] G. Sutanto, Z. Su, S. Schaal, and F. Meier, "Learning sensor feedback models from demonstrations via phase-modulated neural networks," in *Proceedings of the IEEE International Conference on Robotics and Automation (ICRA) 2018*. IEEE, May 2018.

[115] Y. Chebotar, O. Kroemer, and J. Peters, "Learning robot tactile sensing for object manipulation," in *2014 IEEE/RSJ International Conference on Intelligent Robots and Systems*, Sep. 2014, pp. 3368–3375.

[116] F. Stulp, E. Theodorou, J. Buchli, and S. Schaal, "Learning to grasp under uncertainty," in *2011 IEEE International Conference on Robotics and Automation*, May 2011, pp. 5703–5708.

[117] P. Pastor, M. Kalakrishnan, S. Chitta, E. Theodorou, and S. Schaal, "Skill learning and task outcome prediction for manipulation," in *2011 IEEE International Conference on Robotics and Automation*, May 2011, pp. 3828–3834.

[118] R. Murray and S. Sastry, "Nonholonomic motion planning: steering using sinusoids," *IEEE Transactions on Automatic Control*, vol. 38, no. 5, pp. 700–716, 1993.

[119] A. De Luca, G. Oriolo, and C. Samson, *Feedback control of a nonholonomic car-like robot*. Berlin, Heidelberg: Springer Berlin Heidelberg, 1998, pp. 171–253. [Online]. Available: https://doi.org/10.1007/BFb0036073

[120] I. Robert J. Webster, J. S. Kim, N. J. Cowan, G. S. Chirikjian, and A. M. Okamura, "Nonholonomic modeling of needle steering," *The International Journal of Robotics Research*, vol. 25, no. 5-6, pp. 509–525, 2006. [Online]. Available: https://doi.org/10.1177/0278364906065388

[121] W. Park, J. S. Kim, Y. Zhou, N. Cowan, A. Okamura, and G. Chirikjian, "Diffusion-based motion planning for a nonholonomic flexible needle model," in *Proceedings of the 2005 IEEE International Conference on Robotics and Automation*, 2005, pp. 4600–4605.

[122] H. Zhao, Y. Talwekar, W. Lan, C. Sharma, D. Rus, A. Schulz, and J. I. Lipton, "Robotic jigsaw: A non-holonomic cutting robot and path planning algorithm," in *2021 IEEE/RSJ International Conference on Intelligent Robots and Systems (IROS)*. IEEE, 2021, pp. 5809–5816.

[123] S. Vozar, Z. Chen, P. Kazanzides, and L. L. Whitcomb, "Preliminary study of virtual nonholonomic constraints for time-delayed teleoperation," in *2015 IEEE/RSJ International Conference on Intelligent Robots and Systems (IROS)*, 2015, pp. 4244–4250.

[124] T. Xia, S. Léonard, I. Kandaswamy, A. Blank, L. L. Whitcomb, and P. Kazanzides, "Model-based telerobotic control with virtual fixtures for satellite servicing tasks," in *2013 IEEE International Conference on Robotics and Automation*, 2013, pp. 1479–1484.

[125] F. J. Abu-Dakka, M. Saveriano, and V. Kyrki, "A unified formulation of geometry-aware dynamic movement primitives," *arXiv preprint arXiv:2203.03374*, 2022.

[126] Z. Lu, N. Wang, and C. Yang, "A constrained dmps framework for robot skills learning and generalization from human demonstrations," *IEEE/ASME Transactions on Mechatronics*, vol. 26, no. 6, pp. 3265–3275, 2021.

[127] H. Hoffmann, P. Pastor, D.-H. Park, and S. Schaal, "Biologically-inspired dynamical systems for movement generation: Automatic real-time goal adaptation and obstacle avoidance," in *2009 IEEE International Conference on Robotics and Automation*. IEEE, 2009, pp. 2587–2592.

[128] L. Han, P. Kang, Y. Chen, W. Xu, and B. Li, "Trajectory optimization and force control with modified dynamic movement primitives under curved surface constraints," in *2019 IEEE International Conference on Robotics and Biomimetics (ROBIO)*. IEEE, 2019, pp. 1065–1070.

[129] R. M. Murray, Z. Li, and S. S. Sastry, *A mathematical introduction to robotic manipulation*. CRC press, 2017.

[130] F. Udwadia and R. Kalaba, "A new perspective on constrained motion," *Proceedings of The Royal Society A: Mathematical, Physical and Engineering Sciences*, vol. 439, pp. 407–410, 11 1992.

[131] A. Ude, B. Nemec, T. Petric, and J. Morimoto, "Orientation in cartesian space dynamic movement primitives," 05 2014, pp. 2997–3004.

[132] L. Koutras and Z. Doulgeri, "A correct formulation for the orientation dynamic movement primitives for robot control in the cartesian space," in *Conference on robot learning*. PMLR, 2020, pp. 293–302.

[133] K. K. M. Lynch, *Modern robotics : mechanics, planning, and control / Kevin M. Lynch, Frank C. Park.* Cambridge: Cambridge University Press, 2018 - 2017.

[134] X.-M. Zhao, Y.-H. Chen, H. Zhao, and F.-F. Dong, "Udwadia–kalaba equation for constrained mechanical systems: Formulation and applications," *Chinese Journal of Mechanical Engineering*, vol. 31, no. 1, p. 106, Dec 2018. [Online]. Available: https://doi.org/10.1186/s10033-018-0310-x

[135] A. Müller, "Hamel's equations and geometric mechanics of constrained and floating multibody and space systems," *Proceedings of the Royal Society A*, vol. 479, no. 2273, p. 20220732, 2023.

[136] T. R. Kane, "Dynamics of nonholonomic systems," *Journal of Applied Mechanics*, vol. 28, no. 4, pp. 574–578, 1961.

[137] Q. Ghori and M. Hussain, "Poincaré's equations for nonholonomic dynamical systems," *ZAMM-Journal of Applied Mathematics and Mechanics/Zeitschrift für Angewandte Mathematik und Mechanik*, vol. 53, no. 6, pp. 391–396, 1973.

[138] M. Korayem and A. Shafei, "A new approach for dynamic modeling of n-viscoelastic-link robotic manipulators mounted on a mobile base," *Nonlinear Dynamics*, vol. 79, no. 4, pp. 2767–2786, 2015.

[139] P. Virtanen, R. Gommers, T. E. Oliphant, M. Haberland, T. Reddy, D. Cournapeau, E. Burovski, P. Peterson, W. Weckesser, J. Bright, S. J. van der Walt, M. Brett, J. Wilson, K. J. Millman, N. Mayorov, A. R. J. Nelson, E. Jones, R. Kern, E. Larson, C. J. Carey, İ. Polat, Y. Feng, E. W. Moore, J. VanderPlas, D. Laxalde, J. Perktold, R. Cimrman, I. Henriksen, E. A. Quintero, C. R. Harris, A. M. Archibald, A. H. Ribeiro, F. Pedregosa, P. van Mulbregt, and SciPy 1.0 Contributors, "SciPy 1.0: Fundamental Algorithms for Scientific Computing in Python," *Nature Methods*, vol. 17, pp. 261–272, 2020.

[140] A. Fabisch, "pytransform3d: 3d transformations for python," *Journal of Open Source Software*, vol. 4, no. 33, p. 1159, 2019. [Online]. Available: https://doi.org/10.21105/joss.01159

[141] D. Siegel, *Surgery of the skin : procedural dermatology*. London: Elsevier/Saunders, 2015.

[142] Y. Maddahi, L. S. Gan, K. Zareinia, S. Lama, N. Sepehri, and G. R. Sutherland, "Quantifying workspace and forces of surgical dissection during robot-assisted neurosurgery," *The International Journal of Medical Robotics and Computer Assisted Surgery*, vol. 12, no. 3, pp. 528–537, 2016. [Online]. Available: https://onlinelibrary.wiley.com/doi/abs/10.1002/rcs.1679

[143] G. Tholey, J. P. Desai, and A. E. Castellanos, "Force feedback plays a significant role in minimally invasive surgery: results and analysis," *Annals of surgery*, vol. 241, no. 1, pp. 102–109, Jan 2005, 15621997[pmid]. [Online]. Available: https://pubmed.ncbi.nlm.nih.gov/15621997

[144] A. M. Okamura, C. Simone, and M. D. O'Leary, "Force modeling for needle insertion into soft tissue," *IEEE Transactions on Biomedical Engineering*, vol. 51, no. 10, pp. 1707–1716, Oct 2004.

[145] R. B. Singapogu, S. DuBose, L. O. Long, D. E. Smith, T. C. Burg, C. C. Pagano, and K. J. L. Burg, "Salient haptic skills trainer: initial validation of a novel simulator for training force-based laparoscopic surgical skills," *Surgical Endoscopy*, vol. 27, no. 5, pp. 1653–1661, May 2013. [Online]. Available: https://doi.org/10.1007/s00464-012-2648-y

[146] S. S. Vedula, M. Ishii, and G. D. Hager, "Objective assessment of surgical technical skill and competency in the operating room," *Annual review of biomedical engineering*, vol. 19, pp. 301–325, Jun 2017, 28375649[pmid]. [Online]. Available: https://pubmed.ncbi.nlm.nih.gov/28375649

[147] P. D. van Hove, G. J. M. Tuijthof, E. G. G. Verdaasdonk, L. P. S. Stassen, and J. Dankelman, "Objective assessment of technical surgical skills," *British Journal of Surgery*, vol. 97, no. 7, pp. 972–987, 05 2010. [Online]. Available: https://doi.org/10.1002/bjs.7115

[148] K. Atesok, R. M. Satava, J. L. Marsh, and S. R. Hurwitz, "Measuring surgical skills in simulation-based training," *JAAOS - Journal of the American Academy of Orthopaedic Surgeons*, vol. 25, no. 10, 2017. [Online]. Available: https://journals.lww.com/jaaos/Fulltext/2017/10000/Measuring_Surgical_Skills_in_Simulation_based.1.aspx

[149] T. Horeman, J. Dankelman, F. W. Jansen, and J. J. van den Dobbelsteen, "Assessment of laparoscopic skills based on force and motion parameters," *IEEE Transactions on Biomedical Engineering*, vol. 61, no. 3, pp. 805–813, 2014.

[150] J. D. Mason, J. Ansell, N. Warren, and J. Torkington, "Is motion analysis a valid tool for assessing laparoscopic skill?" *Surgical Endoscopy*, vol. 27, no. 5, pp. 1468–1477, May 2013. [Online]. Available: https://doi.org/10.1007/s00464-012-2631-7

[151] V. Datta, A. Chang, S. Mackay, and A. Darzi, "The relationship between motion analysis and surgical technical assessments," *The American Journal of Surgery*, vol. 184, no. 1, pp. 70–73, Jul 2002. [Online]. Available: https://www.sciencedirect.com/science/article/pii/S0002961002008917

[152] T. Horeman, S. P. Rodrigues, F. Willem Jansen, J. Dankelman, and J. J. van den Dobbelsteen, "Force parameters for skills assessment in laparoscopy," *IEEE Transactions on Haptics*, vol. 5, no. 4, pp. 312–322, 2012.

[153] T. Horeman, D. D. Kurteva (DD Kurteva), P. Valdastri, F. W. Jansen, J. J. van den Dobbelsteen, and J. Dankelman, "The influence of instrument configuration on tissue handling force in laparoscopy," *Surgical Innovation*, vol. 20, no. 3, pp. 260–267, Jun 2013. [Online]. Available: https://doi.org/10.1177/1553350612456100

[154] C. Richards, J. Rosen, B. Hannaford, C. Pellegrini, and M. Sinanan, "Skills evaluation in minimally invasive surgery using force/torque signatures," *Surgical Endoscopy*, vol. 14, no. 9, pp. 791–798, Sep 2000. [Online]. Available: https://doi.org/10.1007/s004640000230

[155] J. Rosen, B. Hannaford, C. Richards, and M. Sinanan, "Markov modeling of minimally invasive surgery based on tool/tissue interaction and force/torque signatures for evaluating surgical skills," *IEEE Transactions on Biomedical Engineering*, vol. 48, no. 5, pp. 579–591, May 2001. [Online]. Available: https://doi.org/10.1109/10.918597

[156] S. Misra, K. T. Ramesh, and A. M. Okamura, "Modeling of tool-tissue interactions for computer-based surgical simulation: A literature review," *Presence (Cambridge, Mass.)*, vol. 17, no. 5, pp. 463–463, Oct 2008, 20119508[pmid]. [Online]. Available: https://pubmed.ncbi.nlm.nih.gov/20119508

[157] S. Leeman and J. Jones, "Visco-elastic models for soft tissues," in *Acoustical Imaging*, I. Akiyama, Ed. Dordrecht: Springer Netherlands, 2009, pp. 369–376.

[158] I. Podder, S. Chandra, M. Chatterjee, and L. Field, "Anatomy and applications of the #15 scalpel blade and its variations," *Journal of Cutaneous and Aesthetic Surgery*, vol. 11, no. 2, p. 79, 2018. [Online]. Available: https://doi.org/10.4103/jcas.jcas_70_16

[159] P. WILLIAMSON, "Gentleness in surgery," *Canadian Medical Association journal*, vol. 72, no. 8, pp. 602–604, Apr 1955, 14364411[pmid]. [Online]. Available: https://pubmed.ncbi.nlm.nih.gov/14364411

[160] C. Oberhauser. Ldc device selection guide. [Online]. Available: http://www.ti.com/lit/pdf/SNOA954

[161] C. Oberhauser. Optimizing l measurement resolution for the ldc161x and ldc1101. [Online]. Available: https://www.ti.com/lit/pdf/snoa944

[162] P. Hajikarimi and F. Moghadas Nejad, "Chapter 3 - mechanical models of viscoelasticity," in *Applications of Viscoelasticity*, P. Hajikarimi and F. Moghadas Nejad, Eds. Elsevier, 2021, pp. 27–61. [Online]. Available: https://www.sciencedirect.com/science/article/pii/B9780128212103000036

[163] G. Ackerson and K. Fu, "On state estimation in switching environments," *IEEE Transactions on Automatic Control*, vol. 15, no. 1, pp. 10–17, 1970.

[164] Y. Bar-Shalom and X.-R. Li, "Estimation and tracking: Principles, techniques, and software [reviews and abstracts]," *IEEE Antennas and Propagation Magazine*, vol. 38, no. 1, pp. 62–, 1996.

[165] M. West, *Bayesian forecasting and dynamic models*. New York: Springer, 1997.

[166] J. D. Hamilton, "Analysis of time series subject to changes in regime," *Journal of Econometrics*, vol. 45, no. 1, pp. 39–70, 1990. [Online]. Available: https://www.sciencedirect.com/science/article/pii/0304407690900939

[167] Z. Ghahramani and G. E. Hinton, "Variational learning for switching state-space models," *Neural Computation*, vol. 12, no. 4, pp. 831–864, 2000.

[168] E. Fox, E. Sudderth, M. Jordan, and A. Willsky, "Nonparametric Bayesian learning of switching linear dynamical systems," in *Advances in Neural Information Processing Systems*, D. Koller, D. Schuurmans, Y. Bengio, and L. Bottou, Eds., vol. 21. Curran Associates, Inc., 2009. [Online]. Available: https://proceedings.neurips.cc/paper/2008/file/950a4152c2b4aa3ad78bdd6b366cc179-Paper.pdf

[169] L. E. Baum, T. Petrie, G. Soules, and N. Weiss, "A maximization technique occurring in the statistical analysis of probabilistic functions of Markov chains," *The Annals of Mathematical Statistics*, vol. 41, no. 1, pp. 164–171, 1970. [Online]. Available: http://www.jstor.org/stable/2239727

[170] A. P. Dempster, N. M. Laird, and D. B. Rubin, "Maximum likelihood from incomplete data via the em algorithm," *JOURNAL OF THE ROYAL STATISTICAL SOCIETY, SERIES B*, vol. 39, no. 1, pp. 1–38, 1977.

[171] T. K. Koo and M. Y. Li, "A guideline of selecting and reporting intraclass correlation coefficients for reliability research," *Journal of chiropractic medicine*, vol. 15, no. 2, pp. 155–163, 2016.

[172] P. H. Ramsey, "Critical values for Spearman's rank order correlation," *Journal of Educational Statistics*, vol. 14, no. 3, pp. 245–253, 2021/10/26/ 1989, full publication date: Autumn, 1989. [Online]. Available: https: //doi.org/10.2307/1165017

[173] A. Sorriento, M. B. Porfido, S. Mazzoleni, G. Calvosa, M. Tenucci, G. Ciuti, and P. Dario, "Optical and electromagnetic tracking systems for biomedical applications: A critical review on potentialities and limitations," *IEEE Reviews in Biomedical Engineering*, vol. 13, pp. 212–232, 2020.

[174] A. M. Franz, T. Haidegger, W. Birkfellner, K. Cleary, T. M. Peters, and L. Maier-Hein, "Electromagnetic tracking in medicine—a review of technology, validation, and applications," *IEEE Transactions on Medical Imaging*, vol. 33, no. 8, pp. 1702–1725, 2014.

[175] B. Tang, G. Hanna, and A. Cuschieri, "Analysis of errors enacted by surgical trainees during skills training courses," *Surgery*, vol. 138, no. 1, pp. 14–20, 2005.

[176] Z. Liu, Z. Liao, D. Wang, C. Wang, C. Song, H. Li, and Y. Liu, "Recent advances in soft biological tissue manipulating technologies," *Chinese Journal of Mechanical Engineering*, vol. 35, no. 1, pp. 1–34, 2022.

[177] A. Hussein, M. M. Gaber, E. Elyan, and C. Jayne, "Imitation learning: A survey of learning methods," *ACM Computing Surveys (CSUR)*, vol. 50, no. 2, pp. 1–35, 2017.

[178] T. Matsubara, S.-H. Hyon, and J. Morimoto, "Learning stylistic dynamic movement primitives from multiple demonstrations. in 2010 ieee," in *RSJ International Conference on Intelligent Robots and Systems*, 2010, pp. 1277–1283.

[179] Y. Zhao, R. Xiong, L. Fang, and X. Dai, "Generating a style-adaptive trajectory from multiple demonstrations," *International Journal of Advanced Robotic Systems*, vol. 11, no. 7, p. 103, 2014.

[180] T. Matsubara, S.-H. Hyon, and J. Morimoto, "Learning parametric dynamic movement primitives from multiple demonstrations," *Neural networks*, vol. 24, no. 5, pp. 493–500, 2011.

[181] A. Ude, B. Nemec, T. Petrić, and J. Morimoto, "Orientation in cartesian space dynamic movement primitives," in *2014 IEEE International Conference on Robotics and Automation (ICRA)*. IEEE, 2014, pp. 2997–3004.

[182] R. Rahal, F. Abi-Farraj, P. R. Giordano, and C. Pacchierotti, "Haptic shared-control methods for robotic cutting under nonholonomic constraints," in *2019 IEEE/RSJ international conference on intelligent robots and systems (IROS)*. IEEE, 2019, pp. 8151–8157.

[183] T. E. Rohrer, J. K. Robinson, C. W. Hanke, D. M. Siegel, A. Fratila, and A. C. Bhatia, *Surgery of the Skin E-Book: Procedural Dermatology*. Elsevier Health Sciences, 2014.

[184] A. Baghdadi, S. Lama, R. Singh, and G. R. Sutherland, "Tool-tissue force segmentation and pattern recognition for evaluating neurosurgical performance," *Scientific Reports*, vol. 13, no. 1, p. 9591, 2023.

[185] A. L. Trejos, R. V. Patel, R. A. Malthaner, and C. M. Schlachta, "Development of force-based metrics for skills assessment in minimally invasive surgery," *Surgical endoscopy*, vol. 28, pp. 2106–2119, 2014.

[186] P. I. Frazier, "A tutorial on bayesian optimization," *arXiv preprint arXiv:1807.02811*, 2018.

[187] C. Rasmussen and C. Williams, *Gaussian Processes for Machine Learning*, ser. Adaptive Computation and Machine Learning series. MIT Press, 2005. [Online]. Available: https://books.google.co.uk/books?id=Tr34DwAAQBAJ

[188] D. R. Jones, M. Schonlau, and W. J. Welch, "Efficient global optimization of expensive black-box functions," *Journal of Global optimization*, vol. 13, pp. 455–492, 1998.

[189] M. L. Stein, *Interpolation of spatial data: some theory for kriging*. Springer Science & Business Media, 1999.

[190] M. G. Genton, "Classes of kernels for machine learning: a statistics perspective," *Journal of machine learning research*, vol. 2, no. Dec, pp. 299–312, 2001.

[191] R. D. Howe, "Tactile sensing and control of robotic manipulation," *Advanced Robotics*, vol. 8, no. 3, pp. 245–261, 1993.

[192] A. Bloch and B. Brogliato, "Nonholonomic mechanics and control," *Appl. Mech. Rev.*, vol. 57, no. 1, pp. B3–B3, 2004.

Appendix A

Expert evaluation and commentary

Table A.1: Expert evaluation (scoring from 0 to 3) of task execution based on video of the trials. Note: Matching scores among experts are highlighted in bold. The original scoring by expert B (shown in parentheses) was normalised to a 0-3 scale from provided 0-5 scale, see Supplementary Table 3 for expert's comment.

Subject	Expert A	Expert B	Expert C	Expert D
A (1st trial)	3	1	3	1
A (2nd trial)	3	1 (2)	2	3
B	**1**	**1** (2)	**1**	**1**
C (1st trial)	0	1	0	1
C (2st trial)	**0**	**0**	**0**	**0**
D (1st trial)	2	1 (2)	2	2
D (2nd trial)	3	1 (2)	2	2
E	1	2 (3)	3	3
F	**0**	**0**	**0**	**0**
G	3	1	1	2
H	1	2 (3)	3	3
I	1	1	3	2
J	1	2 (3)	1	1
K	2	2 (3)	1	0
L	2	1 (2)	3	3

Table A.2: Expert A supplementary comment.

Subject	Comments
A (1st trial)	Good even pressure, skin traction, continuous movement.
A (2nd trial)	Good movement, gentle and continuous.
B	Nice flow.
C (1st trial)	Minimal, if any meaningful traction. Movement with knife is not fluid. Seems to be dragging/digging with knife rather than cutting.
C (2st trial)	Awkward saw-like movement of blade.
D(1st trial)	Nice fluid movements.
D (2nd trial)	-
E	Good movement of blade, but awkward movement at wrist.
F	Digging at the material, appears to be sawing through it. Traction is not meaningful.
G	Nice grip and knife movement, fluid re-positioning of fingers for traction.
H	Fluid movement but limited use of hands for traction.
I	Good, but odd grip.
J	Slightly dragging the knife through the material, little traction.
K	Fluid, but limited traction and very firm grip of blade without optimising the use of wrist/hand movements.
L	-

Table A.3: Expert B supplementary comment.

Score	Comments
0	Unable to perform dissection or rough/uneven scalpel use.
1	Able to cut through skin with some care.
2	As 1 + smooth scalpel strokes (did not go over the same area twice, for the same level, nor jerky movement) + uses supporting hand to provide tension.
3	As 2 + held blade 90 degrees to incision line (no bevelling).
4	As 3 + recognises that the epidermal layer should be scored (smooth light cut) first, allowing a smoother dissection of deeper layers.
5	Perfect dissection (all of the above).

Table A.4: Expert D supplementary comment.

Subject	Comments
A (1st trial)	Good use of non-dominant hand, accurate in centre of dots for first two but that accuracy decreased from 3rd ellipse onwards, slightly bevelled cut because knife not at right angles to skin.
A (2nd trial)	Smooth single glide on each half of ellipse, accurate, excellent use of non-dominant hand, good knife angle, confident, very slight bevelling on the first part of lower incision of the ellipse.
B	Fairly consistent accuracy in centre of dots, knife angle OK, less use of non-dominant hand, there seemed to be less need for use of non-dominant hand, bevelling present.
C (1st trial)	More of a stabbing/sawing, sometimes jerky movement, rather than knife gliding over skin. Looks like the operator cut more deeply into the model and there was more friction on the knife, became smoother and quicker from 1-6, good accuracy
C (2st trial)	Stabbing, sawing movements, deep cuts, with possible variation in depth of cut, no glide, accuracy medium to poor, no bevel, ragged edges, knife slipped once, non-dominant hand used well.
D (1st trial)	Fairly deep cuts, smoother action (knife seems sharper), longer continuous knife sweeps, seemed more confident and quicker, accuracy good, except at corners, no bevelling. Top layer of "skin" seemed much more mobile in this specimen. (In marked contrast to subject H) I think this made the incisions more difficult, especially in the first 2 ellipses - leading to ragged edges, where the top layer seemed to be dragged by the knife rather than a clean cut.
D (2nd trial)	Confident glide, non-dominant hand quality good, cuts deeper at start of incision, seemed more superficial at end of each incision, accuracy medium.
E	More shoulder/trunk movements than others, hand obscured view more than in other recordings, no bevelling, knife held more vertically in line of incision possibly resulting in a deeper cut and less glide, but knife glided fairly well with no re-cuts.
F	Non-pencil grip, deep cuts, sawing action, little/no use of non-dominant hand to stabilise skin, accuracy poor, no bevelling.
G	Shorter glides, accuracy OK, no bevelling, good knife angle, more superficial incisions.
H	Confidence, smooth glide single glide for each side of ellipse, limited (need to) use non-dominant hand, good knife angle, accuracy fine, on last side of last ellipse near end - lateral pressure to correct course led to slight ragged edge. Top layer of skin seemed very firmly attached to lower layers with no sheering.
I	OK, but less clean glide of knife, some breaks in continuity of glide, pushing knife to the side to correct inaccurate course, very occasional bevel and slight dragging of top layer of skin which was not as well attached to deeper layer, accuracy medium to poor.
J	Less good use of non-dominant hand (interestingly, non-dominant hand often applied tension along the long axis of the ellipse rather than at right angles to the incision) knife did not glide smoothly, leading to dragging of top layer of skin, with some ragged cuts, no significant bevelling, knife more vertical and made deeper cuts, which may have contributed to the jerky movements while cutting against greater resistance.
K	Accuracy is very poor (missed dots and overshot corners), non-dominant hand use could have been better - did not seem to apply much stretch, side pressure to correct inaccurate course, leading to ragged edges, e.g. ellipse no 2.
L	Non pencil grip, confident although not a single smooth glide, good use of non-dominant hand, some lateral force to correct course, but this was minimal, accuracy - medium.